HEAT TRANSFER ENHANCEMENT IN A SOLAR LATENT HEAT STORAGE SYSTEM

BY

MUHAMMAD KHALIL ANWAR

A Thesis Presented to the
DEANSHIP OF GRADUATE STUDIES

KING FAHD UNIVERSITY OF PETROLEUM & MINERALS

DHAHRAN, SAUDI ARABIA

In Partial Fulfillment of the
Requirements for the Degree of

MASTER OF SCIENCE

In

MECHANICAL ENGINEERING

December 2015

KING FAHD UNIVERSITY OF PETROLEUM & MINERALS

DHAHRAN- 31261, SAUDI ARABIA

DEANSHIP OF GRADUATE STUDIES

This thesis, written by **Muhammad Khalil Anwar** under the direction his thesis advisor and approved by his thesis committee, has been presented and accepted by the Dean of Graduate Studies, in partial fulfillment of the requirements for the degree of **MASTER OF SCIENCE IN MECHANICAL ENGINEERING.**

Dr. Bekir Sami Yilbas
(Advisor)

Dr. Zuhair Mattoug Gasem
Department Chairman

Dr. Shahzada Zaman Shuja
(Member)

Dr. Salam A. Zummo
Dean of Graduate Studies

Dr. Saad Bin Mansoor
(Member)

7/3/16
Date

In the name of Allah, the Most Gracious, the most Merciful.

Dedicated to my father, my mother, my brothers, my sisters, my fiancé and all my friends.

ACKNOWLEDGMENTS

All praise to Almighty Allah (S.W.T), the Lord of the world, Who created me, and gave me the knowledge, wisdom and the resources to complete my thesis at King Fahd University of Petroleum and Minerals, Dhahran, Saudi Arabia. May Allah accept my efforts and give me strength and chance to work hard and excel in future.

I would like to acknowledge King Fahd University of Petroleum and Minerals for providing me with the research facilities and a good environment to complete my thesis work.

First, foremost, and my deepest gratitude to my advisor, **Dr. Bekir Sami Yilbas**, for his excellent guidance at every single step, patience, caring and constant encouragement to complete my research work. He always motivated me and provided me assistance to understand the real problem encountered and helped me to sort out them. I am greatly indebted to him for the valuable time he gave to me to carry out this study and also for his kind efforts and cooperation towards this research work. I felt much honored to work with such a great personality and inspired from his dedications toward the research.

I would like to say thanks to **Dr. Shahzada Zaman Shuja** from the core of my heart for providing the technical assistance to accomplish the goals of this research work. He was always there to help me at every single step and to encourage me to work hard. His invaluable efforts and dedication, toward this work, is really appreciable.

I would like to say deepest thanks to my parents and family for providing me all the facilities to study and live a happy life. They always encouraged me and stood with me

every good and bad times. My heartfelt respect is for my parents who always prayed for me to achieve the goals of my life.

I am very thankful to Dr. Saad Bin Mansoor for being with me in this research work. I am also very thankful to Osman Kaleem Siddiqui for providing me very basic technical assistance. Also my deepest thanks for Dr. Haider Ali, who guided me and provided help to me, whenever I asked.

At last but not the least, my thanks to my colleagues, Mujahid Rafique and Hafiz Abd Ur Rehman, for sharing every good and times with me and making my stay at KFUPM enjoyable.

.

TABLE OF CONTENTS

LIST OF TABLES

LIST OF FIGURES

ABSTRACT

Full Name : Muhammad Khalil Anwar

Thesis Title : Heat Transfer Enhancement in a Solar Latent Heat Storage System

Major Field : Mechanical Engineering

Date of Degree : December, 2015

A concentrated solar volumetric receiver pertinent to a mobile thermal battery is considered. A mobile thermal battery consists of a steel tube, metallic meshes and working fluid. Thermal analysis of the storage capacity of the mobile thermal battery is carried out assessed through introducing the relevant cases. In the first two cases, water is used as working fluid and in the other cases, the phase change material is incorporated as a storage medium. Concentrated solar heating around the steel tube is considered in line with the field data and the governing equations of heat transfer and the flow field, due to natural convection, are solved numerically. In addition, the rotation of the thermal battery along the solar concentrator centerline is introduced in the analysis to satisfy the uniform heating at the outer surface of the thermal battery. Lithium nitrate is used as a phase change material due to its high latent heat of melting and aluminum is used as the metallic mesh inside the thermal battery to increase the thermal conductivity of the storage medium. The maximum and the minimum temperature difference in the tube is predicted and the temperature parameter is introduced to assess the thermal storage performance of the mobile thermal battery. The findings revealed that use of metallic meshes inside the steel tube improves significantly the heat conduction in the working fluid and it reduces the total melting time of the phase change material. The rotation of the thermal battery results in almost uniform temperature rise in the working fluid and lowers the difference between the maximum and

the minimum temperatures in the thermal energy storing medium. This behavior is more pronounced for the case when the rotational speed of the thermal battery increases.

ملخص الرسالة

الاسم الكامل: محمد خليل انور

عنوان الرسالة: تعزيز نقل الحرارة في نظام التخزين الحرارة الكامنة الشمسية.

التخصص: الهندسة الميكانيكية

تاريخ الدرجة العلمية: ديسمبر 2015

يعتبر جهاز استقبال الحجمي للطاقة الشمسية المركزة ذات الصلة إلى البطارية الحرارية المحمولة. تتكون البطارية الحرارية المحمولة من أنابيب الصلب، شبكات المعدنية ومائع العمل. ويتم تحليل الحراري لسعة التخزين البطارية الحرارية المحمولة وتقييمها من خلال إدخال حالات متعلقة. في الحالتين الأوليين، يتم استخدام المياه كمائع العمل وفي حالات أخرى، أدرجت مادة متغيرة الطور كوسيلة للتخزين. يعتبر التدفئة الشمسية المركزة في جميع أنحاء أنابيب الصلب في خط مع البيانات الميدانية والمعادلات التي تحكم انتقال الحرارة ومجال التدفق، بسبب الحمل الحراري الطبيعي، وحلها عدديا. وبالإضافة إلى ذلك، تم إدخال نظام التناوب في البطارية الحرارية حول محور المكثف الشمسية في التحليل لإرضاء التدفئة الموحدة على السطح الخارجي للبطارية الحرارية. يستخدم نترات الليثيوم كمادة تغيير الطور بسبب حرارة الكامنة للذوبان العالية ويتم استخدام الألومنيوم كشبكة معدنية داخل البطارية الحرارية ليزداد التوصيل الحراري إلى وسيلة التخزين. توقعنا الحد الأقصى والحد الأدنى للفرق في درجة الحرارة في الأنبوب، وقدمنا الدرجة الحرارة كمعامل لتقييم أداء التخزين الحراري للبطارية الحرارية المحمولة. وكشفت النتائج أن استخدام المعدنية الحديدية داخل أنابيب الصلب يحسن توصيل الحرارة بشكل كبير في مائع العمل ويقلل الوقت الذوبان الكلي لمادة تغيير الطور. دوران البطارية الحرارية ينتج في ارتفاع درجة حرارة في مائع العمل بشكل موحد تقريبا ويخفض الفرق بين الحد الأقصى والحد الأدنى لدرجات الحرارة في وسيلة التخزين الطاقة الحرارية. هذا السلوك هو أكثر وضوحا عند زيادة سرعة دوران البطارية الحراري.

CHAPTER 1

INTRODUCTION

Increase in energy demand is one of the major challenges associated with the technological development and sustaining the industrial productivity. It is expected that about $12.2 trillion is to be required to invest in energy sector to meet the energy demand in near future [1]. The consumption rate of fossil fuels is higher than the production rate and it is expected to increase more in future [2]. This situation may affect the economy of a country because of increase in prices of fuels. Along with that, the fossil fuels consumption is the main cause of climate changes. The emissions from fossil fuels contain carbon, nitrogen dioxide, sulfur dioxide and other many dangerous particles in it, which is counted as the major factor of global warming and other many serious environmental effects. The acid rain is one of these issues which is the result of acid formed from the acidic particles present in the emissions of fossil fuels. Ultimately the habitants and species living in the environment are the victims of such kind of problems.

Alternative energy sources, such as clean energy, are the focus areas of research because of the environmental measures. The clean energy available to us in the form of wind energy, hydropower energy, solar energy, geothermal energy and biomass energy. Among all the available renewable energies, the solar energy is the abundantly available energy, which is the most popular topic in research field. It is expected that, in future the investment in solar field is to be the large chunk of the total investment in power sector [1]. It will

result in the reduction of fossil fuels use and consequently the reduction in the pollutants by fossil fuels.

The solar energy can be harvested by different ways for the production of electricity. One of them is by using solar PV panels in which the solar energy falls on the panel and it is directly converted into electricity by the cells available in the panel. The second way; in which solar energy is directly used to heat the fluid and that heated fluid is used in electricity generation. The conventional flat plate collectors are only used for low temperature range applications like heating water at domestic level. For the power generation applications, the high energy fluid is required and it is obtained by using solar concentrating panels. These panels are available in the form of parabolic trough, solar tower and Fresnel reflector. In such kind of panels, the energy is focused at a single point ultimately raising the temperature of the fluid and that heated fluid is used to run the turbine.

The variation in the electricity consumption is another issue faced by the power management these days particularly in the countries where the climate is either extremely hot or extremely cold. These variations may result in different pricing of the available power for the peak load and off-peak load periods. Also the solar energy is available for the limited time period and not reliable for the continuous energy supplying units. Such kind of situations can be handled by developing some kind of energy storage system, which can store energy during the presence of sun and can supply it in the absence of solar energy. This way, we can achieve the goals of getting better economic benefits due to a good power management system.

Thermal energy storage is one of the popular topics to be investigated for fulfilling the energy demand in future. It is one of the important, efficient and practical way of saving the available energy. It not only the way to meet the requirement of energy but also has a positive impact on environment. It allows us to collect a large amount of energy and this stored energy can be used later. For example the heat stored in summer season can be used to provide the heat in buildings during the winter season. Similarly the cold storage in winter can be utilized in hot weather for air conditioning purpose. Thermal energy can be stored in many ways; it can be stored in water, pebbles, concrete and in phase change materials. It is stored in the form of sensible heat or latent heat or combination of both. The sensible heat is stored by raising the temperature of liquid or solid and amount of heat stored depends on the heat capacity of the storage medium. In latent heat storage system, the energy is stored and released during the phase change process and the amount of energy depends on the heat of fusion of the storage medium.

1.1 Phase change material

Phase change material (PCM) is the latent energy storage system, which can store a huge amount of energy in it. The energy absorbing and releasing processes take place when the material undergoes the phase change and it occurs nearly at constant temperature. The process of phase change can be in the form of solid phase to liquid phase, liquid to gas phase or solid to gas phase. These types of material has the capability of storing 5 to 14 times more energy than the sensible storage system. Due to its nature of isothermal process and huge amount of energy storage ability, it is being used in many applications like space heating and cooling in commercial, residential and other buildings. The use of PCM in

building heating, is the focus area since 1980. Many reviews are available which describes the different methods of applying PCM in an effective way. Hogn et al [3] presented a study on use of PCM in building applications. They demonstrated that the use of PCM could lower the room indoor temperature variations and control it effectively.

The solar applications require an efficient way of storing energy which is capable of storing enough energy that can be utilized during the absence of solar energy. The phase change material storage system can be the best option to cultivate the solar energy efficiently. The phase change material has attained a great attention in solar applications [4]. For example the space heating in buildings, integrated with phase change material, is the most popular topic the field of research. The phase change material is utilized in such a way that it is mixed with the building material during its manufacturing or a layer of phase change material is applied in between the walls and roof. During the solar time, the energy is stored in it and this stored energy is utilized for space heating in night. It is also used in other applications for example; solar power plants, off-peak load utilization, heat pump systems, computer cooling, solar panel cooling, and in many others.

1.1.1 Classification of Phase Change Material

The phase change material can be categorized into three types, based on the properties; organic type, inorganic type and eutectic type phase materials. The figure 1.1 explains the classification of phase change material [5]. The organic PCM includes paraffin and fatty acids (non-paraffin). They have volumetric heat storage capacity in range of 128 to 200 kg/dm^3. The general advantages of organic phase change material include that they have melt congruently and no supercooling is required during solidification process. Usually they are chemically stable and recyclable. The inorganic type includes salt hydrates and

metals. They have volumetric storage capacity (250 to 400 kg/dm^3) approximately double than the organic type. Along with that, inorganic phase change materials have sharp melting temperature. The disadvantages associated with these type of PCM is that they require supercooling effect during solidification process. Also after some time, they undergo degradation and some nucleating agents are required to make them recyclable. The Eutectic type phase change material includes the combination of both PCM types mentioned above. They may exist in the form of organic-inorganic, organic-organic and inorganic-inorganic mixtures [5].

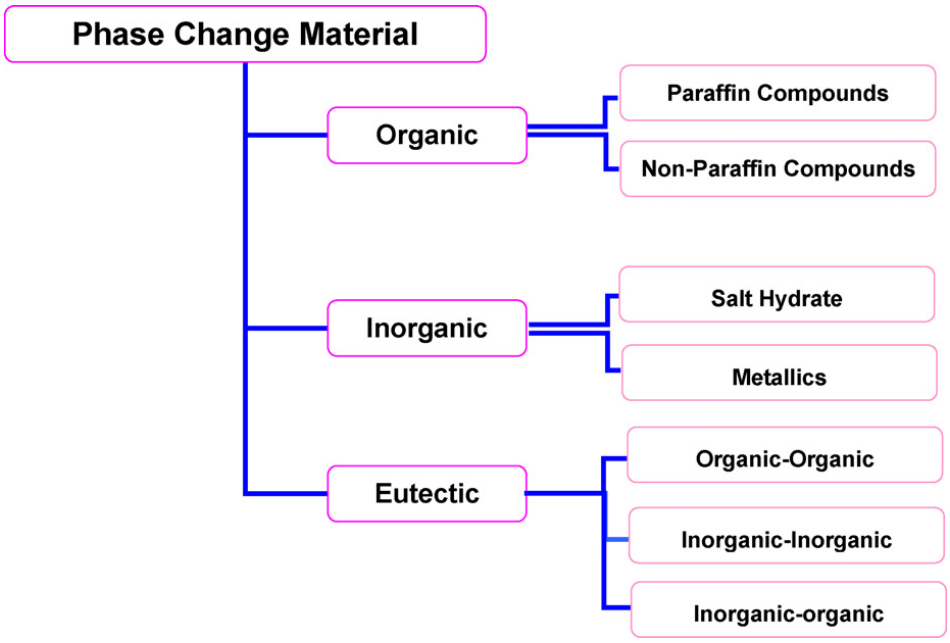

Figure 1.1 Classification of phase change material [5].

The selection of an appropriate phase change material usually depends on the application requirement for which PCM is to be used. In applications, having low operating temperature, usually the organic type is suitable because of their low melting temperatures. But in applications like power generation, a high operating temperature requires a PCM

with high melting temperature for which inorganic is the best candidate. Usually an ideal phase change material have high latent heat, high density, high specific heat capacity, high thermal conductivity and ability to melt congruently. Along with that, it should have high nucleation rate to avoid the supercooling effect and should have high crystallization rate. It also should be chemically stable, non-corrosive, non-toxic, recyclable, and also affordable in terms of cost.

1.2 Heat Transfer Enhancement in Phase Change Material

Phase change materials usually have low thermal conductivity especially the liquid phase. When the PCM starts melting, a layer of liquid is formed which acts as an insulation and prevents the PCM from further melting. Such kind of problem results in increase in total time required for complete melting of phase change material and makes the system inefficient. So to make the effective use of energy storage system with phase change material, it is required to develop some technique to enhance the thermal conductivity of phase change material. This can be done by adding some material with high conductance.

Several techniques are available to increase the thermal conductivity of phase change material. Some of them include the addition of metallic meshes, fins, metallic powder, metal foams, and metallic tubes into the phase change material. Also the encapsulation of phase change material into metal frame is very interesting technique to enhance the heat transfer process in PCM. The addition of metal part into phase change material also reduces the storage capacity of system due to the volume occupied by the metal. So the addition of metal part into phase change material should considered carefully in order to minimize the compromised storage capacity of the system.

Another technique of increasing heat transfer rate in phase change material is the rotation of cylinder or the enclosure in which PCM contained. The rotation of the system provides the uniform temperature distribution inside the domain and uniform melting of phase change material consequently minimizing the problem of segregation of phase change material and supercooling effect. Furbo [6] investigated the rotational effect of phase change material contained in a cylindrical vessel and recommended a speed of 3 rpm to maintain the chemical equilibrium inside. He demonstrated that nucleation problem could be avoided with rotation of cylinder. Also Herrick et al. [7] described some benefits of rotating the cylinder consisting phase change material in it. The benefits included the reduction in complete melting time of PCM, increase in the storage efficiency of the system, increase in the number of charging discharging cycles and increased heat transfer rate with uniform heating inside.

Natural convection inside the melted region also provides the assistance to melting process of phase change material. This heat transfer process occurs due to the flow developed because of density variation with temperature. The effect of natural convection on melting is reported to be small as compare to the processes mentioned above and will be discussed in the succeeding chapters.

1.3 Scope of the work

A thermal energy storing unit is one of the important components of the thermal system to utilize the thermal energy when required. In general, the thermal energy storing units are fixed because of the localized requirements and easiness of operation in the thermal system. This limits the mobility of the storing units in the thermal system. The mobile thermal

batteries are the new concepts and they offer advantages in space heating and cooling applications because of their re-chargeable characteristics and cost effective operations. However, the size and charging/discharging durations of the thermal batteries are critical for the practical applications.

In the present study, thermal characteristics of a mobile thermal battery are investigated. A steel tube with the metallic meshes is considered to resemble the mobile battery and water is incorporated as the working fluid in the storing system. Concentrated solar power heating is considered in the analysis and actual field data is used in the simulations. In order to minimize the localized heating of the thermal battery due to parabolic trough, the rotation of the thermal battery along its symmetry axis is also introduced in some cases.

To estimate the storage time and capacity in the mobile thermal battery, following are considered in this thesis:

i. To investigate the effect of metallic meshes on the thermal performance of the system consisting water in it and to compare the results with the case of without metallic meshes.
ii. To investigate the effect of different rotational speeds of mobile thermal battery, in the focus of trough, on the thermal performance of the system with metallic meshes and water in it.
iii. To investigate the effect of metallic meshes on the melting process of phase change material and to compare the results with the case of without mesh
iv. To investigate the effect of different rotational speeds of mobile thermal battery, in the focus of trough, on the melting of phase change material with mesh inside.

CHAPTER 2

LITERATURE REVIEW

This section provides the literature survey in the related fields of this research work. Extensive literature data is available in the field of heat transfer enhancement in thermal energy storage system. Hence this literature data is divided into four sub sections, describing the heat transfer enhancement in phase change material.

2.1 Heat Transfer Enhancement in PCM by Conductive Additives

An experimental study was conducted by Sari et al [8] to investigate the heat storage characteristics of lauric acid. In the experiment they used 95 % pure lauric acid and vertical double pipe to examine the properties. Their focus was to investigate the influence of temperature in the radial and the axial directions during phase change and the storage characteristics of lauric acid. With the experiment they demonstrated that melting and solidification processes were prominent in the radial direction. In addition, they reported that the buoyancy played an important role in melting process of PCM. Therefore, the heat transfer coefficient was affected by changing Reynolds number and Stefan number. Finally the concluded by their study that 95 % pure lauric acid was a good energy storage material which could be used in building and other applications.

An experimental approach, to enhance the thermal conductivity of paraffin wax, was adopted by Mettawee et al [9]. They mixed aluminum powder in wax to examine the thermal conductivity enhancement. They found that heat storing time was reduced by 60 % as compared to the using pure wax only and the useful heat gain was increased. They

also described the development of the solid-liquid profiles during melting and solidification processes and observed a different profile in solidification process than that of melting. They reported the mean thermal efficiency of the composite studied as in the range of 82 % to 94 %.

Heat transfer characteristics in phase change material (PCM), embedded with copper metal foam, was investigated by Tian and Zaho [10] numerically and they validated the predictions with the experimental data. In the numerical part they considered two equations to investigate the non-equilibrium heat transfer by conduction in the solid part and heat transfer by natural convection in the liquid phase. They demonstrated that heat conduction rate was improved with use of metal foam in phase change material, but the phenomenon of natural convection, in liquid phase, was suppressed due to resistance in flow caused by the metal foam. They also suggested that it could be further improved by using a metal foam having low pore size and porosity.

A similar analysis was also carried out experimentally by Zhao et al [11] in which they used wax RT58 as PCM which was embedded with copper metal foam. A constant heat flux from bottom was applied to examine the melting process in the phase change material. They determined the temperature difference between the PCM and the heated wall to investigate the effect of presence of the metal foam on the melting process. They found that a significant effect of metal foam on melting and solidification processes of PCM occurred as compared to the case using pure PCM only. Increase in heat transfer rate by 3 to 10 times was reported in the case of metal foam with PCM. In addition, the solidification process under cooling conditions, like natural and forced convection, was examined and they found that the time required for complete solidification was reduced to half with the

use of metal foam. A numerical approach was also adopted by them to validate the data obtained from the experimental part. They also found a good agreement between the numerical predictions and experimental data.

Heat transfer enhancement in phase change material, using aluminum fins, was studied by Gharebaghi and Sezai [12] numerically. They investigated the effect of different types of arrangements of fins, on process of energy absorbing and releasing by phase change material. After the analysis, they reported that the heat transfer rate was increased by 80 times with the addition of fins than in the case of using pure phase change material. Among the different arrangement of fins discussed in their study, they found the vertical arrangement of fins more useful for Nusselt number enhancement. The rate of heat transfer was higher in the case of vertical and closed spaced arrangement. They also reported that the process of heat transfer in phase change material was higher in the case of closed spaced fins than the case of increasing fin thickness.

Composites of paraffin wax with different mass fractions of expanded graphite were prepared and analyzed by Sari et al [13] to investigate the thermal characteristics of these composites, used as phase change material (PCM). They prepared composites by using graphite like 2%, 4%, 7% and 10 % by mass. They determined the parameters like melting temperature of PCM, time required for melting of PCM and amount of energy stored by PCM by adopting differential scanning calorimetry technique. They reported the decrease in melting time of PCM because of increase in the thermal conductivity value with addition of expanded graphite. Among all the tested samples of composite, they found the composite with 10 % expanded graphite was more stable than others and also concluded that PCM

composite with 10% mass fraction of graphite was useful in all aspect of high storage capacity, high thermal conductivity and good melting temperature.

A similar study of paraffin-expanded graphite composite, used as phase change material, was also carried out by Zhang and Fang [14] . They prepared composite of paraffin wax with expanded graphite by using average size of 300 μm graphite particle. They reported that there was no change in melting temperature and the latent heat of the composite equal to the calculated value of latent heat, based on mass ratio of paraffin in the composite. They also reported due to the high values of thermal conductivity of composite, the heat transfer rate was increased; consequently reducing the melting and solidification time of PCM. They also observed that they experienced no leakage of liquid during its solid-liquid phase change process.

An experimental study was conducted by Fang et al [15] to investigate the increase in thermal conductivity of eicosane, an organic type PCM, with addition of various mass fractions of graphene nanoplatelets in it. They prepared the composites by addition of graphene nanoplatelets 1, 2, 5 and 10 %, by weight into liquid eicosane. They carried out the study by using transient plane source technique at temperatures 10 to 35℃. They used differential calorimeter to measure the melting point and latent heat of fusion of the composite. They demonstrated that with addition of nanoplatelets, thermal response of PCM could be enhanced due to increase in its thermal conductivity. They also reported that with addition of nanoplatelets10 % by weight, the thermal conductivity was enhanced to 400 %. They achieved these results at expense of reduction in heat storage capacity up to 16 %.

An experiment was conducted by Agyenim et al [16] to analyze the heat transfer characteristics in phase change material. They the shell and tube heat exchanger in which they considered single tube inside the outer shell and multi tubes inside the shell as a heat transfer medium. They used phase change material having melting temperature of 117.7℃ in their experiment. They measured the temperature variations in the radial, axial and the angular directions. They found that the temperature gradient was higher in radial direction compared to the other directions for both type of systems. The phase change in multi tube system was more prominent with convective heat transfer, reported by the authors. They also reported that creation of convective cells in the multi tube system changed the shape of the solid liquid interface fluid flow.

A mathematical model for heat transfer in latent energy storage system was developed by Stritih [17] to investigate the enhancement of the heat transfer rate in phase change material (PCM). He considered paraffin wax enclosed in fins with water outside the fins as a heat carrier medium. He neglected the natural convection heat transfer, during the solidification process, for the considered problem. He used FORTRAN for simulation of his problem and considered different distances between fins, thickness of the fins and depths of the fins. With variation of these parameters, he concluded that the distance between fins was more influential on heat transfer process.

An experimental study was carried out by Xiao et al [18] in which they prepared a shape stabilized PCM, paraffin with thermoplastic elastomer, which was capable of retaining its shape in solid state even with above melting temperature of paraffin and also having the similar phase transition as that of simple paraffin with 80 % of latent heat of fusion of paraffin. The thermal conductivity of prepared composite was reported to be high with

addition of graphite in PCM. They reported that the time required for complete melting of the composite was reduced by 2/5 of the time required for melting of pure paraffin and, for complete solidification, it reduced by 2/9 of the time required for solidification of pure paraffin. They also mentioned that the thermal properties and the mechanical strength can be controlled by the use of different kind of polymer and paraffin.

A study on heat transfer enhancement with fins in latent heat storage medium was conducted by Zhang and Faghri [19]. They considered a geometry, in which phase change material was filled in annular section of cylinder. The fins were attached inside the cylinder in which flow of water was considered as a heat carrier. They assumed one dimensional heat conduction in shell wall and used finite difference technique to solve the problem. They found that adding fins improved the performance of heat transfer phenomenon when heat carrier fluid, with low thermal conductivity, was used at low Reynolds number.

An experimental study was presented by Cabeza et al. [20] to analyze the heat transfer enhancement in a cold storage with three different techniques. The deionized water was used as a phase change material (PCM) in the experiment. They adopted three different methods to enhance the heat transfer rate in PCM. One of them is addition of stainless steel, second is addition of copper and third is addition of graphite soaked into PCM. They concluded that heat or cold storage was mainly due to the latent heat as sensible heat was only 15 to 25 % of total stored heat. The addition of stainless steel did not show good results in case of melting and freezing process. However the addition of copper and graphite showed a better performance of the system. Among the copper and graphite, the graphite showed superior results.

An experimental work to compare the heat transfer characteristics of latent energy storage system with finned surface and without fins was conducted by Stritih [21]. The paraffin with melting temperature 30℃ was considered as phase change material in the study. He measured transient variations of temperature and heat flux to investigate the process of melting and solidification of phase change material. He developed a dimensionless correlation between Nusslet number as a function of Rayleigh number to explain the phenomenon of natural convection in melting and solidification process. He concluded that conduction heat transfer was prominent during solidification process and heat transfer rate could be increased with use of fins. He also investigated the fin effectiveness which was less than 1 for low Fourier number. He reported the reason behind it that was the natural convection, which was dominant in melting process and also reduced because of the presence of fins. On other hand the fin effectiveness was more in solidification process due to fins. He observed 40 % reduction in time for freezing process.

Analysis of numerical simulation of latent heat storage system was presented by Costa et al. [22] to examine the thermal performance of the system. The enthalpy formation and fully implicit finite difference method was adopted by them to carry out their study. A detailed comparison between the thermal performances of the models, with and without fins, was described by them. The magnitude of melting fraction was chosen as a performance deciding factor of the system. They demonstrated by their work that use of fins improved the heat transfer rate, during conduction heat transfer mode, than the case of without fins.

A theoretical study of heat transfer enhancement mechanism in latent heat storage system with fins was presented by Lacroix [23]. He considered a system resembling shell and tube

heat exchanger, in which the phase change material (PCM) was filled to the shell side and the heat transfer fluid was circulating inside the finned tubes. An enthalpy based technique, coupled with convective heat transfer, was adopted by him to solve the problem. A parametric study was given to analyze the effect of different parameters like shell radius, mass flow rate of the fluid and the inlet temperature of the fluid on the thermal performance of the system. He concluded by his study that the fins were more influential for the thermal performance of the system in case of average value of the fluid mass flow rate and at lower values of the inlet fluid temperatures.

The effect of different shapes of metallic meshes, on thermal performance of phase change material (n-octadecane), was studied by Shuja et al. [24] numerically. They selected different shapes of mesh like triangular, hexagonal and rectangular for the analysis. They made the analysis by considering geometric shapes in such a way that the area is kept constant in one case and the perimeter is constant for the second case keeping the same amount of phase change material in both cases. The effect of each type of mesh on melting of phase change material was compared in their work. They found from their analysis that the melting of phase change material started early in case of triangular mesh and the total also the total time required for complete melting of phase change material was less in case of triangular mesh, compared to the other mesh geometries. Finally they conducted an experiment to validate their predictions with experimental data and found a good agreement between their predictions and the experimental work.

An experimental study was conducted by Velraj et al. [25] to investigate the performance of the different methods of heat transfer enhancement in latent energy storage system. They discussed three types of methods; one of them was using longitudinal fins inside the

cylinder and phase change material was filled inside the tube. In the second method, they filled tube with steel lessing rings having diameter 1 centimeter and rest of the space was filled with molten phase change material. The third method, they adopted, was the addition of small amount of water in tube with phase change material and the vacuum was created to make the saturation temperature of water nearly equal to the melting temperature of phase change material. In the last method, they considered that the steam bubbles created from water, may involve in heat transfer enhancement process. They concluded by their work that addition of fins and lessing rings were suitable for the solidification process and they were feasible economically. While on other hand, they found that the steam bubbles were more suitable for the case of melting process of phase change material.

An experimental investigation to examine the thermal performance of mesh composite was conducted by Kim et al. [26]. The effect of wire mesh layers, filler material, material size and the temperature range on the thermal characteristics of the system was presented. They demonstrated that the number of mesh layers was the dominate factor enhancing the heat transfer in fluid but the addition of hollow glass and fillers did not affected the system performance as significant as the wire mesh case.

A study on melting enhancement of phase change material with metal foam was conducted by Mustaffar et al. [27]. They cut the aluminum expanded metal sheets to make layers and arranged them in perpendicular direction to make a metal foam. They arranged the layers in such a way that the porosity of the created metal foam was equal to 0.9. A Phase change material having melting temperature 45℃ was used filled into the empty spaces of the metal foam. They heated the prepared composite until the temperature value 55℃. A comparison between the melting time of phase change material, with and without metal

foam, was established by them to examine the performance of the composite. They found that the time required for complete melting of phase change material was reduced by 14% with the use of expanded metal foam. A numerical study was also presented by them in which the metal layers were arranged in different directions like parallel and perpendicular. They found that the parallel arrangement of metal layers reduced the melting time by 81%.

The effect of metal mesh sizes on melting of phase change material and its capacity was presented by Shuja and Yilbas [28] numerically. The phase change material (n-octadecane) with various metal mesh sizes was used for analysis purpose. They found that the increase in mesh numbers resulted in reduction of total time required for complete melting of phase change material due to high thermal conductivity of metal mesh. On the other hand, it also reduced the storage capacity of the system. An experiment was also carried out by them to validate the results obtained from the simulations and they reported a good agreement between the numerical and experimental data.

2.2 Natural Convection Effect on Melting of Phase Change Material

Natural convection heat transfer is the way of heat transfer in which flow is developed due to change in density of fluid with temperature variation and it plays significant role in some cases. During the melting process of phase change material (PCM), the natural convection phenomenon occurs in molten PCM and contributes towards the further melting of the phase change material.

A numerical study for the effect of natural convection process on the melting of phase change material was presented by Khodadadi and Zhang [29]. Transient equations of continuity, momentum and energy equations were solved iteratively for the analysis. The Darcy's law was considered to solve the flow developed similar to that of flow through

porous media. They reported that the conduction mode of heat transfer was dominated at start, but after developing the molten region of phase change material, the melting became faster because of convection heat transfer. They kept the value of Rayleigh number constant and varied the Prandtl number value from 0.03 to 1 and found that the Prandtl number played a major role in melting of phase change material. While making the comparison, they also showed the prominent effect of the natural convection process on melting of phase change material as compare to the diffusion-controlled melting.

A study on melting of encapsulated phase change material was conducted by Tan et al. [30] to investigate the effect of bouncy-driven convection on melting process. The iterative finite-volume method was adopted in which enthalpy formulation technique was considered to solve the phase change phenomenon. They used n-octadecane, enclosed in a glass tube, as a phase change material. They observed the melting fraction and melting phase front occurred in phase change material and compared these results with numerical predictions. They observed the quick melting of top region of phase change material due to the wavy surface at the bottom. They reported that thermal stratification was formed at upper half region of sphere due to elevation of molten phase change material. The results obtained from experiment and simulation indicated that the wavy behavior at bottom was due to formation of unstable fluid layer and also stable layer at the top region. They also observed the deviation of the temperature values from top to bottom region due to thermal stratification.

Thermal analysis of phase change material in the steel cavity, with consideration of void inside and the natural convection effect, was presented by Elmozughi et al. [31]. They considered the Sodium nitrate as phase change material in their analysis. They examined

the charging and discharging durations by applying different boundary conditions for laminar and turbulent conditions. The flow developed inside was calculated by adopting the volume of fluid method and the enthalpy porosity technique. A cylindrical shape, with different sizes, was considered in the analysis. The air and the Therminol/VP-1, flowing in cross flow arrangement, were considered as heat transferring fluids. They also investigated the 3-D heat transfer effect by considering a spherical shaped encapsulated phase change material with constant heat walls. They reported that due to presence of void, the melting and the solidification processes took a longer time. They also reported that due to lack of properties and smaller effect of convection, the solidification process took more time than the melting process.

A study of melting process of phase change material and the natural convection process inside the liquid phase was presented by Beckermann and Viskanta [32]. The volume averaged transport equations and phase change occurrence at small temperature value were assumed in numerical part. The gallium, incorporating glass beads and enclosed within square shaped container, was considered as a phase change material in the experiment. They measured the temperature and melting front inside the phase change material. They found that natural convection played a dominated role in molten region and conduction heat transfer was dominant in solid region. Upon comparison between the experimental data and the numerical predictions, they observed a good agreement between them.

A numerical investigation of melting process of phase change material, enclosed inside a cylindrical container, was presented by Drazi et al. [33]. They considered N-eicosane as phase change material which was sub-cooled to 1℃. The inner part of concentric and eccentric cylinder was taken as a heated wall and outer surface was assumed adiabatic in

the analysis. They demonstrated that conduction was dominated at start, but after some time the natural convection became dominated at upper region and it increased the melting rate in upper region. They also reported that when inner cylinder moved downward, the melting process became faster than earlier because of natural convection heat transfer taking place in most of the area.

Effect of natural convection on phase change characteristics was presented experimentally by Hirata et al. [34]. The phase change material was filled in rectangular shapes with aspect ratios 3, 1, 1/3 and they were heated isothermally. They also presented a correlation for calculation of mass fraction by natural convection coefficient inside the rectangular horizontal or vertical shape. They found that the change in aspect ratio did not have significant effect on melting of phase change material, but the natural convection played an important role in melting process. They also compared the predicted results, obtained from correlation, with the experimental data and found a good agreement between them.

A numerical study of melting of phase change material in a spherical enclosure was presented by Roy and Sengupta [35] to investigate the effect of natural convection on melting process. They applied uniform temperature at the walls for melting of phase change material. They observed the pressure difference in the domain and the effect of various dimensionless parameters on the flow field. They found that the natural convection had a significant effect on flow and pressure distribution inside the enclosure. They also found that the heat transfer process was greater in lower region than the upper region because of natural convection process taking place in lower region. They found a significant amount of melted region in upper part because of Grashof and Prandtl number.

The numerical investigation of melting process of the phase change material, driven by natural convection, was conducted by Bertrand et al. [36]. They considered a 2D square geometry in which a constant temperature, at the walls, was applied. They selected two ranges of Prandtl numbers, which covered the melting of metals and organic materials. They demonstrated that the natural convection process played a major role in melting process of material. They also recommended that the work could be extended to next stage with more effective calculations.

The investigations on the process of melting of phase change material in a sphere were presented by Assis et al. [37] experimentally and numerically. A parametric study was given to examine the effect of sphere diameters (40, 60 and 80 mm) and various wall temperature values (2℃ to 20℃) on the melting process of paraffin wax. During the melting process, they observed the natural convection in the melted region, volumetric expansion because of melting, close contact melting and the dipping of solid material into liquid material. The analysis was presented in the form of dimensionless numbers and the melt fraction of phase change material. They concluded that the melting process of phase change material had significant effect of the temperature difference (between wall temperature and bulk temperature) and the diameter of the sphere. They compared the numerical predictions with the experimental data and found a good agreement between them.

The effect of natural convection on solidification of lead was investigated experimentally by Szekely and Chhabra [38] and compared with numerical predictions. They observed the shape and the movement of solid-liquid interface in the domain. During the solidification process, they found a reasonable shape and position of interface that could be predicted by

considering the theory of natural convection and it confirmed the presence of natural convection process in the melted region. They also found that the natural convection had significant effect on the solid structure formed and on its floatability.

The experimental and numerical studies on the effect of natural convection on conjugate thermal characteristics of liquid and melting performance, during the melting process of phase change material, were presented by Mansour [39]. The water was considered as a heat carrier fluid and the paraffin wax was chosen as phase change material for the analysis. He conducted a parametric study by considering the combinations of two inlet temperature values and two inlet velocity values. He determined the temperature values in the domain, the Nusselt number, melting fraction and time required for complete melting of phase change material. He found some irregular thermal behavior of the fluid during the melting process of phase change material. He concluded that this inconsistency in the temperature values was because of natural convection process. He observed the high values of Nusselt number at some regions and also the rapid decrease in it at certain regions in the channel considered. He also demonstrated that the natural convection increased the melting rate in phase change material. Among all the cases he considered, the case of lowest inlet velocity and highest inlet temperature resulted in drastic decrease in the melting time of phase change material. He also reported a good agreement in between the predicted values and the data obtained from the experimental work.

A numerical study was conducted by Tan et al. [40] to investigate the effect of natural convection on the storage characteristics of latent heat storage system embedded with fins and spiral fillers. A paraffin wax with moderate melting temperature was considered and the enthalpy-porosity technique was adopted to carry out the analysis. They calculated the

melting fraction, the temperature and the velocity due to the natural convection in the molten phase change material. They found that the natural convection effect was suppressed at start because of adding more fins in the phase change material later on the natural convection increased the melting rate of phase change material. They reported that the natural convection currents were supported by spiral fillers and it resulted in improved melting performance than the case of using fins. They recommended the addition of spiral fillers was the best method to enhance the heat transfer rate in latent heat storage system.

Natural convection process inside the pipe was also studied experimentally by Martini and Churchill [41]. The halves of cylinder were set at different temperature values. The temperature and velocity of air inside the cylinder was measured to calculate the rate of air movement inside and heat transfer rates. The rate of circulation of air inside the cylinder was reported to increase initially with increasing temperature difference and then decreased when this difference became large. The local heat transfer coefficient was also reported to increase in angular direction of pipe, but this increase was small with wall temperature difference. The Nusselt number was remained almost constant. A numerical solution was also described to compare the results with experimental measurements and they found these results were in a good agreement.

The study on melting process with natural convection inside an enclosure was presented by Jany and Bejan [42] by adopting the method of scaling. The square enclosure, heated from sides, was considered in the study. The study was divided into 4 stages; 1^{st} was the pure conduction heat transfer, 2^{nd} was the mixed conduction and the convection heat transfer, 3^{rd} was the pure convection heat transfer and the last was the dipping of solid part into liquid. In the first three stages, they observed the variation of Nusselt number with

time resembling to a van der Waals isotherm and in the fourth stage the solid part was vanished. They also conducted a simulation based study to verify the predictions made previously. They obtained a correlations for Nusselt number and melting front as a function of time by combining the theory predictions and numerical part.

An experiment was conducted by Webb and Viskanta [43] to investigate the natural convection effect on the melting process of phase change material contained in an inclined rectangular shape. They demonstrated that the due to the inclination, a 3D flow field was developed by natural convection which resulted in no-uniform melting of phase change material. They found the initial solid subcooling and the angle of inclination had significant effect on the developed flow field. They presented a correlation between transient variations in the liquid fraction and the angle of inclination. A numerical study was also presented by them to verify the experimental findings.

The melting and the solidification processes of phase change material were investigated by Lamberg et al. [44] experimentally and numerically. In the numerical part, they adopted the effective method and the enthalpy method and carried out calculations by using FEMLAB software. The technical grade paraffin was considered as a phase change material. They transient temperature variations were measured in the domain and compared these results with the numerical predictions. They reported to achieve a good agreement in between them. They also reported that the natural convection was the influential parameter for the process of melting of phase change material because they observed that the less time was required for melting of phase change material when the natural convection was included than the case of without natural convection involvement.

2.3 Volumetric Solar Absorber

Volumetric solar absorbers are the focus area now a day to cultivate the solar energy efficiently. The absorption of solar energy includes heat losses which consequently lowers the system efficiency. One of these losses is emissive heat energy loss which occurs due to large temperature difference in absorber and fluid. To minimize these kinds of losses, temperature distribution in the system should be made uniform. Many studies have been conducted to improve the absorption process of solar energy.

A numerical study on nanofluid volumetric solar absorber was conducted by Lenert and Wang [45] by considering a 1 dimensional problem to estimate the effect of solar concentration, optical thickness and height of nanofluids on thermal performance of the system. They also validated the numerical predictions by conducting an experiment in which the Therminol with suspended carbon coated cobalt particles was used. Their experimental study was in good agreement with numerical study. Their parametric study concluded that the efficiency of the system increased with increase in solar concentration and nanofluid height. They also predicted that the efficiency could be increased to 35 % by using nanofluids volumetric absorbers combined with power cycle and adjusted according to the solar time exposure.

The analytical model of volumetric solar absorber was developed by Veeraragavan et al [46] to investigate the effect of different parameters like height of the channel, heat losses and solar concentration on the efficiency of the absorber. Volumetric receiver with Therminol VP-1, as a heat transfer fluid, along with suspended particles of graphite was taken to carry out the analysis. They also considered the surface heat losses like the convective heat loss and the radiative heat loss in the study. The system performance and

the temperature profile were investigated by variation of different dimensionless numbers. They determined the optimized length of the receiver, by coupling receiver efficiency with ideal power cycle efficiency, at which the combined efficiency of the system was maximized. Their results indicated the dependence of maximum temperature on surface heat loss Nusselt number. They found the maximum efficiency of system 35 % at receiver dimensionless length of 0.86 and at the Nusselt number equal to one. The solar flux and the Nusselt number were found as the system efficiency controlling parameters.

A numerical model of solar absorber, composed of with mixture of water and aluminum nanoparticles, was presented by Tyagi et al. [5]. The performance of the system was examined as a function of geometric configuration of geometry, nanoparticle size and volume fraction. A comparison, in terms of efficiency, of the volumetric solar absorber with flat plate collector was also given in the study. The effect of the dispersion of nanoparticles into the fluid and the absorption was observed. They reported that the absorption was increased by 9 times with nanoparticles than in case of the using pure water. The efficiency of the collector was reported to increase with glass transmissivity, volume fraction of suspended particles and height of the receiver. While making the comparison, 10 % higher efficiency of the solar collector with nanofluid was observed than the conventional flat plate collector.

A numerical investigation of volumetric solar air receiver to observe the temperature profile in the fluid was carried out by Zhiyong Wu et al. [47]. The solid ceramic foam was used as an absorber in the study. While calculating the solution, they also accounted the pressure drop associated with metal foam and the heat transfer between the solid foam and the flowing fluid over it. Validation of their numerical predictions with the previous

experimental study was also given. They observed the effect of inlet velocity, porosity of foam, thermal conductivity of solid and cell size on temperature profile. They demonstrated that the material properties and working conditions have effect on temperature profile and at steady state condition, thermal conductivity of solid phase absorber had no significant effect on performance of volumetric solar receiver. They also concluded that mean cell size has foremost effect on temperature profile among all other tested parameters.

A similar work was presented by Wu et al. [48] to understand the phenomenon of convective heat transfer between ceramic foam and air flow passing by it. They solved the equations of flow inside the foam and energy balance simultaneously to carry out the analysis. They observed the effect of porosity, inlet velocity and mean cell size on heat transfer coefficient. Based on the obtained results, they developed a correlation for volumetric heat transfer coefficient between the ceramic foam and air, which was true for various values of velocities, temperatures, cell sizes and porosities. By comparing the obtained numerical results with experimental data from literature, they observed a good agreement between the predictions and experimental data.

The thermal characteristics of solar volumetric latent energy storage system were investigated by Osman and Yilbas [49] numerically. They considered the Lauric acid as an energy storage medium and the water as a heat transfer fluid for the analysis. They carried out the parametric study by changing the locations of absorber plate (top, middle and bottom of channel), the Reynolds number values and the solar concentration values. They found the highest thermal performance of the system by locating the absorber plate at the top surface of channel. In addition to that increasing Reynolds number and solar concentration also improved the thermal response of the system, reported by the authors.

They also considered the pump losses, which may occur in the system, in their analysis and found the maximum losses with the absorber plate placed at middle position of channel.

An numerical investigation of radiation attenuation in volumetric solar absorber was conducted by Fabrisio et al. [50] using Monte Carlo ray-tracing method. They considered a stack of multichannel monoliths, with square cross section, as an absorber of incident radiations. The effects of optical properties of surface, geometric configuration and incident radiation profile on the system were considered for the analysis. They demonstrated that the optical efficiency was maximized at large monoliths layers and large spacing between these layers. It was also found that the attenuation length increased with the increase in spacing distance and was maximum for longer element. However due to change in the relative positions between elements, the losses in proposed system were increased than classical multichannel system at the constant pitch size.

The effect of channel depth on the performance of solar air heater was described by Sun et al. [51] numerically. The study was carried out by using CFD method, in which laminar and turbulence models were assumed to calculate the flow and temperature profiles in the solar air heater. Their study revealed a great influence of the channel depth on the performance of the solar air collector. They recommended the channel height equal to 10 mm as the best height for the performance of solar air collector. However with selective coating surface, it was required to maintain a suitable distance between absorber plate and glass to avoid the convective losses. The minimum distance recommended by them was 20 mm to avoid the losses. They also described that with the increased inlet temperature and the decreased flow rate of air, the efficiency of the system reduced. Also the best performance of solar air heaters, with black coated absorber surface and with selective

surface, was reported at temperature difference (between inlet temperature and ambient temperature) of 50 K.

Thermal analysis of volumetric solar absorber with multichannel configuration was carried out by Lee et al. [52]. A one dimensional model with convective, conductive and radiation was presented by using Monte Carlo ray-tracing method. The effect of geometry dimensions and material properties, on the system performance, was investigated. The study showed that the maximum solar radiations were absorbed at the smaller length of channel, which was equal to 15 mm. It was also reported that at low absorptivity, the collector efficiency was low because of high reflection losses. Also the increase in emission losses was reported with increase in radius or decrease in mass flow rate and these losses were maximum in case of the model considered.

2.4 Effect of rotation on thermal performance of the system

The rotation of cylinder provides uniform heating inside lowering the difference between maximum and minimum temperatures.

A numerical study of natural convection inside the rotating cylinder was conducted by Hasan et al. [53] to examine the effect of rotation on thermal performance of the system. The cylinder walls were heated periodically and rotation of the cylinder was along the axial direction. They adopted finite difference method to solve the governing equations and carried out the analysis with the dimensionless numbers like Rayleigh number, Taylor number and Prandtl number. They fixed the value of Prandtl number to 0.71 and gravitational Rayleigh number equal to $10^{5.}$ The rotation speed was set enough that the gravity effect was very small as compare to the Coriolis effect due to rotation. They

demonstrated that the convection induced inside fluid had significant of Coriolis forces. Also the centrifugal force affected the convection inside the domain.

The effect of rotation on convective heat transfer inside the cylinder was presented by Seghir-Ouali et al. [54] experimentally. They heated the outside cylinder walls with infrared lamp and three different methods were adopted to observe the heat transfer inside. The cylinder was rotated at speed from 4 to 880 rpm with Reynolds numbers 10^3 to 10^5 and air flow rate was set varied from 0 to 530 m^3 per hour. They found that the heat transfer rate had significant effect of rotational speed and air flow rate. They reported that the heat transfer rate had very strong effect of rotation and negligible effect of air flow rate at high rotational speeds. They also presented two correlations of Nusselt number for low rotational speed values and high rotational speed values.

An experiment study of natural convection inside the rotating cavity was conducted by Abell and Hudson [55] to investigate the effect of rotation on convection inside. They carried out analysis in a rectangular cavity with dimensions equal to 27.94 cm length, 2.54 cm width and 2.62 cm height and it was rotated at speed equal to 565 rev/min along its vertical axis passing through the center. They selected fluids with Prandtl number varying from 7 to 3000 and provided the heat to cavity from top surface and cooled from bottom side. They observed the Nusselt number value for each type of fluid and found variation in it with power of 0.4 of temperature difference applied, for the fluids having low Prandtl number and with power of 0.25, for the case of high Prandtl number fluids. Also the effect of rotation speed on temperature gradient was observed to be independent of the rotational speed.

The heat transfer characteristics inside the rotating cylinder was presented by Song et al. [56] experimentally. They selected two cylinder; one of them was of straight walls shape and second was tapered from inside. The cylinders were rotated at 4000 rev/min and was filled with water as working fluid inside. The effect of rotational speed, pipe geometry and working fluid loading on the thermal performance of the system was given. They found that the pipe geometry had significant effect on heat transfer process inside the fluid. Also the heat transfer rate was reported to increase with rotational speed. Upon comparison of the obtained results and previous findings, they found that the natural convection effect showed more prominent on heat transfer process at high rotation speeds.

The effect of rotation on flow field and heat transfer rate inside the cylinder was presented by Reich et al. [57]. They assumed a cylinder rotating about its central axis and examined the effect of rotational speed on temperature profile inside the fluid, coefficient of friction and heat transfer rate inside the fluid with and without natural convection effect. They found that the rotation of cylinder provided the disturbed fluid inside which resulted in turbulence and increase in heat transfer rate. They also found that the natural convection effect was suppressed by the high rotational speeds at small heat flux values. They compared their results with experimental data and found a good agreement between them.

An experimental study was presented by Song et al. [58] to investigate the rotation effect on heat transfer mechanism in pipes rotating at high speeds. They adopted a modified Nusselt film technique to carry out the analysis. They found that the effect of natural convection was significant at high rotational speeds. They reported that the heat transfer rate was higher at high rotational speeds because of turbulence effect inside the fluid. They also investigated the effect of fluid loadings on heat transfer process and found no

significant effect on it. They compared the obtained results with the previous study and found good agreement between them.

The heat transfer enhancement on a cylinder was investigated by Cheng et al. [59] experimentally. The cylinder was heated with a wire heater around it and the air was flown at maximum speed of 20 m/s over the heated cylinder. They calculated the Nusselt number values for different rotational speeds. They demonstrated that the heat transfer coefficient was affected by the stream flow produced by the rotation. This effect of rotation on heat transfer coefficient was higher in case of high rotational speed and low Reynolds number value, reported by the authors. They also reported that the heat transfer rate was increased due to mixing phenomenon induced by the rotational effect.

CHAPTER 3

PROBLEM DESCRIPTION AND MATHEMATICAL MODEL

A transient model for all the cases is presented in this thesis and the mathematical formulations and problem descriptions, for all the cases, are given here in this section. The study is divided into five different cases. In first two cases, the water is considered for testing of thermal performance of the model, and then the phase change material is introduced for the other cases. The mathematical model for each case along with its problem definition is presented below.

3.1 Mobile Thermal Battery

The mobile thermal batteries can be designed and possibly be used for the heating and cooling applications. The energy can be stored into them and can be moved to other place for utilization of stored energy. In this work, a mobile thermal battery, with metallic meshes inside, is considered. The cross section of thermal battery is shown in figure 3.1.

3.2 Heating Profile

The solar flux in all cases is taken as the solar flux magnified by the parabolic trough [60]. The heat profile is the function of the angle, as at half portion of the tube the direct solar flux is applied and at the other portion, facing toward the trough, the concentrated solar flux is applied. The schematic profile is shown in figure 3.2.

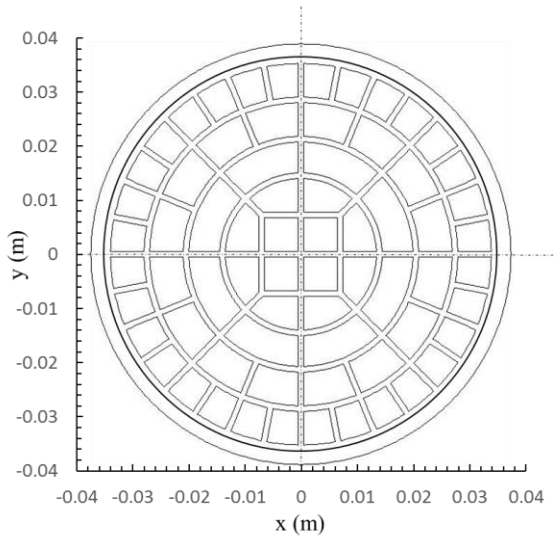

Figure 3.1 Schematic view of Mobile Thermal Battery

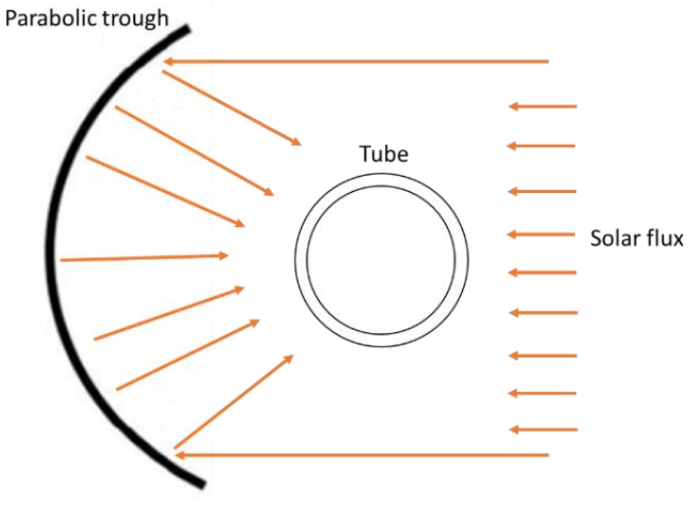

Figure 3.2 Schematic of concentrated solar flux around the tube.

3.3 Water as Working Fluid without Rotation of Thermal Battery

The transient analysis inside the steel tube subjected to solar concentrated heating is carried out. The aluminum meshes are introduced inside the tube and flow field developed due to buoyancy driven flow during density variation of water is simulated. The governing

equations for heat transfer and natural convection inside the tube due to solar concentrated heating include the continuity, momentum and energy equations, which are given below.

The continuity equation is:

$$\vec{\nabla}.\vec{V} = 0 \tag{3.1}$$

The momentum equation is

$$\frac{\partial\left(\rho\vec{V}\right)}{\partial t} + \vec{\nabla}\cdot(\rho\vec{V}\vec{V} - \mu\nabla\vec{V}) = \vec{g}\rho\beta(\mathrm{T}-\mathrm{T}_{\infty}) \tag{3.2}$$

The energy equation is

$$\frac{\partial(\rho c_p \mathrm{T})}{\partial t} = \vec{\nabla}.(k\nabla T - \rho\vec{V}c_p \mathrm{T}) \tag{3.3}$$

Here c_p is specific heat, ρ is density, $\vec{V}$ is velocity, g is gravitational acceleration, β is coefficient of thermal expansion, κ is thermal conductivity and T is temperature.

The thermal properties of water and aluminum mesh is presented in table 3.1 below.

3.3.1 Initial Conditions

Initially water has uniform temperature and it is in temperature equilibrium with the tube material. In addition, water is considered to be stagnant inside the tube initially, which is:

At t = 0

T = 298 K , u = 0 , v = 0

3.3.2 Boundary Conditions

The solar flux is applied at the surface of the steel tube according to the profile given in figure 3.3, which resembles the solar concentrated heating [60]. At steel pipe walls and meshes, no slip boundary conditions are assumed. Temperature and flux continuity are

incorporated at the surface between water and aluminum mesh. The density variation of fluid with temperature is taken according to Boussinesq approximation. Water is used as working fluid and aluminum is incorporated as the mesh material.

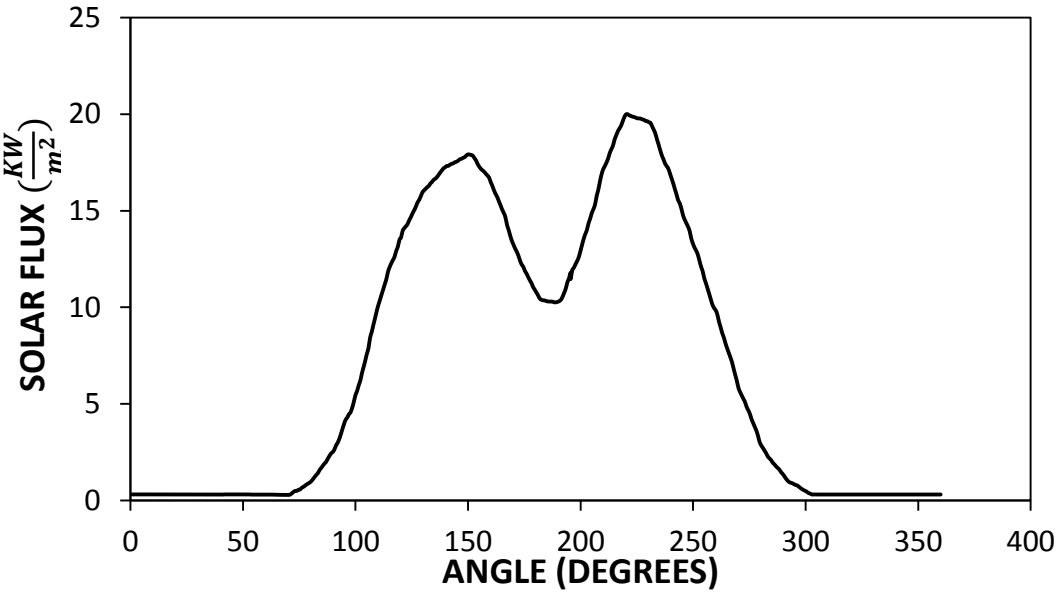

Figure 3.3 Solar flux resembling the trough and incident onto the tube, which is used to simulate the heat transfer [60].

3.4 Rotation of Thermal Battery and Water as Working Fluid

A circular steel tube with presence of aluminum meshes and water as working fluid are incorporated to resemble the thermal battery. Figure 3.4 shows the schematic view of the cross-section of the thermal battery. Since the thermal battery is considered to rotate along its symmetry axis at the trough centerline, a transient analysis of a rotating cylinder with a constant angular velocity ω in counter clockwise is introduced. In the analysis, the total heating duration of the thermal battery is constant for all the rotational speeds, so the energy input remains same for all cases. The rotational speeds of the thermal battery are adjusted in such a way that the thermal battery completes the total revolutions in this time (t = 540 s). The working fluid is assumed to be homogeneous and flow developed inside the thermal battery because of the fluid density variation, and the Coriolis and centripetal accelerations

developed during rotation is modelled. The governing conservation equations for the case of rotation, describing the heat transfer process and fluid flow inside the domain, are given below:

Continuity equation:

$$\vec{\nabla}.\vec{V} = 0 \tag{3.4}$$

Momentum equation:

$$\frac{\partial\left(\rho\vec{V}\right)}{\partial t} + \vec{\nabla}\cdot(\rho\vec{V}\vec{V}) + \rho(2\vec{\omega}\times\vec{V} + \vec{\omega}\times\vec{\omega}\times\vec{r}) = \vec{g}\rho\beta(\mathrm{T}-\mathrm{T}_{\infty}) + \vec{\nabla}\cdot(\mu\vec{\nabla}\vec{V}) \tag{3.5}$$

The momentum equation includes Coriolis acceleration and centripetal acceleration terms in left hand side of equation which describes the rotational effect on flow. The flow developed is assumed as laminar flow in the study.

Energy equation

$$\frac{\partial(\rho c_p \mathrm{T})}{\partial t} = \vec{\nabla}.(k\vec{\nabla}T - \rho\vec{V}c_p \mathrm{T}) \tag{3.6}$$

Here c_p is specific heat, ρ is density, $\vec{V}$ is velocity, g is gravitational acceleration, β is coefficient of thermal expansion, κ is thermal conductivity, ω is angular velocity and T is temperature.

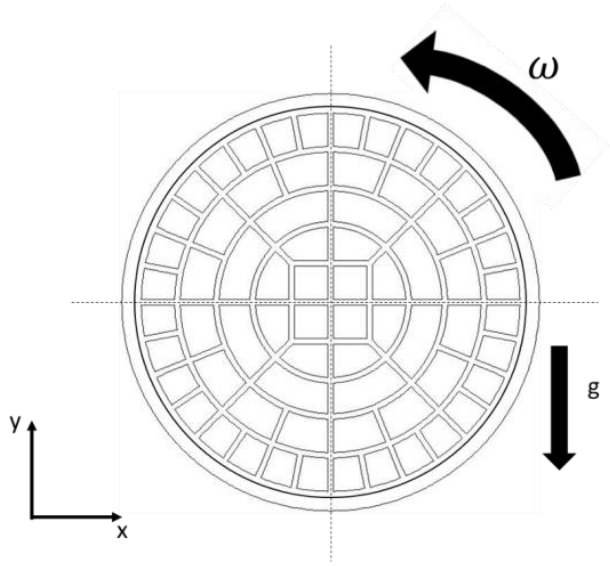

Figure 3.4 Rotational direction and gravity field.

3.4.1 Initial Conditions

The working fluid (water) is considered to be stationary inside the tube initially at uniform temperature. The solution is initialized with following appropriate conditions:

At $t = 0$

T = 298 K , $u = 0$, $v = 0$

3.4.2 Boundary Conditions

At start the standard temperature is set which is 298 K. The solar flux is applied at boundary of steel pipe according to the profile obtained from the field data [60]. The solar power intensity distribution along the outer surface of the thermal battery is shown in figure 3.5. At walls of steel pipe and wire, no slip conditions are assumed. The properties of fluid are assumed constant except density which is function of temperature. The density variation with temperature is taken according to Boussinesq approximation.

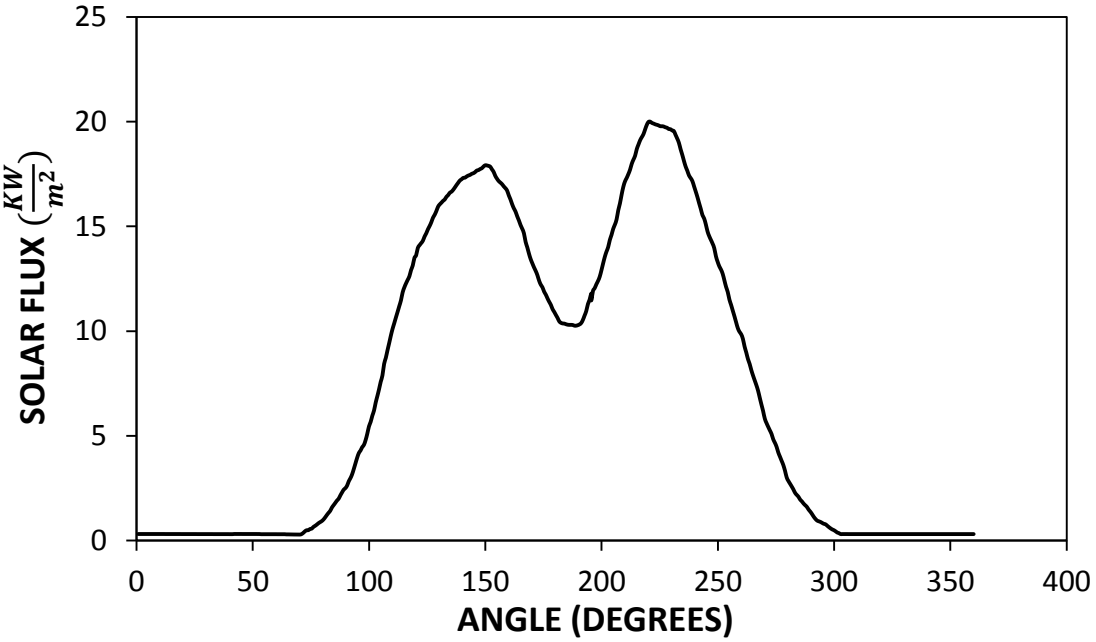

Figure 3.5 Concentrated solar flux, which is incident onto the thermal battery outer surface and used in the simulations [60].

3.5 Thermal Performance of the System with Phase Change Material ($LiNO_3$)

In this case, the analysis of heat transfer and flow field pertinent to a thermal battery consisting of the steel tube, the phase change material the metallic meshes as shown in figure (3.6). Lithium nitrate ($LiNO_3$) is considered as phase change material and aluminum is incorporated as the mesh material. Table 3.2 gives the data used in the simulations for this case. The phase change material is assumed to have uniform properties. The natural convection flow and heat transfer are also incorporated in the liquid phase of the phase change material. The density change in taken by considering the Boussinesq approximation. The flow developed inside the liquid region is assumed as laminar flow. The governing equations are described below:

The continuity equation is

$$\vec{\nabla}.\vec{V} = 0 \tag{3.7}$$

The momentum equation is

$$\frac{\partial\left(\rho\vec{V}\right)}{\partial t}+\vec{\nabla}\cdot(\rho\vec{V}\vec{V}-\mu\vec{\nabla}\vec{V})=\vec{g}\rho\beta(\mathrm{T}-\mathrm{T}_{\infty})+S \tag{3.8}$$

The energy equation is

$$\frac{\partial(\rho H)}{\partial t}+\vec{\nabla}.(\rho\vec{V}\,\mathrm{H})=\vec{\nabla}.(k\vec{\nabla}T) \tag{3.9}$$

Here H is the total enthalpy of the fluid which is sum of sensible enthalpy and latent enthalpy:

$$H=h+\Delta H \tag{3.10}$$

Where ΔH is latent enthalpy and h is sensible enthalpy which is computed as follows:

$$h=h_{ref}+\int_{T_{ref}}^{T}c_p dT \tag{3.11}$$

Here h_{ref} is the reference enthalpy, T_{ref} is the reference temperature and c_p is the specific heat.

The S is the source term which is added in equation (3.8), as the mushy zone is treated as porous media, and it can be written as:

$$S=\frac{(1-\gamma)^2}{(\gamma^3+c)}A_{mush}\vec{V} \tag{3.12}$$

In above term, A_{mush} is the mushy zone constant which defines the melting front, c is the computational constant, γ is the liquid fraction and $\vec{V}$ is the velocity. The values of A_{mush} and c are taken equal to 10^5 and 0.001, respectively.

The liquid fraction γ is computed as follows:

$$\gamma = \begin{cases} 0 & T < T_{solidus} \\ \dfrac{T - T_{solidus}}{T_{liquidus} - T_{solidus}} & T_{solidus} < T < T_{liquidus} \\ 1 & T > T_{liquidus} \end{cases} \tag{3.13}$$

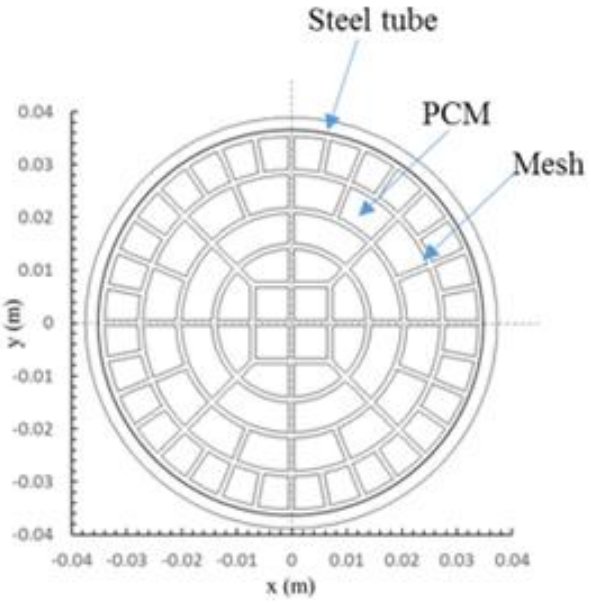

Figure 3.6 Schematic view of model (With PCM case).

3.5.1 Initial Conditions

Initially the steel tube, the metallic meshes and the phase change material are considered to have uniform initial temperature. Since the phase change material is in solid state initially, no convection current flow is considered. Therefore, the initial conditions are:

At $t = 0$

$T = 298$ K ; $u = 0$; $v = 0$

3.5.2 Boundary Conditions

The concentrated solar flux is introduced around the surface of the steel tube in accordance with the solar irradiation profile reported in the early study [60], which is shown in figure 3.7.

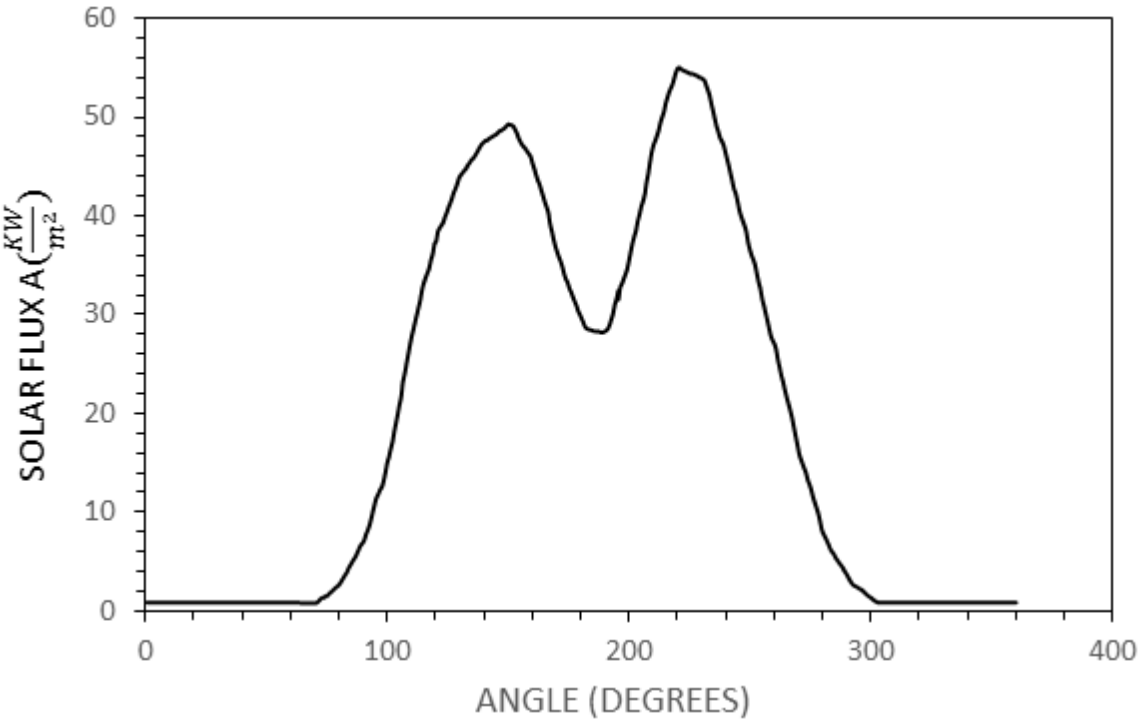

Figure 3.7 Solar flux distribution along the surface of the steel tube while resembling the solar irradiation emanating from the trough and incident onto the tube outer surface [60].

3.6 Analysis with Rotation of Thermal Battery and PCM ($LiNO_3$)

In this case the thermal battery, with metallic meshes, is assumed to be rotated at focus of parabolic trough, similar as in the water case. Figure 3.3 shows the schematic view of the cross-section of the rotating thermal battery. Again the thermal battery is considered to rotate along its symmetry axis at the trough centerline, a transient analysis of a rotating cylinder with a constant angular velocity ω in counter clockwise is introduced. In the analysis, the total duration of the thermal battery is identified in order to secure the total

energy flux received by the thermal battery remains constant for all the rotational speeds. Therefore, the rotational speeds of the thermal battery are adjusted in such a way that the thermal battery completes the total revolutions in this time (t = 4480 s).

The governing equations for this case are the same as described in the equations in previous case of PCM without rotation of thermal battery except the momentum equation in which Coriolis acceleration and centripetal acceleration terms are added in left hand side of equation which describes the rotational effect on flow.

The continuity equation is

$$\vec{\nabla}.\vec{V} = 0 \tag{3.14}$$

$$\frac{\partial\left(\rho\vec{V}\right)}{\partial t} + \nabla\cdot(\rho\vec{V}\vec{V}) + \rho(2\vec{\omega}\times\vec{V} + \vec{\omega}\times\vec{\omega}\times\vec{r}) = \vec{g}\rho\beta(\mathrm{T}-\mathrm{T}_{\infty}) + \nabla\cdot(\mu\nabla\vec{V}) + \mathrm{S} \tag{3.15}$$

The energy equation is

$$\frac{\partial(\rho H)}{\partial t} + \nabla.(\rho\vec{V}\,\mathrm{H}) = \nabla.(k\nabla T) \tag{3.16}$$

Total enthalpy *H* calculation procedure is described in equation 3.10.

The change in density is assumed according to the Boussinesq approximation and given as:

$$\rho_l = \rho_m - \rho_m\beta(T - T_m) \tag{3.17}$$

Here β is coefficient of thermal expansion and ρ_m is the density of PCM at melting point. Again the flow developed inside the liquid region is considered as laminar. The temperature dependent properties of PCM ($LiNO_3$), aluminum mesh and outer steel tube are given in table 3.2.

3.6.1 Initial conditions

The battery is assumed to be stationary at start and PCM is considered with uniform temperature and it is in temperature equilibrium with the tube material. Assumed initial conditions are given below:

At t = 0

T = 298 K , u = 0 , v = 0

3.6.2 Boundary conditions

The solar flux is applied around the surface of the steel tube of according to the profile given in figure 3.8.

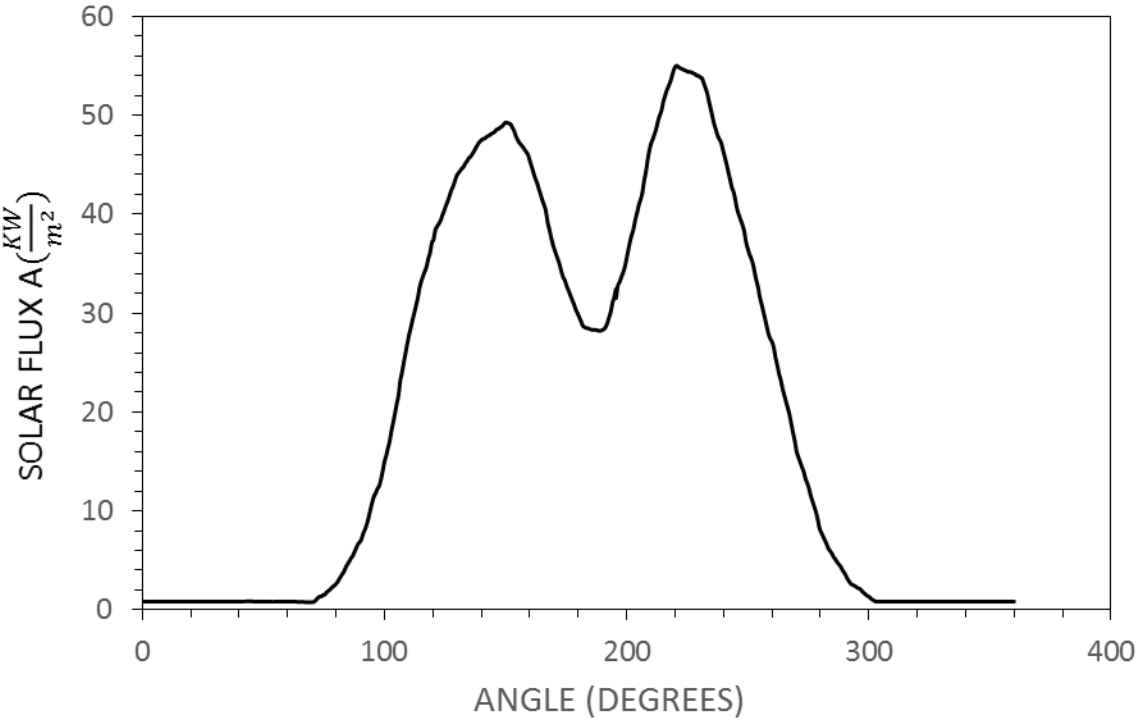

Figure 3.8 Solar flux distribution around the tube.

Table 3.1 Properties of working fluid (water), Aluminum and steel pipe

	Density (kg/m^3)	Density at T= 298 K (kg/m^3)	Specific heat (kJ/kg-K)	Viscosity (kg/m-s)	Thermal conductivity (W/m-K)	Thermal expansion coefficient (1/K)
Water	-	998	4.182	0.001003	0.56	0.000214
Aluminum	2719	-	0.871	-	204	-
Steel pipe	7897	-	0.452	-	73	-

Table 3.2 Properties of PCM (Lithium Nitrate), Aluminum and steel pipe

	Density **(kg/m^3)**	**Specific heat** **(kJ/kg-K)**	**Viscosity** **(kg/m-s)**	**Thermal conductivity** **(W/m-K)**	**Latent heat** **(kJ/kg)**	**Solidus and liquidus temperatures** **(K)**
Solid $LiNO_3$	2140	1.972	-	1.37	360	527
Liquid $LiNO_3$	1780	2.04	0.00584	0.58	-	534
Aluminum	2719	0.871	-	204	-	-
Steel pipe	7897	0.452	-	73	-	-

3.7 Performance parameters

A temperature parameter and difference in local and initial temperature, are calculated along the x and y rakes. Also the temperature values at three different locations is computed. The locations of points and rakes (along x and y axis) are shown in figure 3.9.

The temperature parameter is

$$\varphi = \frac{T - T_{in}}{T_{\max} - T_{in}} \tag{3.18}$$

Here T is local temperature, T_{in} is initial temperature and $T_{\max}$ is maximum temperature.

The temperature difference is

$$\Delta T = T - T_{in} \tag{3.19}$$

Here T is local temperature and T_{in} is initial temperature.

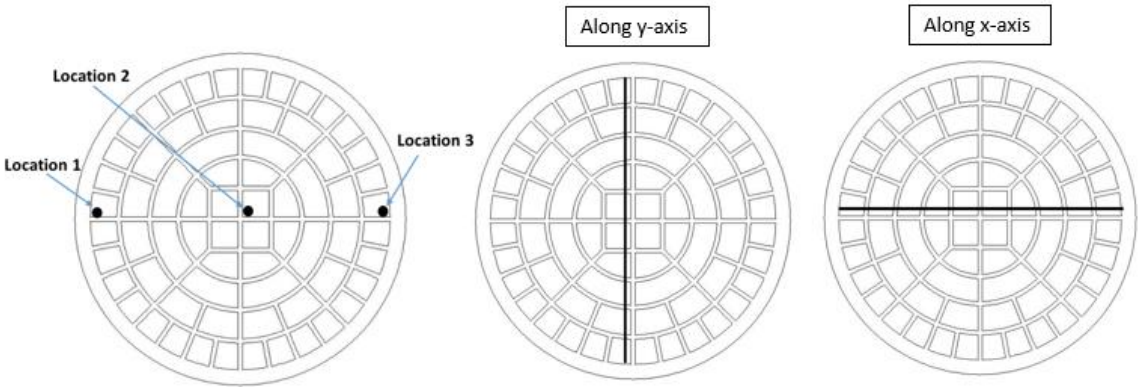

Figure 3.9 Locations of the points and rake inside the tube.

CHAPTER 4

NUMERICAL SOLUTION

This chapter provides the numerical calculation method adopted to carry out the analysis.

Fluent CFD code [61] is used to simulate the temperature and flow field in the solution domain, for all the cases. The enthalpy-porosity and VOF technique has been adopted for the cases of phase change material. Pressure based unsteady solver was chosen for computation of solution. The SIMPLEC algorithm is adopted for linkage of velocity and pressure. A control volume approach is used in the solution for discretization of equations. The discretization of pressure was carried out by PRESTO method. The 2nd order upwind method was incorporated to discretize the momentum and energy equations. The non-linear sets of equations are solved using iterative method incorporating the specified convergence criteria. The values of the residuals ($|\psi^k - \psi^{k-1}|$) for continuity and momentum are set 10^{-6} and for energy it is 10^{-10}. The convergence is ensured by setting the monitors of maximum, minimum and average temperature with time.

4.1 Grid Independence Test

A grid independent study was conducted; in which total number of cells were reduced to half approximately from the number of cells created in domain. Also the number of cells were increased approximately equal to 1.6 times the number of cells used in solution domain. The comparison can be seen in figure 4.1 below. It is clear from the figure that the increase in number of cells from current value will have no significant effect on solution but the decrease in the number of cells will affect the solution.

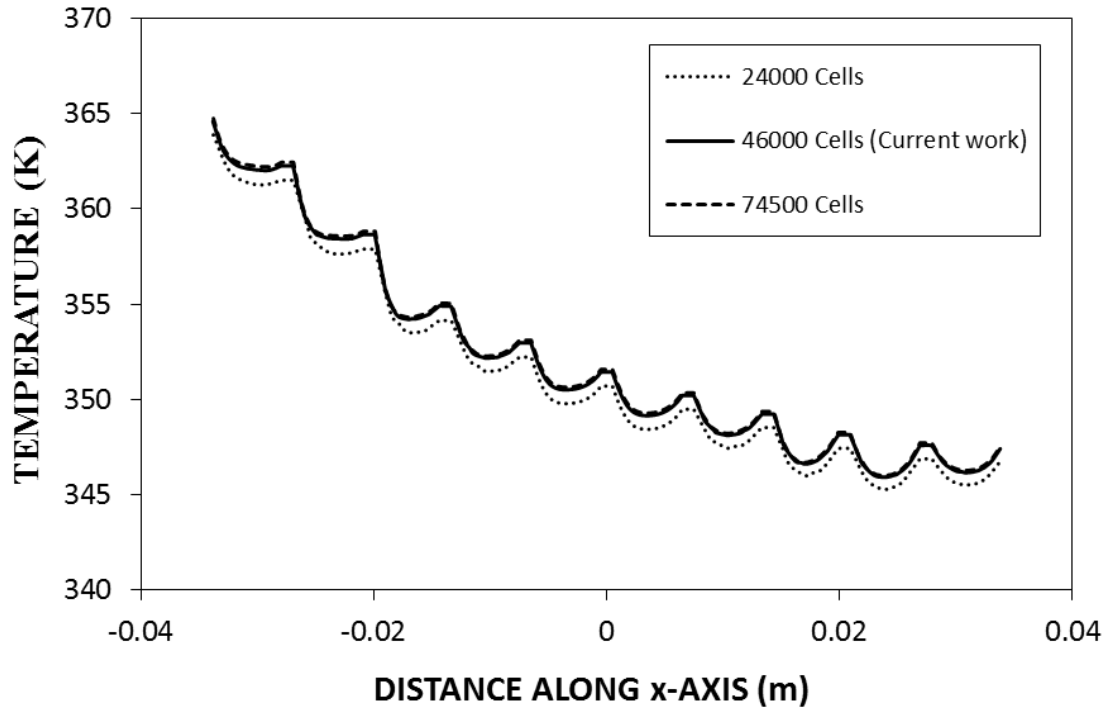

Figure 4.1 Comparison of different grids generated.

4.2 Code Validation

The validation of CFD codes was carried out by comparing the results of simulations and the data obtained from experimental work conducted by Huang et al. [62]. The problem was set exactly according to the geometry (Shown in figure 4.2) and the boundary conditions as described in [62], for comparison purpose. The porosity of the porous media was set equal to 0.975 in simulations. The temperature values, $T_{w,i}$ and $T_{a,m}$ are taken from simulation data and the heat transfer coefficient is calculated by:

$$h = \frac{q}{T_{w,i} - T_{a,m}}$$

Here q is the heat flux, $T_{w,i}$ is the inside wall temperature and $T_{a,m}$ is the air bulk temperature inside the tube. Hence the Nusselt number is calculated by using formula

$Nu = \frac{hD}{\kappa}$, in which D is the inside tube diameter and κ is the thermal conductivity of fluid inside.

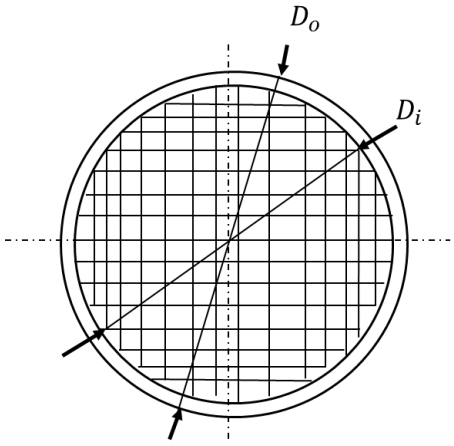

Figure 4.2 Schematic of mesh type used in experiment [62]

The Nusselt number calculated from simulation data, is compared with experimental [62] data in figure given below. The uncertainty of Nusselt number was reported equal to ± 5.93% in experimental results [62]. The average value of error, between experimental [62] and the numerical, is equal to 7.74 %. The error is associated with assumption of homogeneous properties of fluid in simulations. The comparison shows that the values are close to each other and a good agreement exists between experimental [62] and numerical values. Hence the results obtained from numerical study are satisfactory.

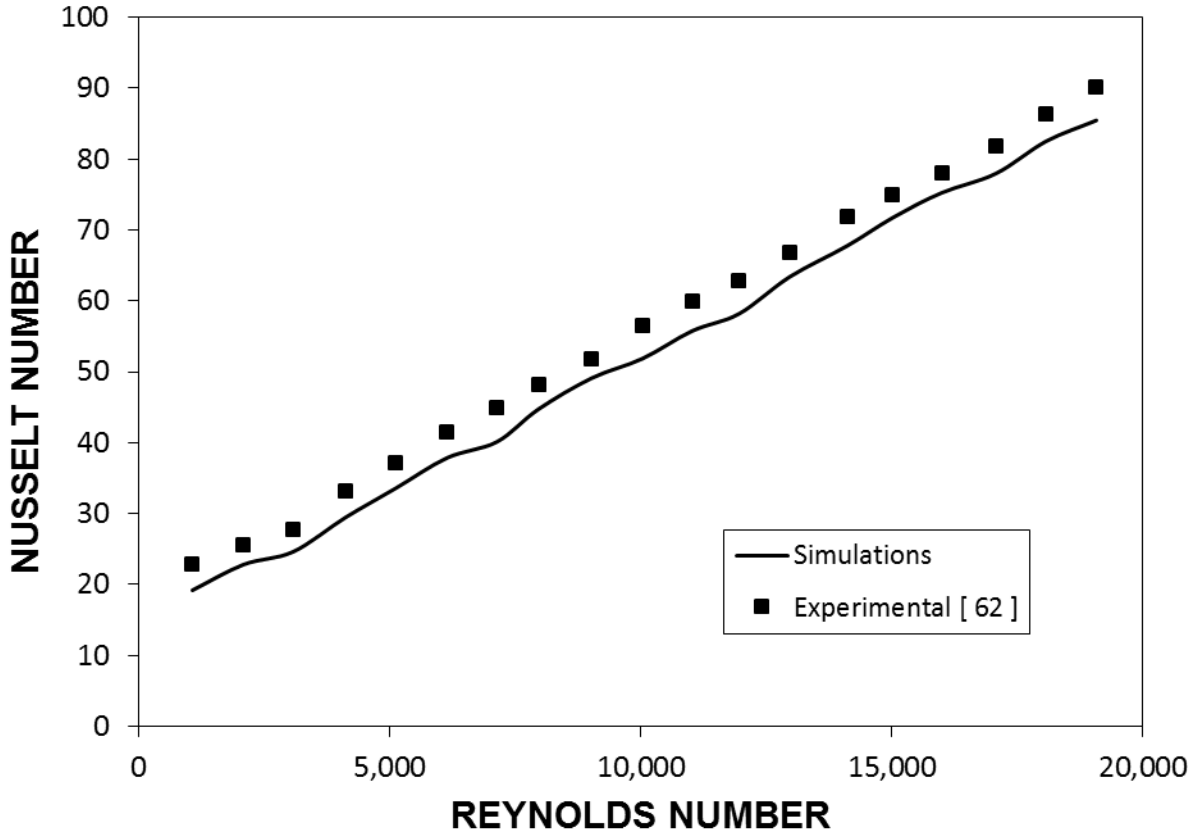

Figure 4.3 Comparison of numerical predictions with previous experimental data [62]

CHAPTER 5

RESULTS AND DISCUSSIONS

This chapter will describe the outcomes of the cases described previously. In the first two sections of this chapter, the results of the testing of the model is given. Third and fourth sections will describe the results of the case of phase change material ($LiNO_3$), with and without rotation respectively. In the last section, thermal performance of the composite of phase change material and CNT is presented.

5.1 Thermal Analysis with Water and Without Rotation Case

Solar concentrated heating of stagnant water in a circular steel tube with and without presence of meshes inside the tube is investigated. Heating conditions are simulated resembling the actual solar intensity distribution along the tube surface, described in chapter 3.

Figures 5.1 and 5.2 show temperature difference ($\Delta T = T - T_{in}$) along the rake located in the x-axis (figure 3.9) for the cases with and without meshes inside the tube while figures 5.3 and 5.4 show the contour plots of temperature distribution inside the tube for the same cases considered. The temperature difference represents the difference between the local temperature and the initial temperature of the water inside the tube. It should be noted that temperature curves are shown for two different times with and without incorporation of the natural convection effect in the simulations, respectively. Temperature difference attains large values in the near region of the high intensity irradiated wall and it reduces as the

distance increases towards the tube wall where the normal solar radiation takes place. However, temperature increases to considerably high values in water for the case of no mesh inside the tube. This is associated with the local heating of water in the near region where the high intensity thermal irradiation is received at the tube surface by the trough. Consequently, relative low thermal conductivity of water is not able to dissipate energy from the heated tube surface towards the bulk of water inside the tube. This is more pronounced for the long heating periods. The influence of the natural convection current on the temperature distribution is significant in water for the case of without mesh inside the tube. This effect is observed for both heating durations presented in figure 5.2. On the other hand, the effect of natural convection current on water temperature becomes less important at some locations along the rake where temperature remains low in the water. This region appears to be within 0.01 m away from the tube center towards the low intensity heating surface. Since the solar intensity at both sides of the tube surface is not the same, this results in temperature variation in water and alters the intensity of the natural convection current accordingly. In the case of the tube with the presence of mesh, temperature difference remains high along the rake; in which case, the maximum and the minimum temperature difference becomes smaller than that corresponding to the case without meshes inside the tube. Therefore, the meshes act like a conduction tree in the tube while enhancing the heat diffusion in water, which is true for both heating durations. However, the effect of natural convection current on the heat dissipation in water is not significant as compared to that corresponding to the without mesh case. This is attributed to: i) the presence of the meshes reduce the volume of the water occupied in the each metallic cell; therefore, convective acceleration ($V_s = V_s \frac{\partial V_s}{\partial s}$, where Vs is the velocity of

the natural convection current along the s direction) becomes smaller than that occurring in the tube without mesh case, and ii) temperature difference remains low in water inside the metallic cell while suppressing the density variation of water in the cell.

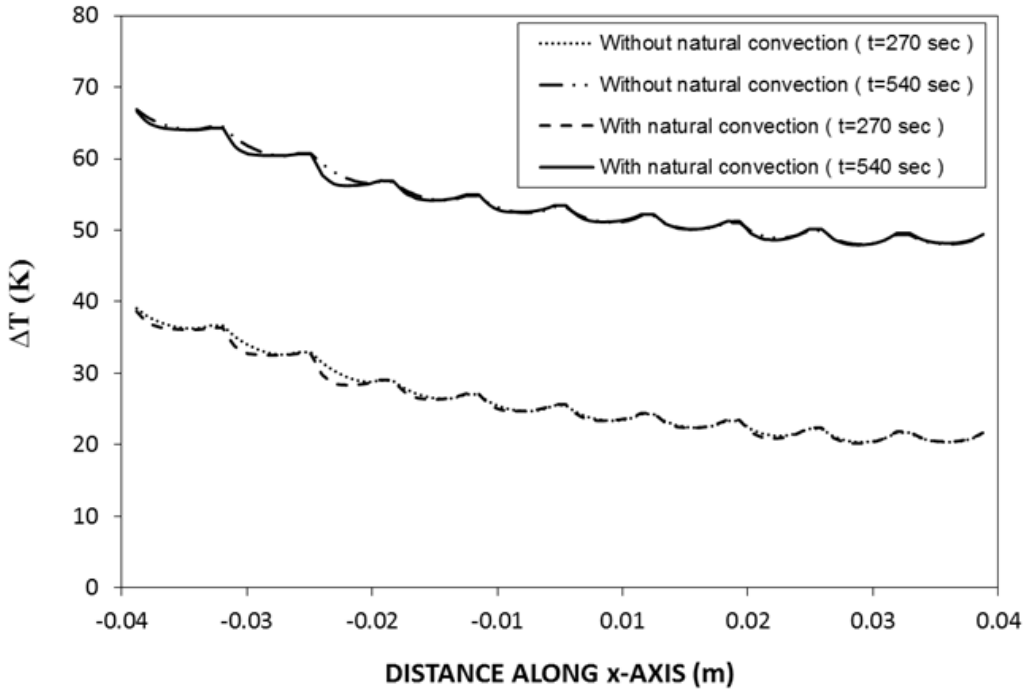

Figure 5.1 Temperature difference along the rake located in x-axis for the case of with presence of meshes inside tube.

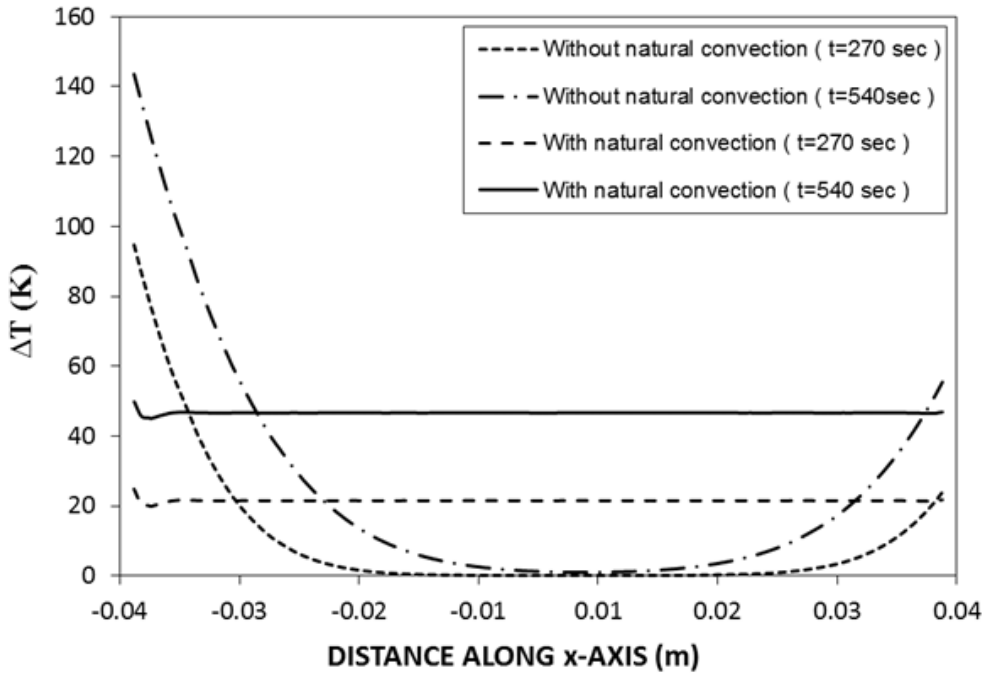

Figure 5.2 Temperature difference along the rake located in x-axis for the case of without meshes inside tube.

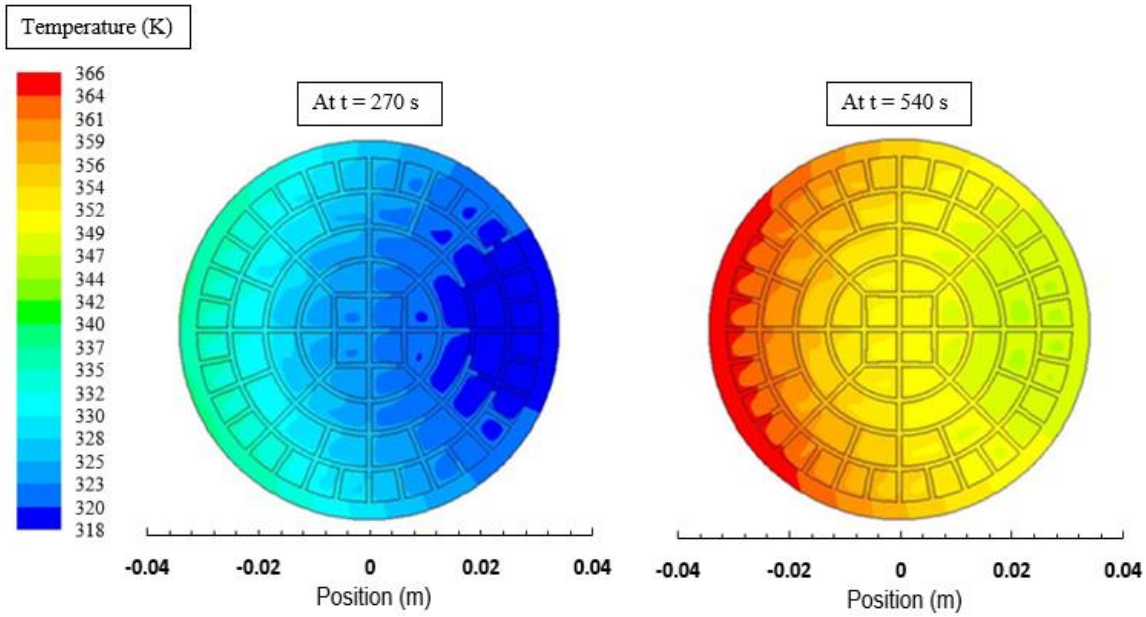

Figure 5.3 Temperature contours inside tube for the case of presence of meshes.

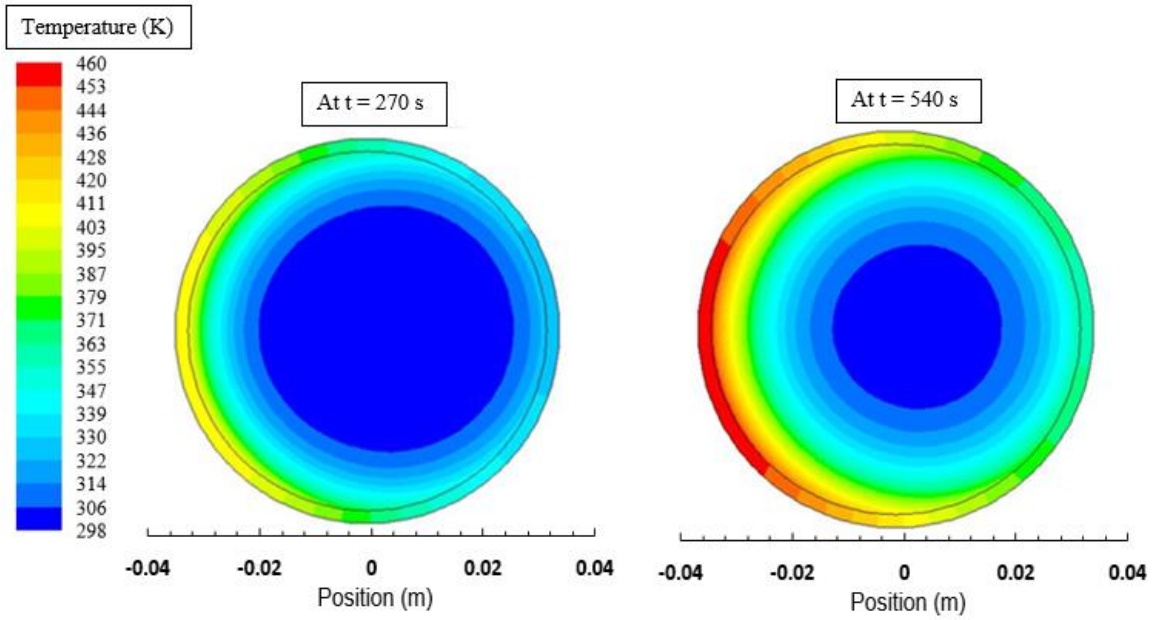

Figure 5.4 Temperature contours inside tube for the case of without meshes.

This situation can also be seen from figures 5.5 and 5.6, in which the velocity contours of the natural convection current is shown with and without meshes inside the tube. The maximum velocity is about seven times higher for the case without mesh as compared to that corresponding to the presence of the mesh case. The maximum water temperature remains extremely high in the close region of the heated side of the tube for the case of without mesh, which demonstrates the local heating of water in this region. Consequently, the use of mesh inside tube provides almost uniform heating of water inside the tube while eliminating the possible local evaporation of water inside the tube.

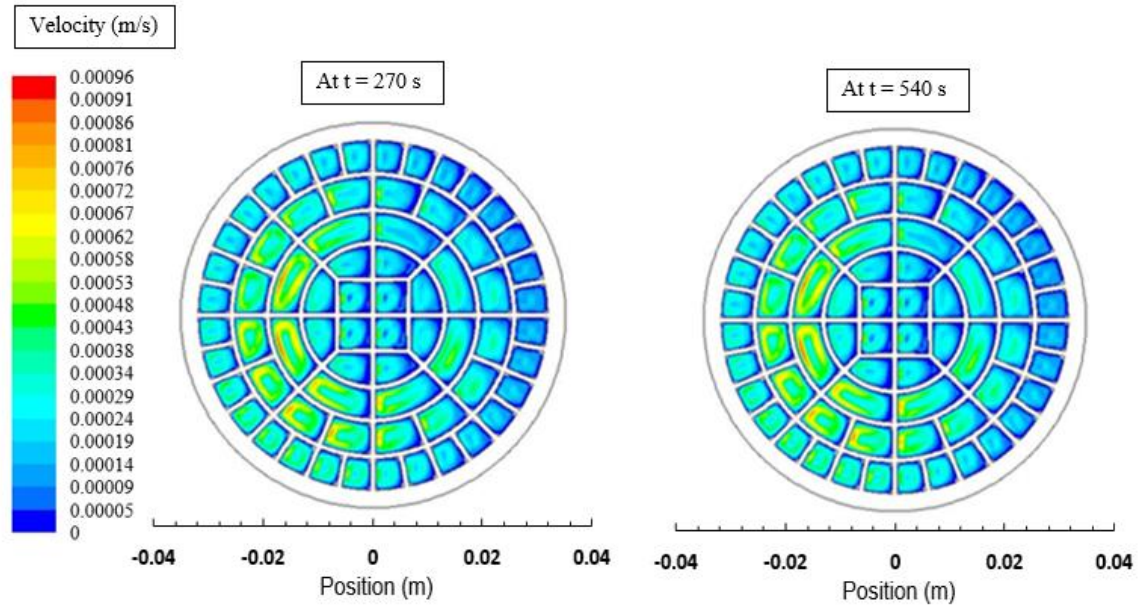

Figure 5.5 Velocity magnitude contours inside tube for the case of presence of meshes.

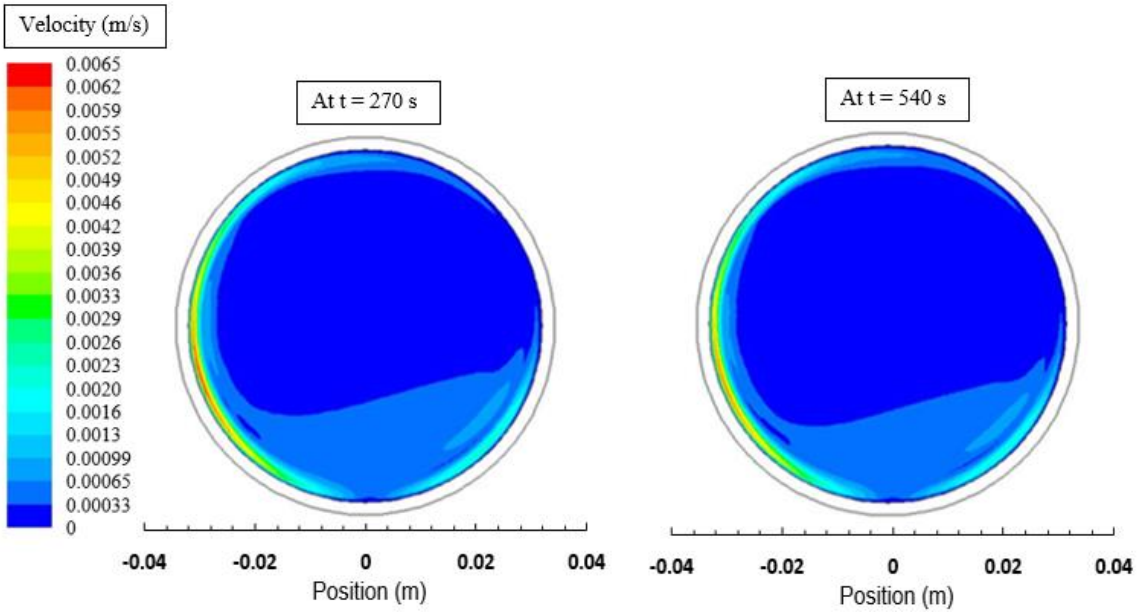

Figure 5.6 Velocity magnitude contours inside tube for the case of without meshes.

Figures 5.7 and 5.8 show temperature difference ($\Delta T = T - T_{in}$) along the rake located at the y-axis (figure 3.9) for the cases with and without the presence of the meshes inside the tube, respectively. Temperature difference behaves similar to that shown in figures 5.1 and 5.2 for the x-axis variation, provided that the value of temperature is less for the case, which

corresponds to the rake along the y-axis. This behavior is related to the heat conduction along the y-axis, since the temperature difference at the top and bottom locations on the surface of the tube due to solar irradiated power is almost the same. Therefore, the diffusion along the y-axis due to heat conduction in water inside the tube is responsible for the temperature distribution along the rake located in the y-axis.

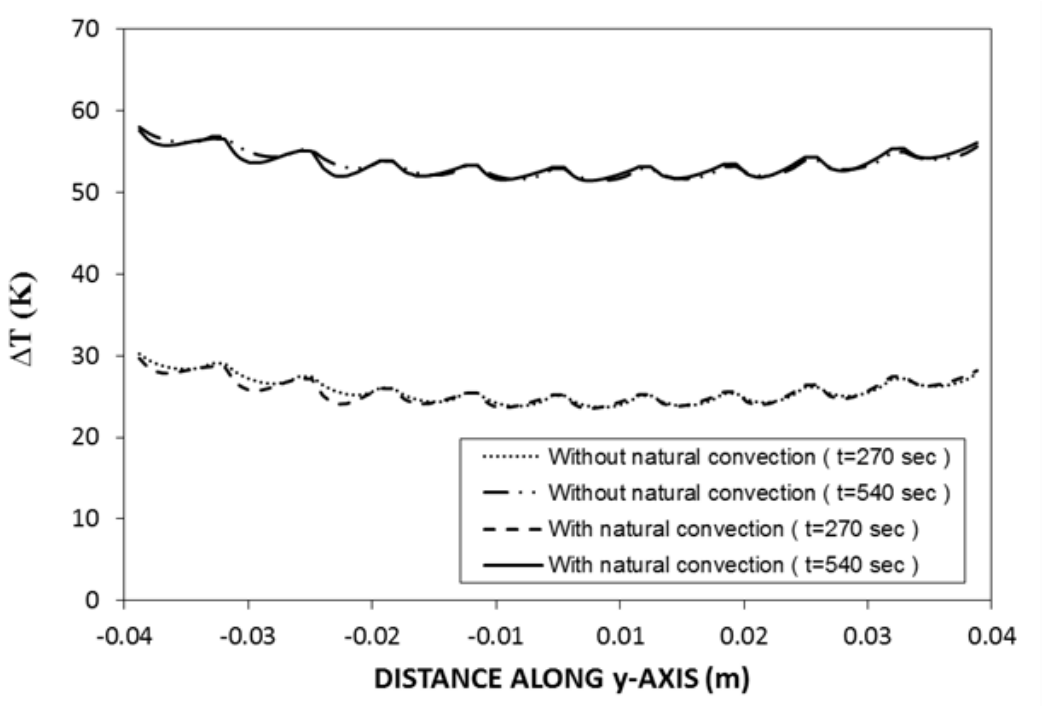

Figure 5.7 Temperature difference along the rake located in y-axis for the case of with presence of meshes inside tube.

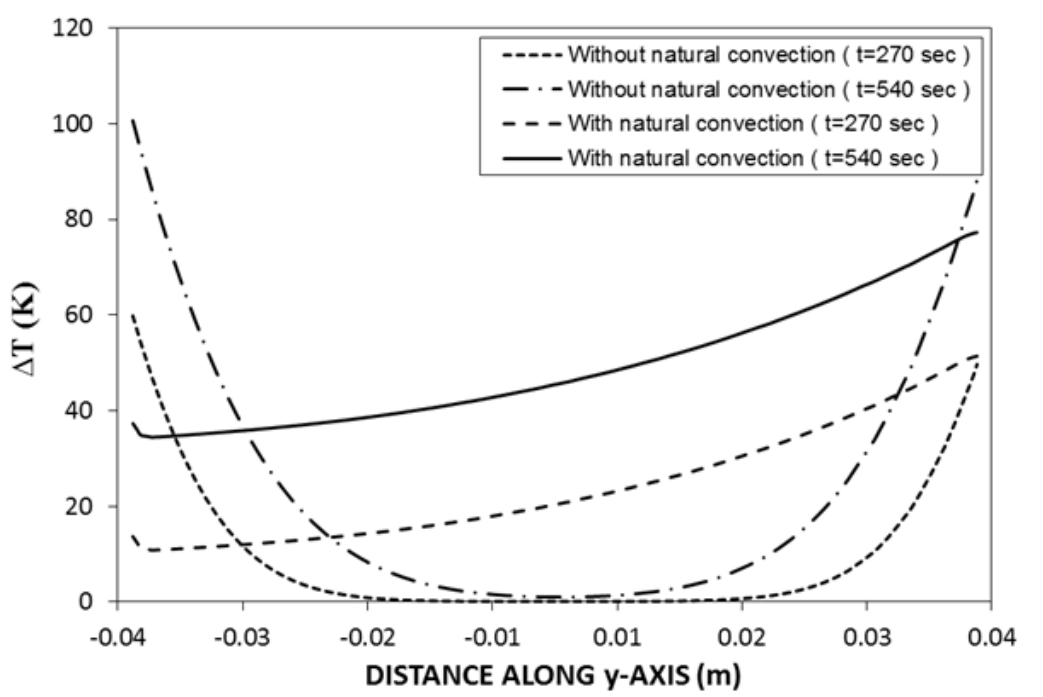

Figure 5.8 Temperature difference along the rake located in y-axis for the case of without meshes inside tube.

Figures 5.9 and 5.10 show temporal variation of temperature at three locations (figure 3.9) inside the tube for the cases of with and without meshes inside the tube, respectively. Temperature rise shows a parabolic rise at location 1 because of the high rate of heat input as a result of solar concentrated heating in the near region of location 1. Consequently, internal energy gain of water due to the heat diffusion from the high temperature tube inner surface becomes high, particularly in the early heating period. This, in turn, causes rapid rise of the internal energy gain and temperature of the fluid. However, as the time progresses, temperature increase in this region causes increased temperature gradient in the neighborhood of this region, which accelerates conduction heat transfer from this region towards the fluid bulk in the tube. Therefore, temperature increase becomes gradual in this region with progressing time. In region 2, where it is located in the center region of the tube, temperature remains low with progressing heating period.

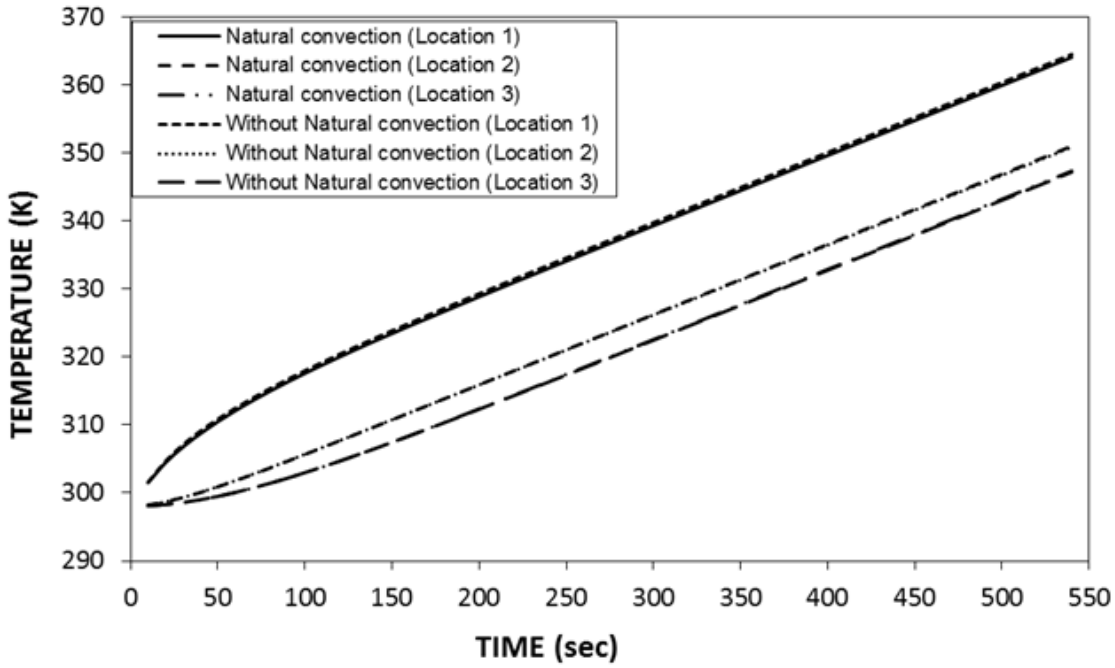

Figure 5.9 Temporal variation of temperature at three locations inside tube for the case of with presence of meshes inside tube.

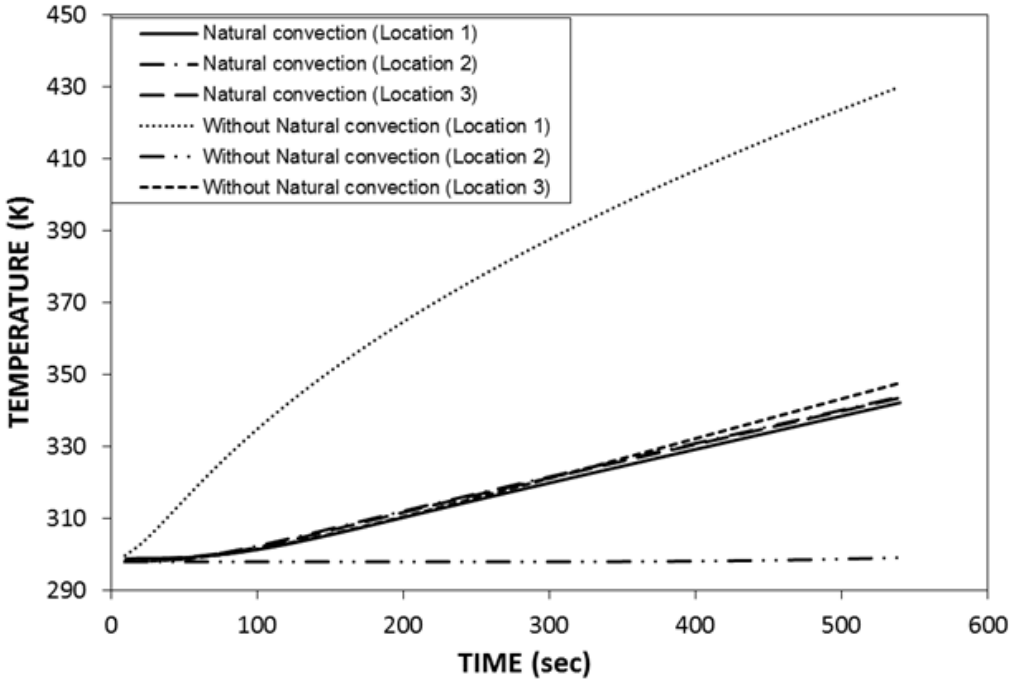

Figure 5.10 Temporal variation of temperature at three locations inside tube for the case of without meshes inside tube.

This is because of the heat conduction, which is suppressed by the low thermal conductivity of water (0.563 W/mK at 293 K). At location 3, Temperature rise is slow in the early heating period and it increases gradually with further progressing of time. Temperature increase is less than that of the location 1. The slow rise and attainment of relatively lower temperature as compared at location 1 are attributed to the solar radiation intensity irradiating the tube surface at location 3, which is less than that corresponding to location 1. It should be noted that exposing of the direct solar radiation is considered at the tube surface in the close region of location 3. On the other hand, the use of aluminum meshes enhances the heat conduction in water inside the tube and minimizes the local heating and high water temperature increase inside the tube. This behavior is associated with the high thermal conductivity of aluminum wire (204.3 at 293 K); in which case, aluminum mesh acts as a conduction three and mesh temperature increases in the tube. Heat conduction from the meshes towards water enhances temperature increase inside the tube. It should be noted that meshes form the cells in the tube where water occupies and heat conduction from the meshes towards water takes place from the mesh edges; therefore, the conduction heating takes place from the circumference of the water cell rather than the heating from the tube side as observed in the without mesh case. The maximum temperature difference between locations 1, 2 and 3 is small for the presence of the meshes case. This situation can also be seen from figure 5.11 in which the maximum and minimum temperature differences with time in water are shown due to the cases with and without meshes inside the tube. In addition, temporal variation of the maximum water temperature inside the tube due to with and without presence of the meshes is shown in figure 5.12. The maximum water temperature rises sharply in the tube in the early heating period and the rise becomes

gradual with progressing time, which is particularly true for the tube without the meshes. In the case of tube with meshes, the maximum temperature increase remains almost gradual throughout the heating period. Since the maximum temperature remains lower for the mesh case than that of no mesh case, local heating is avoided in the tube by using the aluminum mesh inside the tube.

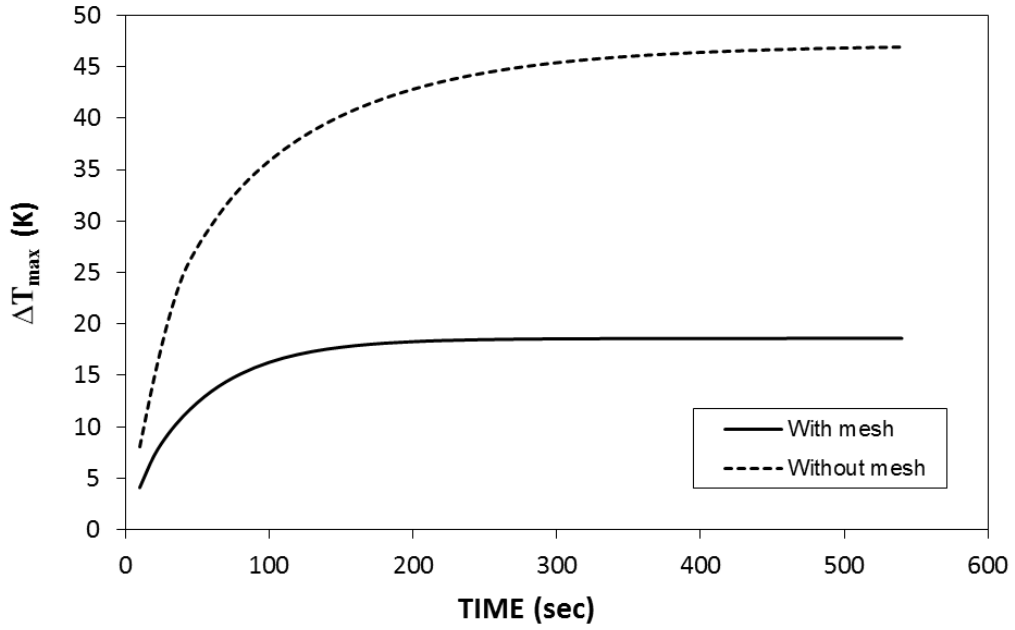

Figure 5.11 Temporal variation of the difference between maximum and the minimum temperatures inside tube.

Figures 5.13 and 5.14 show the temperature parameter ($\varphi = \frac{T-T_{in}}{T_{max}-T_{in}}$, where T is the local temperature, T_{in} is the initial temperature, and T_{max} is the maximum temperature in the tube) along the rake located in the x-axis for the cases of with and without presence of meshes inside the tube.

Temperature parameter distribution almost follows the distribution of temperature difference (figures 5.1 and 5.2) in water, particularly for the no mesh case. However, the value of the temperature parameter varies within the range of $0 \leq \varphi \leq 1$ for the both cases.

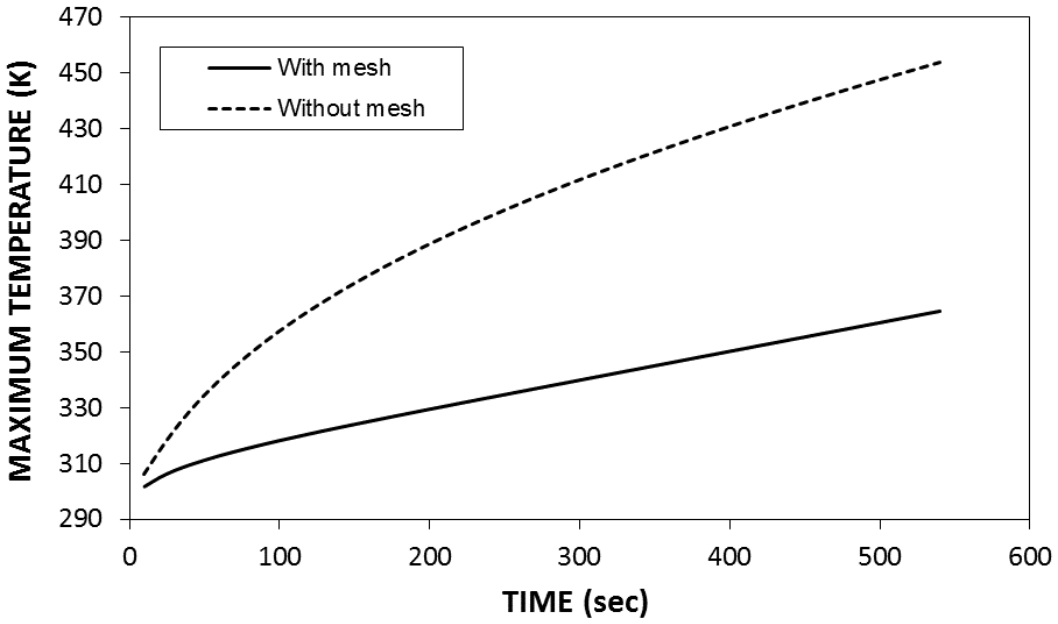

Figure 5.12 Temporal variation of the maximum temperature inside tube for the cases of with presence and without meshes.

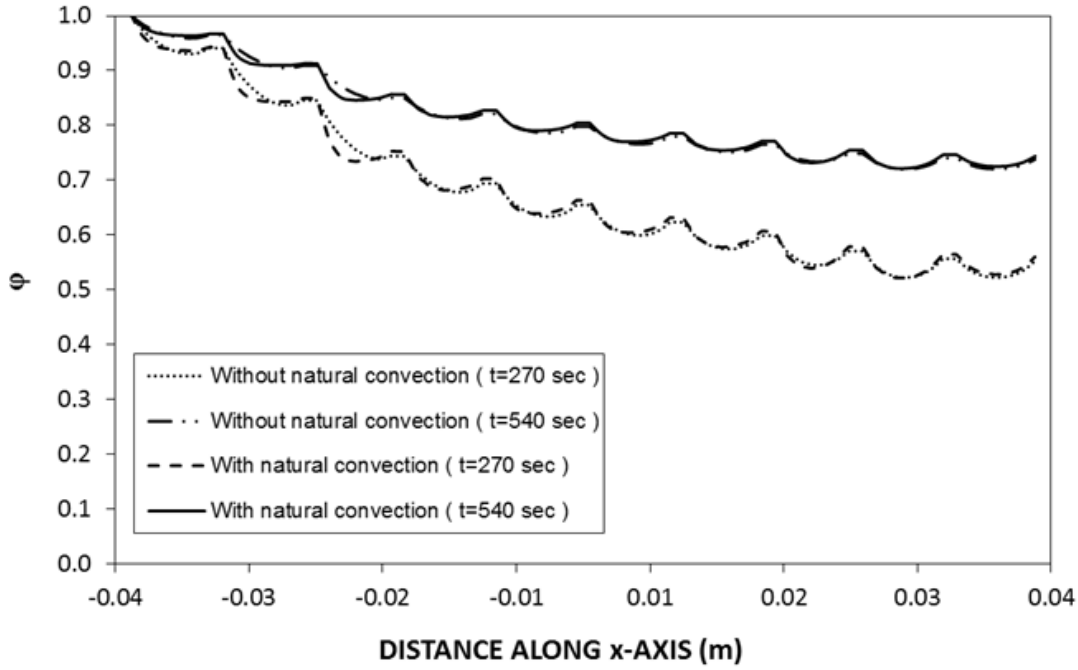

Figure 5.13 Temperature parameter (φ) along the rake located in x-axis for the case of presence of meshes inside tube.

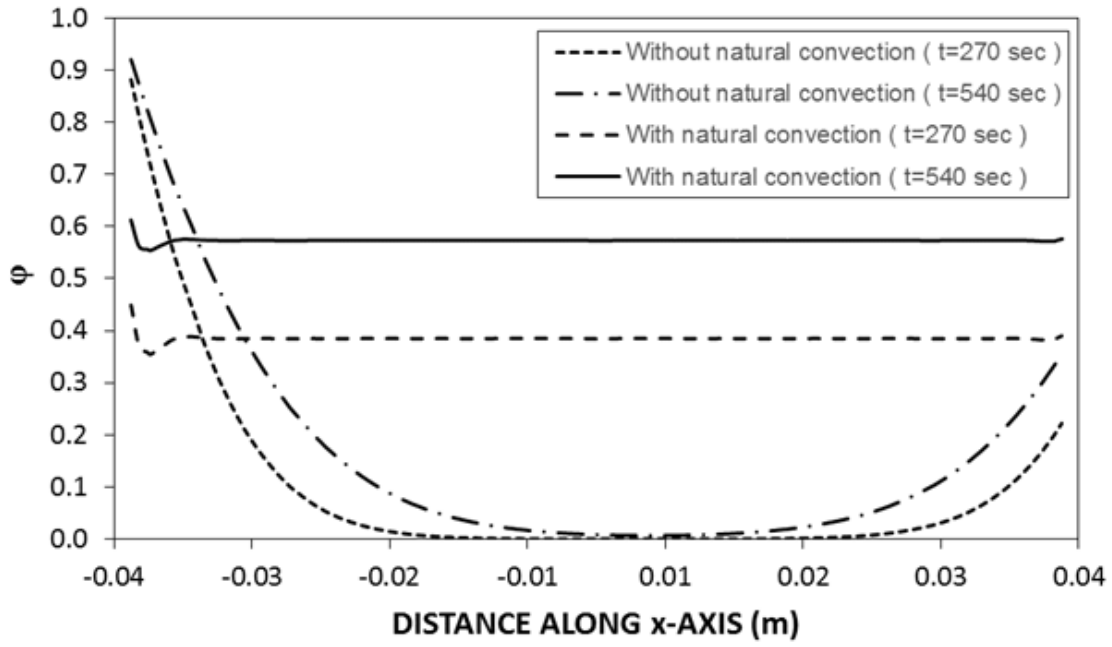

Figure 5.14 Temperature parameter (φ) along the rake located in x-axis for the case of without meshes inside tube.

The oscillatory behavior of the temperature parameter for the case of the meshes inside the tube is associated with the attainment of high temperature along the meshes due to the heat conduction from the tube wall, which is subjected to the solar radiative heating by the trough. In this case, the heat conduction enhances towards water bulk in the near region of the meshes along the rake. This, in turn, increases water temperature in the tube while causing oscillatory behavior of temperature parameter along the rake. This situation is only observed for the case of the meshes inside the tube. Moreover, similar behavior is also observed for the temperature parameter along the rake located in the y-axis (Figures 5.15 and 5.16). However, the variation of the temperature parameter remains almost constant along the rake for the presence of the mesh case inside the tube. The influence of natural convection on the temperature parameter is not significant for the presence of the mesh case as compared to that of the without mesh case. This is because of the relatively low temperature difference in water in the mesh cell, which suppresses the attainment of the

large density variation and convection current in the water cell. However, in the no mesh case, large variation in the temperature difference causes large variation of water density inside the tube and natural convection current improves the heat transfer rates while lowering the temperature difference inside the tube. Consequently, in the case of without mesh inside the tube, the temperature parameter becomes smaller for the natural convection inclusion in the analysis than that corresponding to the exclusion of the natural convection in the analysis. However, this situation is not observed clearly for the presence of the meshes inside the tube case. In general, temperature parameter indicates the ratio of the local enthalpy change during the heating period over the maximum enthalpy change inside the tube during this period. Therefore, large variation of the temperature parameter along the rake indicates the presence of the local excessive heating inside the tube. This is the case, which is observed for without mesh case inside the tube.

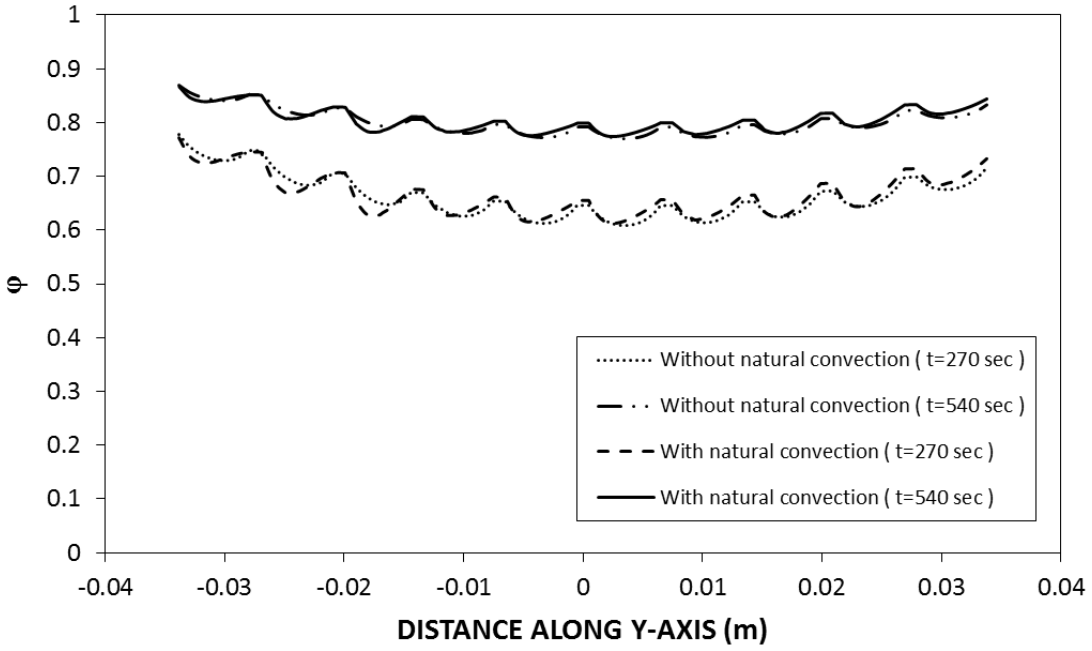

Figure 5.15 Temperature parameter (φ) along the rake located in y-axis for the case of presence of meshes inside tube.

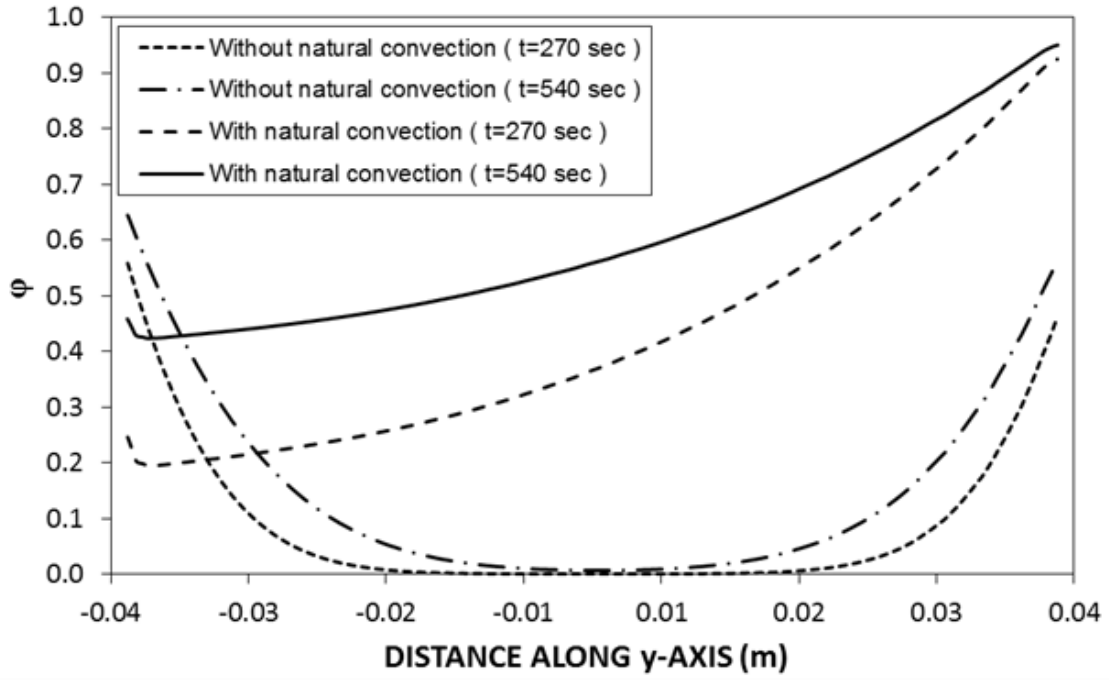

Figure 5.16 Temperature parameter (φ) along the rake located in y-axis for the case of without meshes inside tube.

5.2 Thermal Analysis with Water and Rotation of Thermal Battery

Thermal storage characteristics of a mobile thermal battery are described in this section. A concentrated solar heating of the thermal battery together with the rotation along its symmetry axis is incorporated in the analysis. The temperature parameter is introduced to assess the thermal performance of the thermal battery.

Figure 5.17 shows temperature contours across the cross-section of the thermal battery for different rotational speeds. Temperature of the working fluid attains high values in the near region of the aluminum meshes. This is because of high temperature of the aluminum meshes inside the thermal battery. It should be noted that the thermal conductivity of aluminum (205 W/mK) is higher than that of the working fluid, which is water (0.6 W/mK). The heat conduction from the heat source, resembling the concentrated solar heating at the outer surface of the thermal battery, conducted through the aluminum meshes at a higher

rate than that of water. Therefore, aluminum meshes act like a conduction tree enhancing the heat conduction towards the working fluid. Moreover, the convection current generated in the near region of the metallic mesh surfaces contributes to the heat transfer enhancement in the working fluid. This situation can be seen from figure 5.18 in which velocity contours are shown for various rotational speed of the thermal battery. It should be noted that the rotational speed of the thermal battery influences the convection current in the working fluid, which can be seen when comparing velocity contours at different rotational speeds. However, this effect appears to be small, since the variation of the maximum velocity magnitude due to rotational speed is small. Temperature inside the working fluid becomes almost uniform when the rotational speed increases. This is related to the heat source location around the outer surface of the thermal boundary, which changes with rotation at the outer surface of the thermal battery. In this case, solar irradiation emanated from the parabolic trough shines at different locations of the surface during the rotation of the thermal battery. Therefore, rotating the thermal battery at high speeds results in almost uniform heat source at the outer surface of the thermal battery. This, in turn, gives rise to almost uniform heating of the working fluid from the heat source located at the battery surface. Consequently, incorporating the metallic meshes in the working fluid and thermal battery rotation provide uniform heating and energy storage with a small temperature difference in the working fluid.

Figure 5.19 shows temporal variation of the maximum temperature inside the tube with and without meshes. The maximum temperature remains significantly higher for the without mesh case than that of with the presence of mesh case. Therefore, the aluminum meshes act like a conduction tree while lowering the maximum temperature and resulting

in almost uniform temperature in the working fluid. Consequently, almost uniform temperature of thermal storage could be possible inside the thermal battery when the metallic meshes are incorporated in the storing medium.

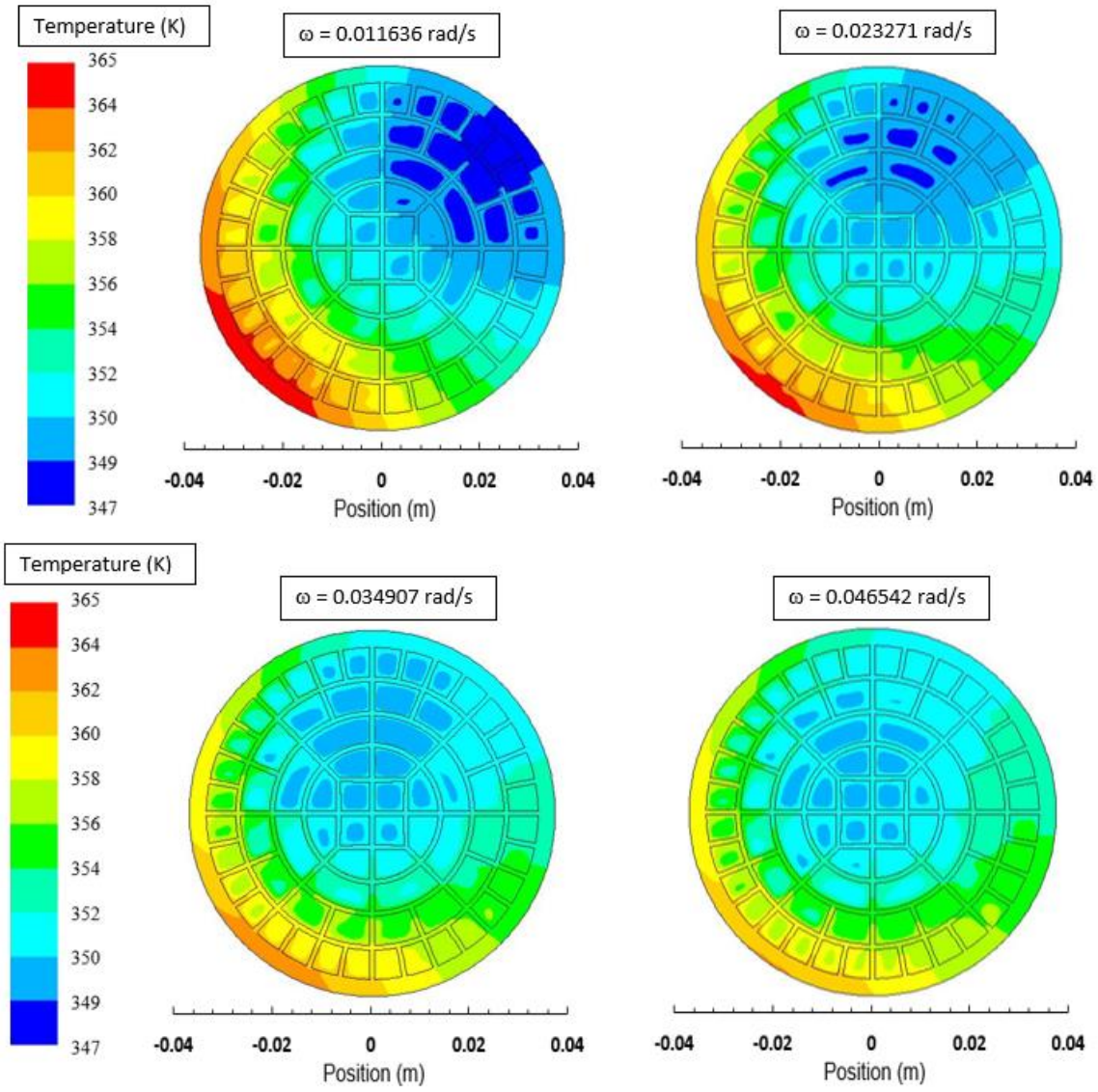

Figure 5.17 Temperature contours in the thermal battery for different rotational speed and total heating duration is 540 s.

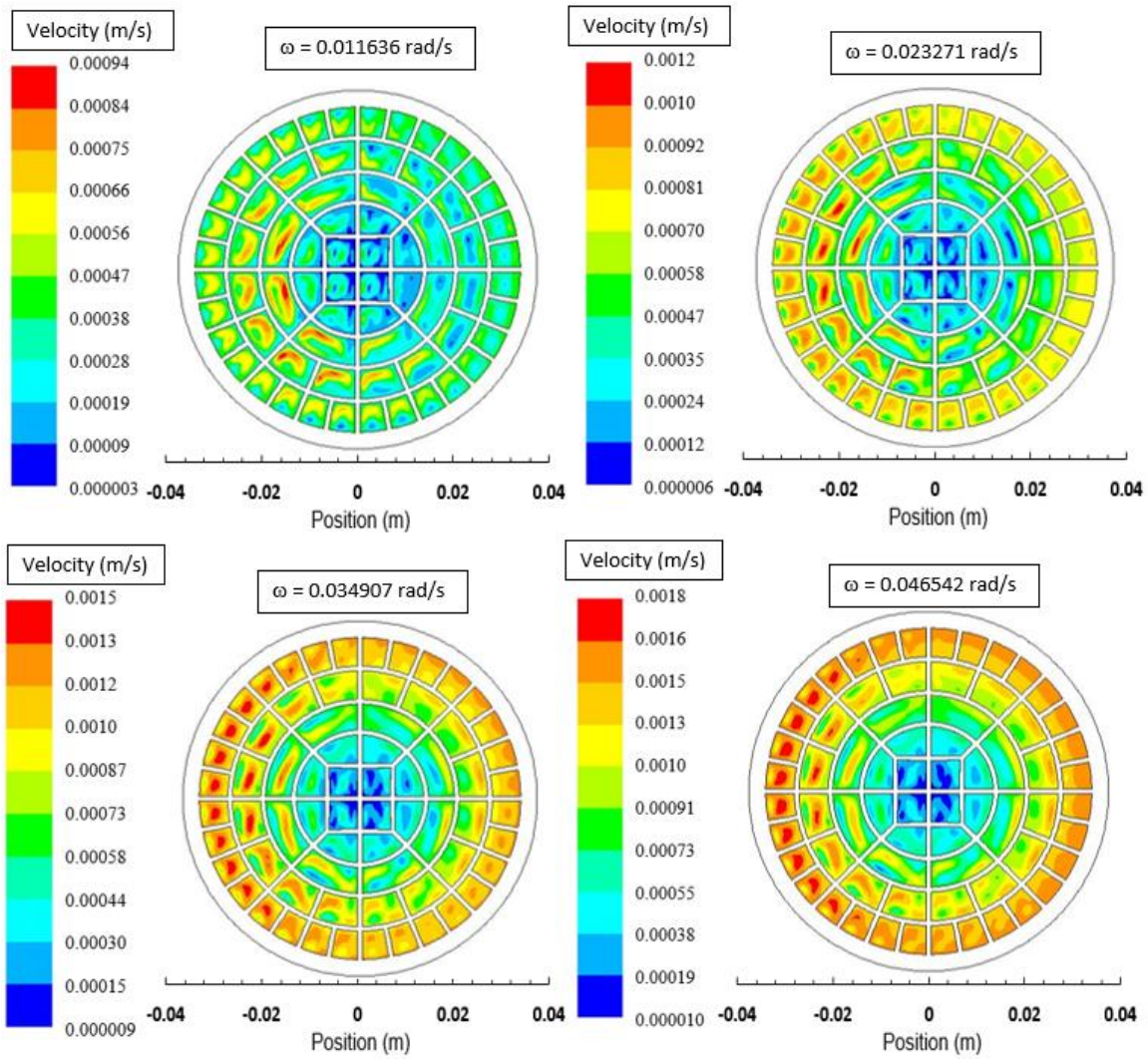

Figure 5.18 Velocity magnitude contours in the thermal battery for different rotational speed and total heating duration is 540 s.

Figure shows 5.20 temperature difference ($\Delta T = T - T_{in}$, where T is the local temperature and T_{in} is the initial temperature in the working fluid) along the x-axis (horizontal rake) for different rotational speed of the thermal battery while figure 5.21 shows temporal variation of temperature difference along the y-axis (vertical rake).

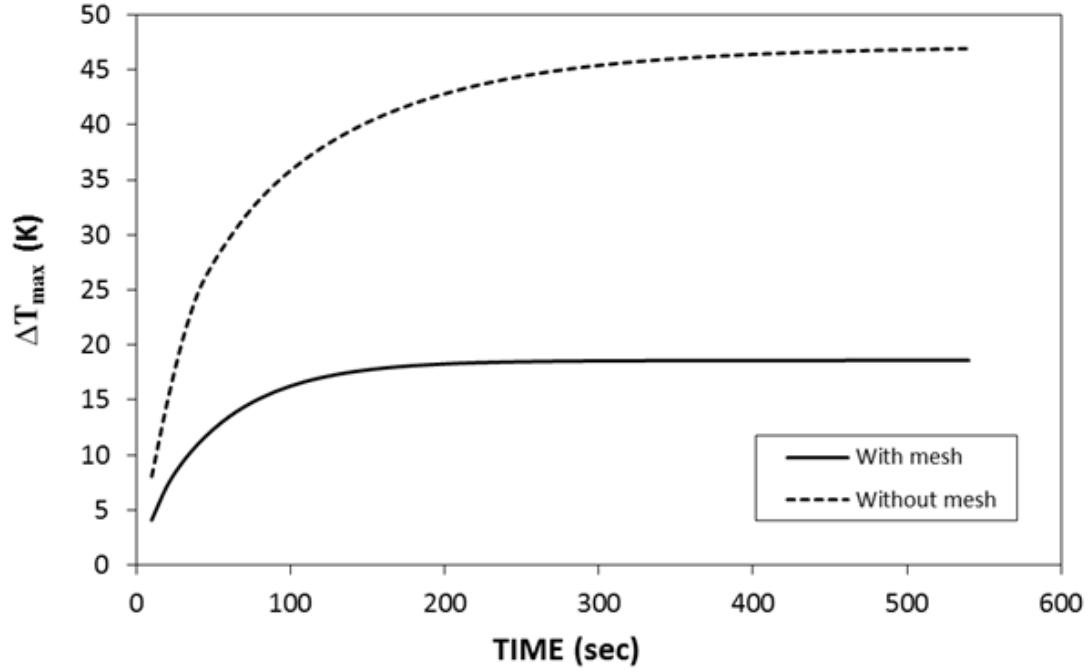

Figure 5.19 Temporal variation of difference between the maximum and the minimum temperatures in the thermal battery for the cases of with and without meshes

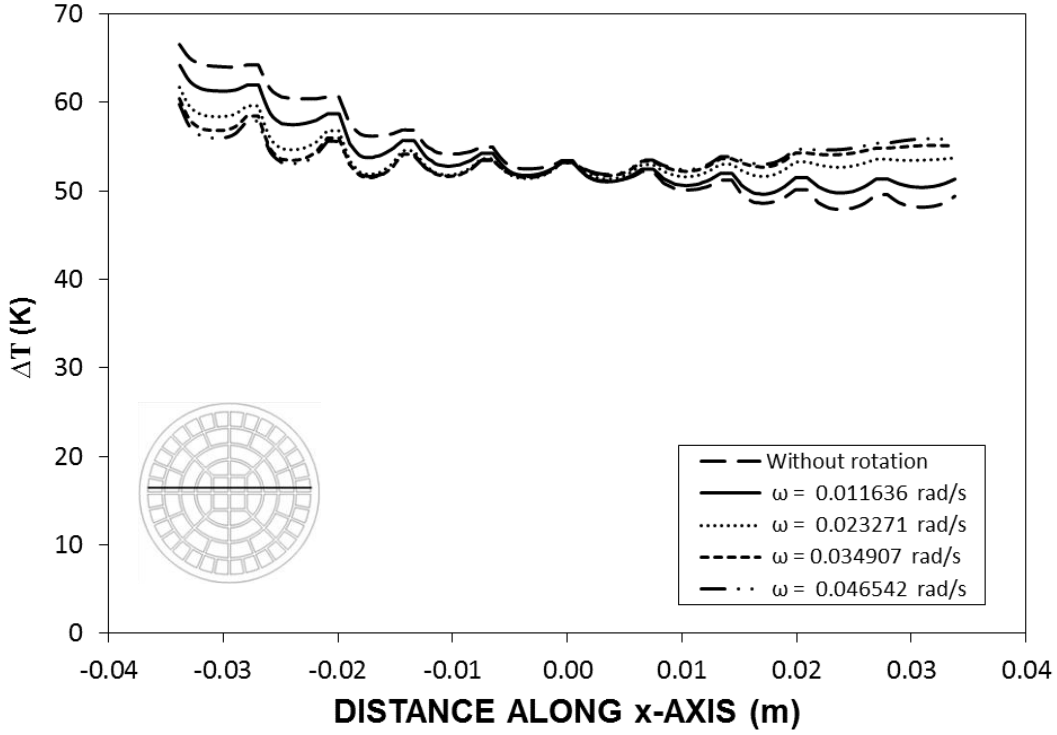

Figure 5.20 . Temperature difference (ΔT) along the x-axis for various rotational speeds of thermal battery after heating time of 540 s

Temperature difference remains high in the near region of the steel tube wall where the heat source resembling the solar concentrated heating is located. As the distance along the x-axis increases, temperature difference reduces. The wavy behavior of temperature variation is associated with the aluminum meshes where temperature remains high. It should be noted that temperature at the aluminum mesh surface remains high because of the high thermal conductivity of aluminum as compared to the working fluid, which is water. Therefore, heat conducted from the heat source towards the thermal battery increases aluminum mesh temperature significantly as compared to that of water. However, temperature difference reduces along the x-axis towards the section opposing to the heat source side for the case of without rotation of the thermal battery. This is related to the thermal diffusion taking place inside the tube; in which case, the heat conduction is governed by the thermal conductivity and the temperature gradient. As the temperature gradient reduces along the x-axis so that the heat conduction, which in turn lowers temperature rise in this region. Moreover, heat transfer from the aluminum mesh towards the working fluid enhances temperature increase in the working fluid. Since the mesh temperature reduces along the x-axis so that working fluid temperature also reduces. In the case of the thermal battery rotation, temperature difference attains low values in the working fluid, which is more pronounced for the high speed rotation (0.046542 rad/s). This behavior is attributed to the location of the heat source around the outer surface of the thermal battery, which changes during the rotation. Consequently, almost uniform temperature is resulted in the working fluid when rotating the thermal battery during the period of the thermal energy storage. In the case of figure 5.21, temperature difference behaves similar to that of shown in figure 5.20, provided that temperature variation

becomes small. This is because of the location of the heat source along the outer surface of the thermal battery. Therefore, heat conduction from the heat source causes small temperature variation along the y-axis, which is more pronounced for the rotation with high speeds.

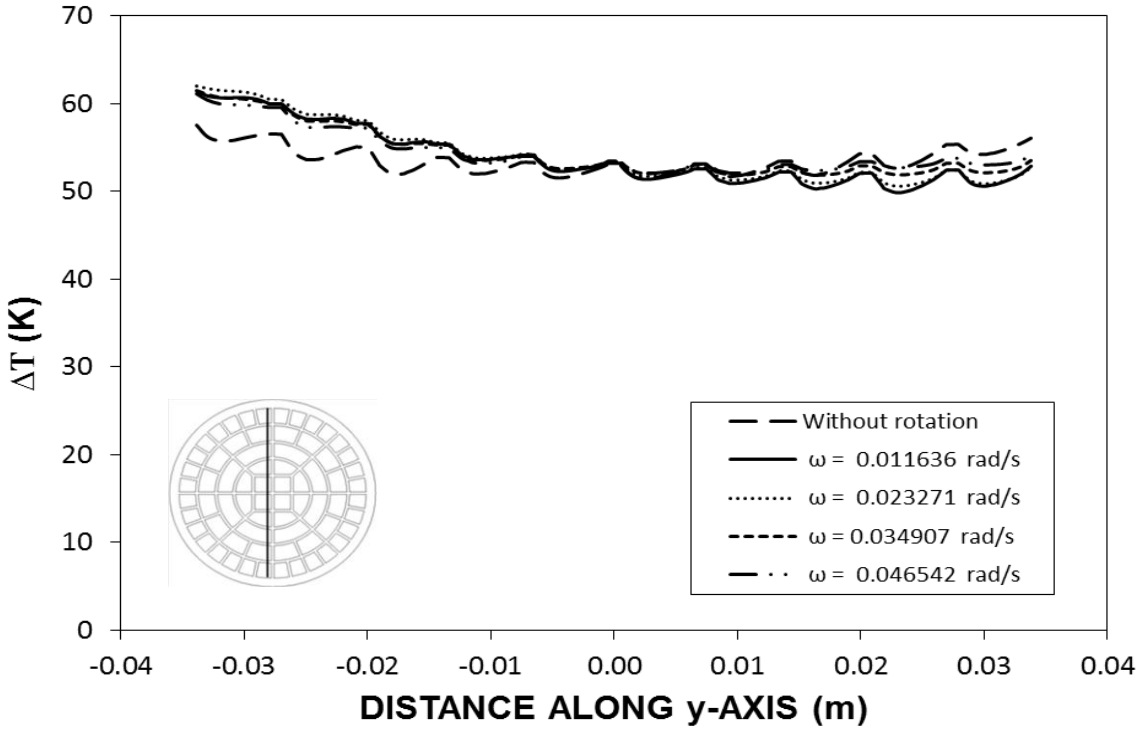

Figure 5.21 . Temperature difference (ΔT) along the y-axis for various rotational speeds of thermal battery after heating time of 540 s.

Figure 5.22 shows the temperature parameter $(\varphi = \frac{T-T_{in}}{T_{max}-T_{in}}$, where T is the local temperature of the working fluid, T_{in} is the initial temperature of the working fluid, T_{max} is the maximum temperature of the working fluid) along the x-axis (horizontal rake) while figure 5.23 shows the temperature parameter along the y-axis (vertical rake) for various rotational speeds of the thermal battery. The temperature parameter represents the ratio of local energy storage over the maximum energy storage in the thermal battery. The temperature parameter remains high in the close region of the heat source due to the heat

conduction taking place in this region. As the distance along the x-axis increases, the temperature ratio reduces, particularly for the without rotational case. This is associated with the energy transfer from the aluminum mesh surfaces to the working fluid. Since temperature of aluminum meshes reduces with increasing distance along the x-axis (figure 5.20), energy transfer from aluminum mesh through conduction and convection towards the working fluid also reduces. This in turn lowers the temperature parameter along the x-axis for the case of without rotation. The wavy behavior of the temperature parameter is also observed in figures 5.22 and 5.23, which is related to the high temperature of the mesh along the x-axis, which causes temperature oscillation. In the case of the thermal battery rotation, the temperature parameter attains high values along the x-axis towards the opposite side of the heat source location, which is more pronounced with increasing rotational speed of the thermal battery. Consequently, increasing rotational speed results in almost uniform heating of the thermal battery from the outer surface while resulting in high local temperature rise inside the working fluid. In addition, temperature difference between the local fluid temperature and the maximum temperature in the fluid remains low. This cases the attainment of the high values of the temperature parameter along the x-axis for the case of the thermal battery rotation at high speeds. In the case of figure 5.23, temperature parameter behaves similar to that of shown in figure 5.22. However, the difference in the temperature parameter, due to various speeds of the rotation of the thermal battery, remains lower along the y-axis than that of the x-axis. This behavior is attributed to the heat source distribution along the outer surface of the thermal battery, which results in almost uniform heating along the y-axis. Consequently, thermal battery rotation along

the centerline line of the trough results in notable improvement in the storage capacity of the thermal battery.

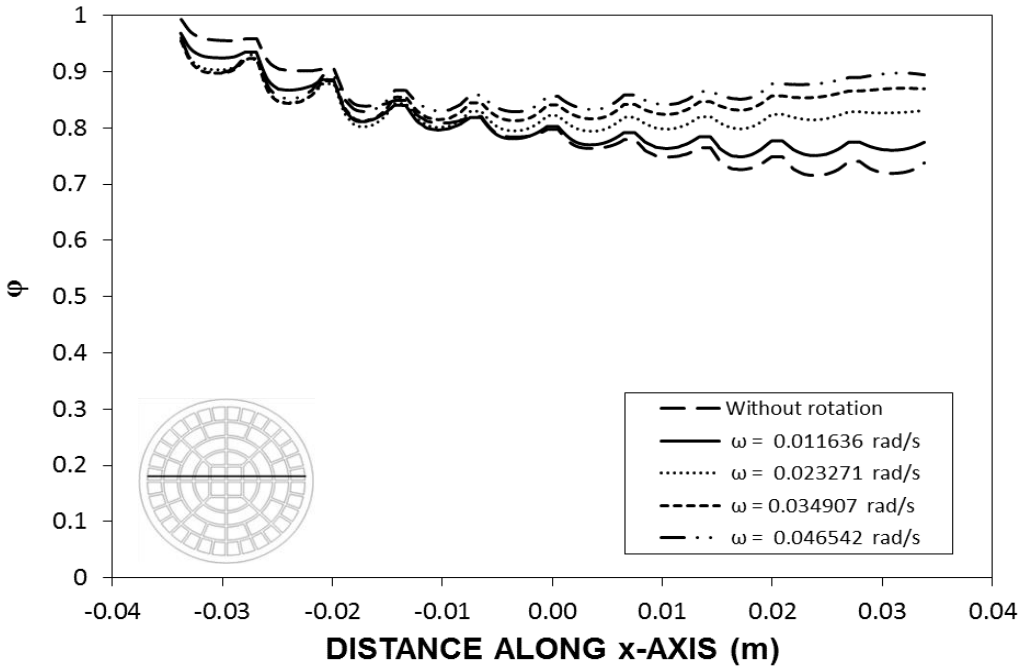

Figure 5.22 . Temperature parameter (φ) along the x-axis for various rotational speeds of thermal battery after heating time of 540 s.

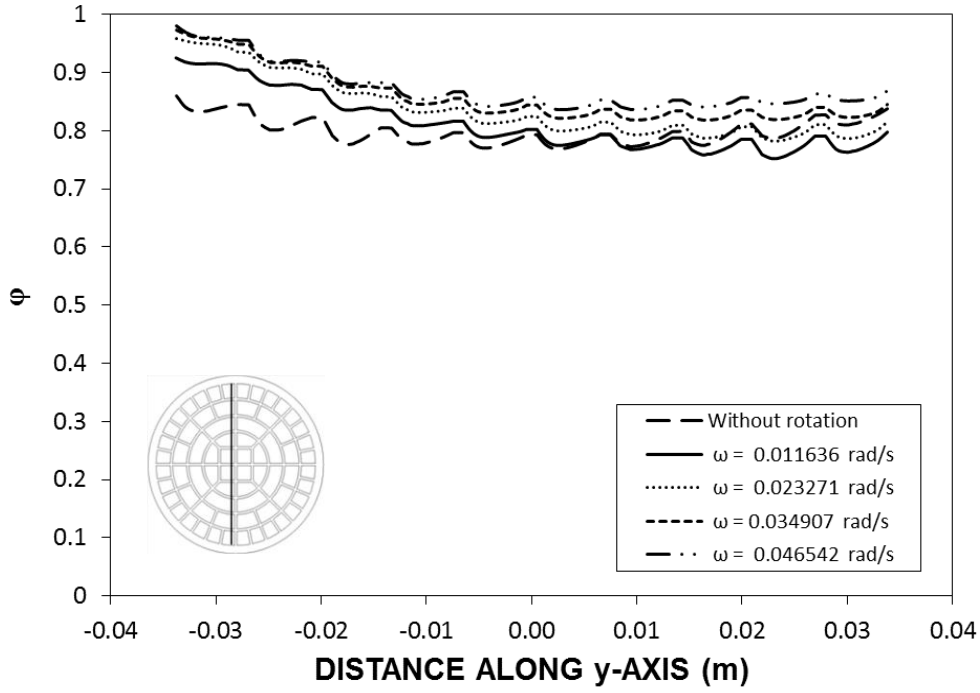

Figure 5.23 Temperature parameter (φ) along the y-axis for various rotational speeds of thermal battery after heating time of 540 s.

Figure 5.24 shows temporal variation of temperature difference ($\Delta T_{max} = T_{max} - T_{min}$) between the maximum and the minimum temperature in the thermal battery for various rotational speeds. Temperature difference remains high for the cases of low rotational speeds and without rotation of the thermal battery. This is because of the local heating in the close region of the heat source, which in turn enhances temperature increase locally in the thermal battery.

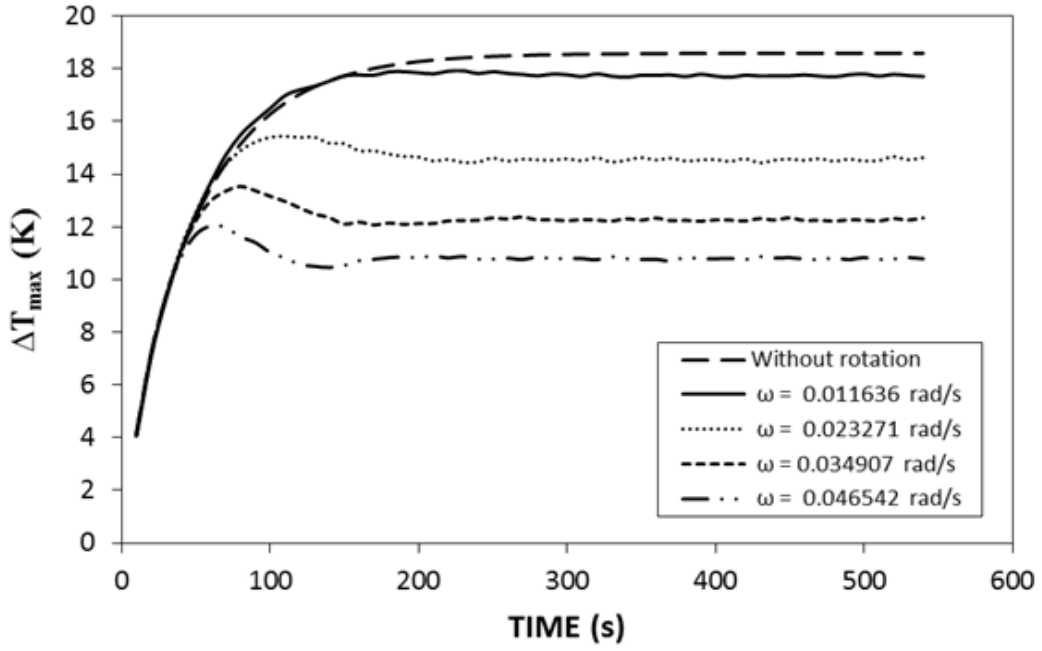

Figure 5.24 Temporal variation of temperature difference (ΔT_{max}) for various rotational speeds of thermal battery.

In general, temperature increases rapidly during the early heating period and becomes gradual as the heating period progresses. Temperature rise is associated with the internal energy gain of the working fluid and the metallic meshes. Consequently, the temperature rises rapidly in the close region of the heat source and becomes gradual as the distance from the heat source increases away from the heat source towards the bulk of the thermal battery. The maximum temperature occurs in the close region of the heat source in the thermal battery. In the case of the rotation, temperature rise becomes almost the same in

the early heating period for all rotational speeds; however, as the time progresses, temperature difference becomes less than that of the low speed rotations. In addition, temperature difference attains a quasi-steady value as the heating period progresses further. This occurs earlier for the case of rotation at high speeds than that of the case for the without rotation. Consequently, rotation of thermal battery results in short duration to reach quasi-steady temperature and almost uniform heating of the working fluid. In addition, incorporating the metallic mesh inside the thermal battery contributes significantly to the achievement of uniform heating of the working fluid in the thermal battery.

5.3 Thermal Analysis with PCM ($LiNO_3$) and Without Rotation of Thermal Battery

A mobile solar thermal energy storage unit incorporating the phase change material and the metallic mesh is considered.

Figure 5.25 shows temporal behavior of the maximum temperature in the phase change material for the cases with and without the presence of aluminum meshes inside the tube. Temperature rises continuously in the phase change material for the non-meshing configuration. This behavior is attributed to the local heating from the heat source around the steel tube, which resembles the concentrated solar intensity distribution. In the case of the mesh configuration, the aluminum meshes act like a conduction tree while minimizing the local heating in the phase change material. This in turn results in almost homogeneous temperature distribution inside the tube.

Figure 5.26 shows temperature contours for two heating periods inside the tube. In the early heating period, temperature remains high in the region close to the solar heating source.

The phase change takes place in this region because of the liquidus temperature of the phase change material (534 K). This situation can also been from figure 5.27, in which contours of liquid fraction is shown inside the tube. Melting takes place in the near region of the aluminum meshes inside the tube. In this case, meshes act like a conduction tree while carrying heat from the irradiated surface of the tube, due to concentrated solar heating, towards the phase change material. It should be noted that the thermal conductivity of the aluminum mesh is 204 W/mK while the thermal conductivity of the phase change material is 1.37 W/mK. Therefore, the high thermal conductivity of meshes is the main driving force for the heat diffusion inside the tube.

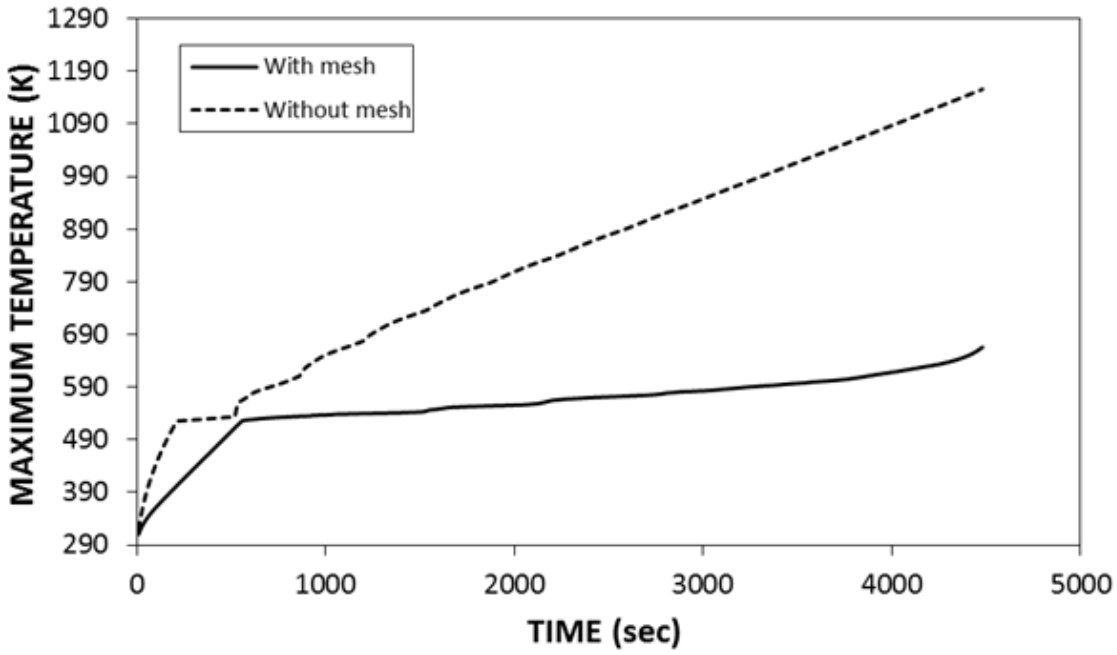

Figure 5.25 Temporal variation of the maximum temperature inside the tube with and without presence of aluminum meshes.

As the time progresses, temperature increases and the phase change completes while resulting in liquid fraction of 1 inside the tube. However, in the early heating period, temperature difference between the mesh and the phase change material is large, which causes the high rate of heat conduction from the metallic meshes towards the phase change

material. As the heating period progresses, temperature difference becomes small and the phase change is initiated in the vicinity of the mesh surfaces. Moreover, the thermal conductivity of the liquid phase of the phase change material reduces significantly (0.58 W/mK), which causes a thermal resistance between the meshes and the solid phase of the phase change material. Therefore, temperature increases in the vicinity of the metallic meshes and the liquid fraction slows down in the phase change material inside the tube with progressing time. As time progresses further, solid phase of the phase change material forms like a small island in the cell of the aluminum meshes and it gradually melts in the tube with progressing time. Consequently, temperature rise in the tube is relatively faster in the early heating period and, as the time progresses, temperature rise becomes gradual. The main reasons for this behavior is that: i) initial formation of the liquid layer in between the mesh and the phase change material suppresses the heat conduction towards the solid phase of the phase change material, ii) energy gain by the phase change material is consumed via phase change rather than sensible heating, and iii) the difference between solidus and liquidus temperatures of the phase change material is small; therefore, temperature difference in the phase change material remains low while suppressing the heat conduction from the melt front towards the solid phase.

Figure 5.28 shows streamlines of the natural convection current developed in the liquid phase of the phase change material during the melting process. The convection current enhances the melting in the phase change material because of the contribution of the convection heating in this region.

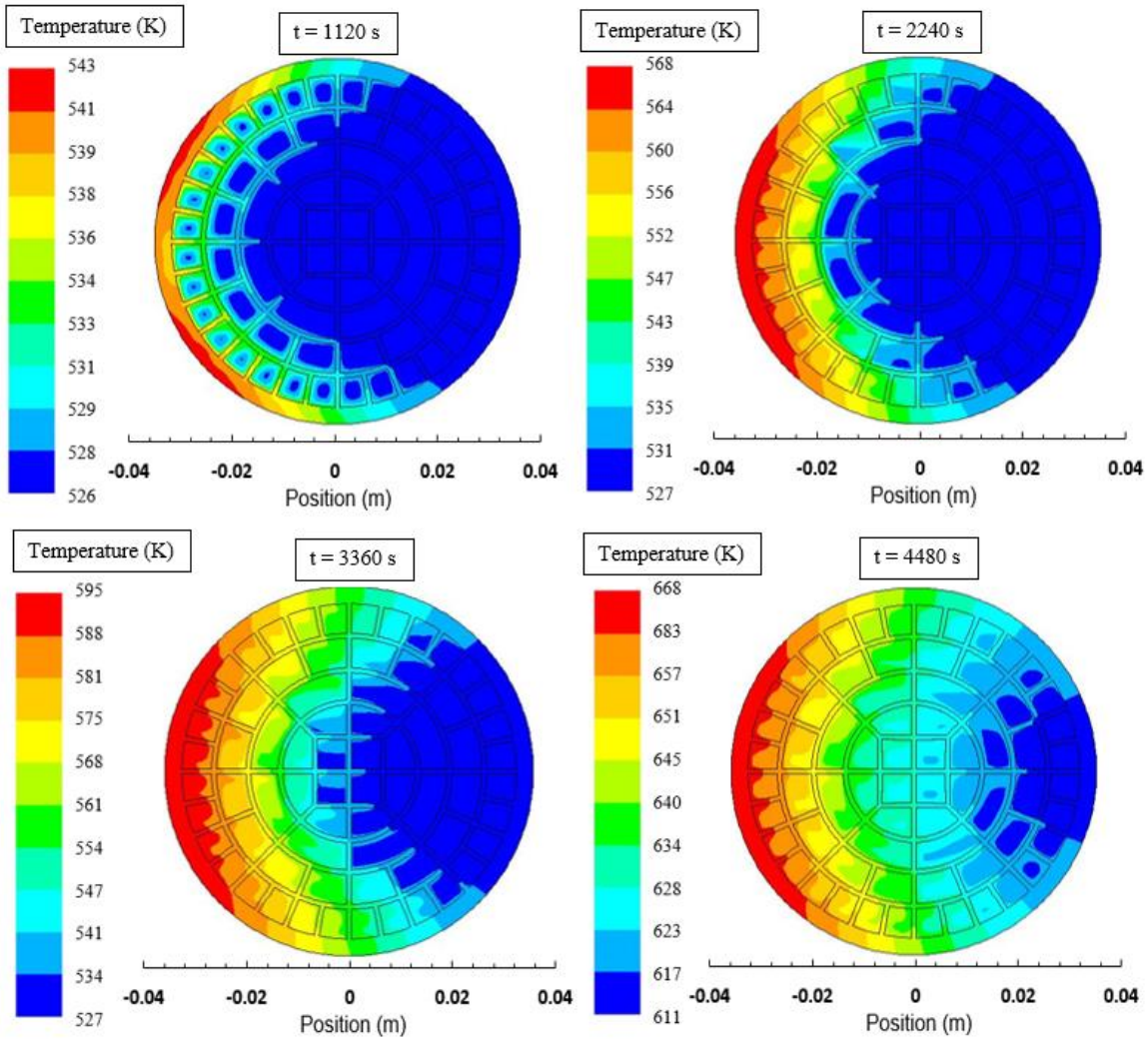

Figure 5.26 Temperature contours inside the steel tube for various heating durations.

Figure 5.29 shows the local and initial temperature difference along the x-axis (along the horizontal rake) while figure 5.30 shows temperature difference along y-axis for different heating periods. Temperature difference decays relatively sharp along the x-axis in the early heating period as compared to late heating periods. As the time progresses, temperature difference decays sharply in the near region of the heated surface of the tube and the decay becomes gradual as the distance increases along the x-axis. The wavy behavior of the temperature difference is associated with the metallic mesh temperature,

which remains higher than temperature of the phase change material along the x-axis in the early heating period.

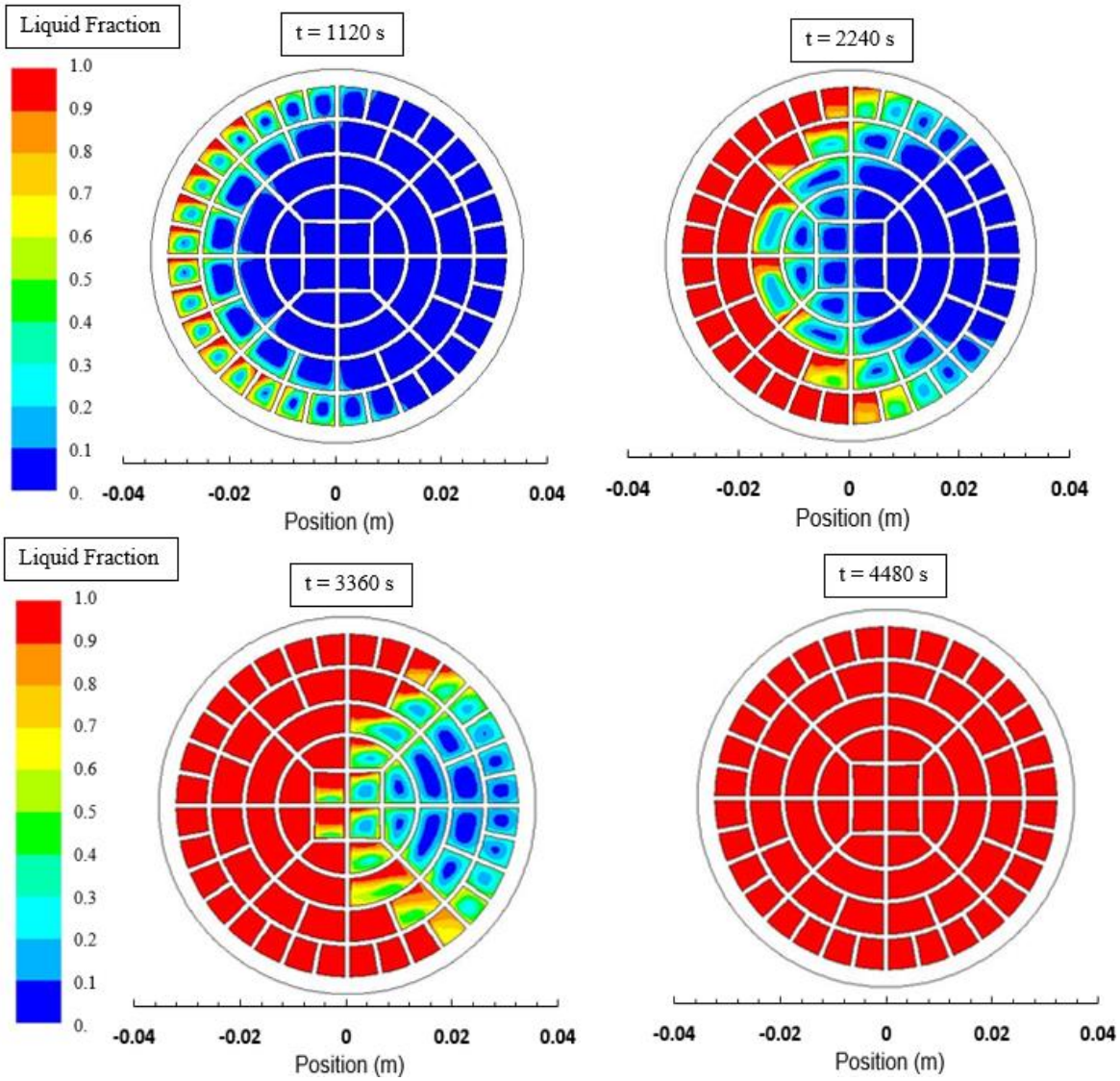

Figure 5.27 Contours of liquid fraction inside the tube for various heating periods.

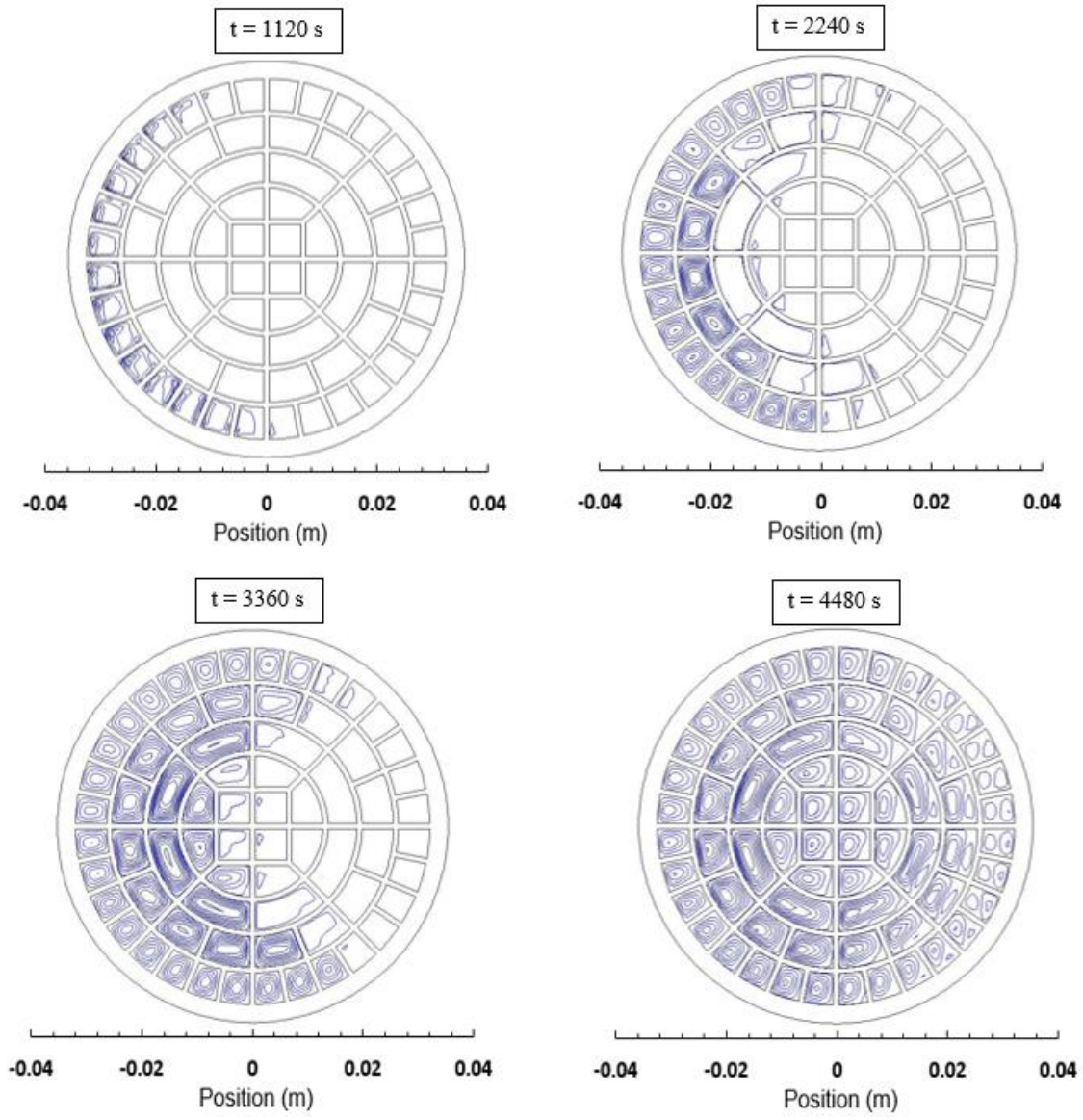

Figure 5.28 Stream lines inside the tube due to natural convection current generated in the liquid phase of the phase change material.

Since thermal conductivity of aluminum is much higher than the solid phase of the phase change material, heat conduction along the wire results in high temperature in the wire. The attainment of high temperature difference in the late heating period (t = 4480 s) is attributed to the sensible heating of the liquid phase of the phase change material. Since the melting of the phase change material completes at t = 4480 s (figure 5.25), the heating results in increased temperature of the phase change material inside the tube. Moreover, as

the heating period progresses, the difference between the local temperature and the initial temperature becomes large and the wavy behavior of temperature difference replaces with the steady behavior. This is attributed to the heat conduction and temperature of the phase change material, which becomes almost similar to temperature of the metallic mesh. However, sensible heating of the liquid phase modifies temperature difference in the close region of the heat source. It should be noted that the specific heat of the phase change material is significantly higher than aluminum and thermal conductivity of the liquid phase of the phase change material is considerably smaller than that of the aluminum mesh. Consequently, high specific heat capacity suppresses temperature rise in the liquid phase of the phase change material despite the fact that internal energy gain of the liquid phase of the phase change material is high in this region. This observation is not strictly valid for temperature difference along the y-axis (figure 5.30). This is associated with the heat conduction along the y-axis inside the tube. Since the heat source distribution along the tube surface, resembling the distribution of the concentrated solar intensity, generates similar temperature distribution inside the tube along the y-axis through heat conduction. Therefore, temperature gradient remains lower along the y-axis than that of the x-axis.

Figure 5.31 shows the temperature parameter ($\varphi = \frac{T-T_{in}}{T_{max}-T_{in}}$) along the x-axis (along the horizontal rake) while figure 5.32 shows the temperature parameter along the y-axis (vertical rake) for different heating periods. It should be noted that the temperature parameter represents the local energy gain over the maximum energy gain by the phase change material. Temperature parameter first reduces with progressing time due to the attainment of high value of the maximum temperature in the tube.

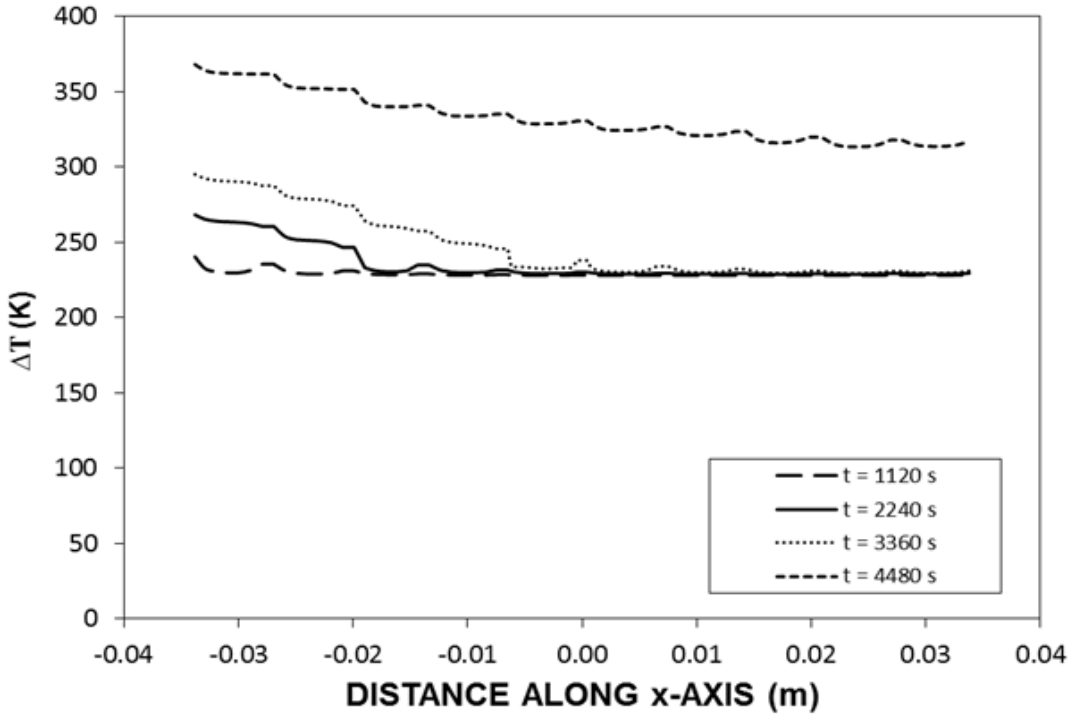

Figure 5.29 Temperature difference (ΔT) along the x-axis (horizontal rake) inside the tube for various heating periods.

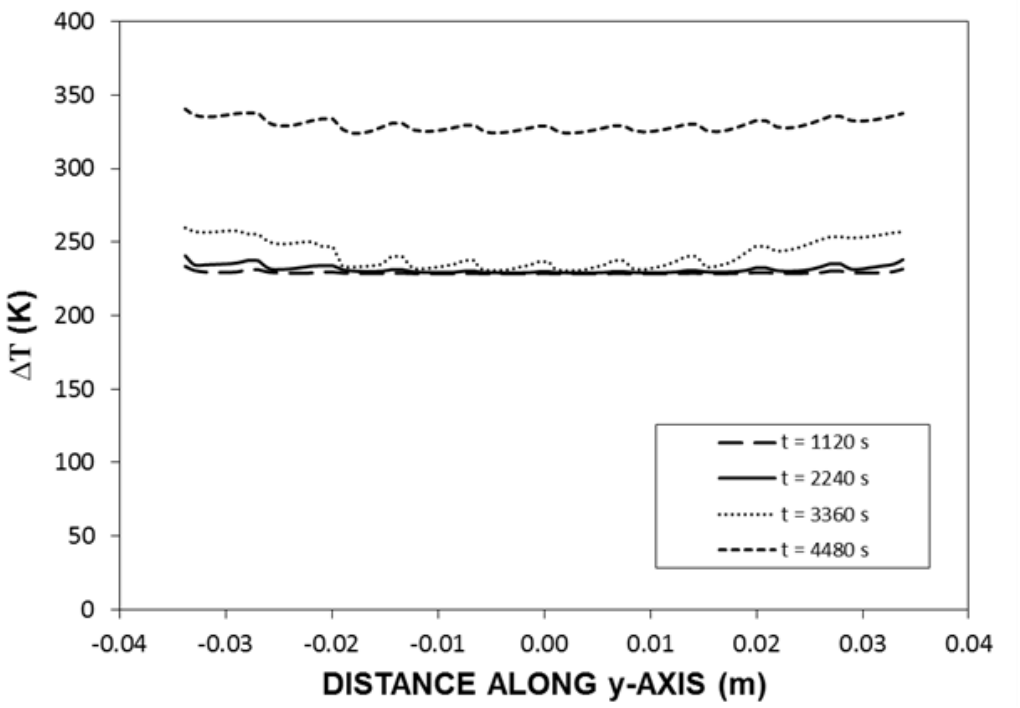

Figure 5.30 Temperature difference (ΔT) along the y-axis (vertical rake) inside the tube for various heating periods.

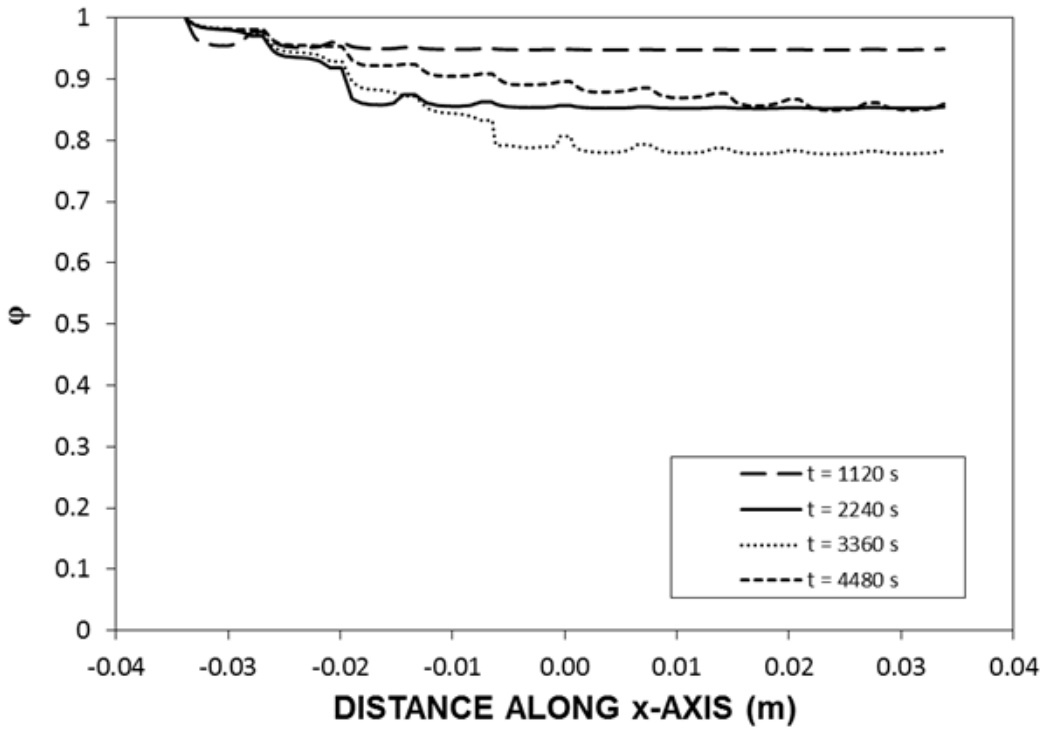

Figure 5.31 Temperature parameter (φ) along the x-axis (horizontal rake) inside the tube for various heating periods.

Since temperature of the phase change material remains almost same during the phase change process, the temperature parameter remains steady along the x-axis accordingly. This occurs in the early heating period (t = 2240 s). However, as the heating period progresses, the difference between the maximum temperature and the local temperature remains small (figure 5.29). This in turn causes increasing temperature parameter at t = 3360 s. As the heating period progresses further (t = 4480 s), temperature parameter reduces because of the increase of the maximum temperature. It should be noted that once the phase change is completed in the tube, sensible heating causes the rise of temperature in the liquid phase at a high rate (figure 5.29). Therefore, the difference between the maximum temperature and the initial temperature of the phase change material increases while reducing the temperature parameter along the x-axis. In the case of figure 5.32, the temperature parameter behaves similar to the parameter that is shown in figure 5.31,

provided that it remains almost steady along the y-axis. This occurs because of temperature rise along the y-axis due to the heat source located at the outer surface of the tube resembling the concentrated solar intensity. Therefore, the energy storage in the tube with the presence of the mesh results in high temperature parameter along both x- and y-axes when the thermal storage is governed by the latent heat of melting.

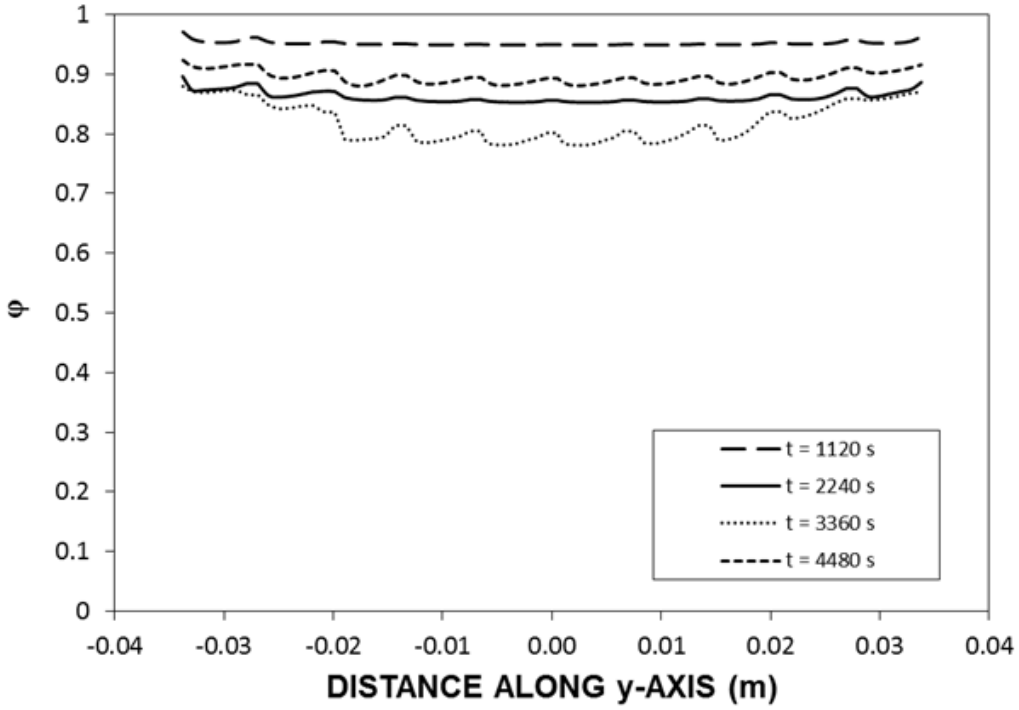

Figure 5.32 Temperature parameter (φ) along the y-axis (horizontal rake) inside the tube for various heating periods.

As the thermal storage continues through the sensible heating, then the temperature parameter reduces because of the local increase of temperature in the liquid phase of the phase change material. In this case, temperature uniformity in the mobile thermal energy storage system is not possible. Nevertheless, temperature difference as depicted in figures 5.31 and 5.32 reveals that local temperature increase is not significantly high in the liquid phase of the phase change material.

Figure 5.33 shows temporal variation temperature at three locations (figure 3.9) inside the tube. Location 1 is near to the heat source where the intensity of concentrated solar radiation is high at the tube outer surface, location 2 corresponds to the central region of the tube, and location 3 is at the distance farther away from the heat source.

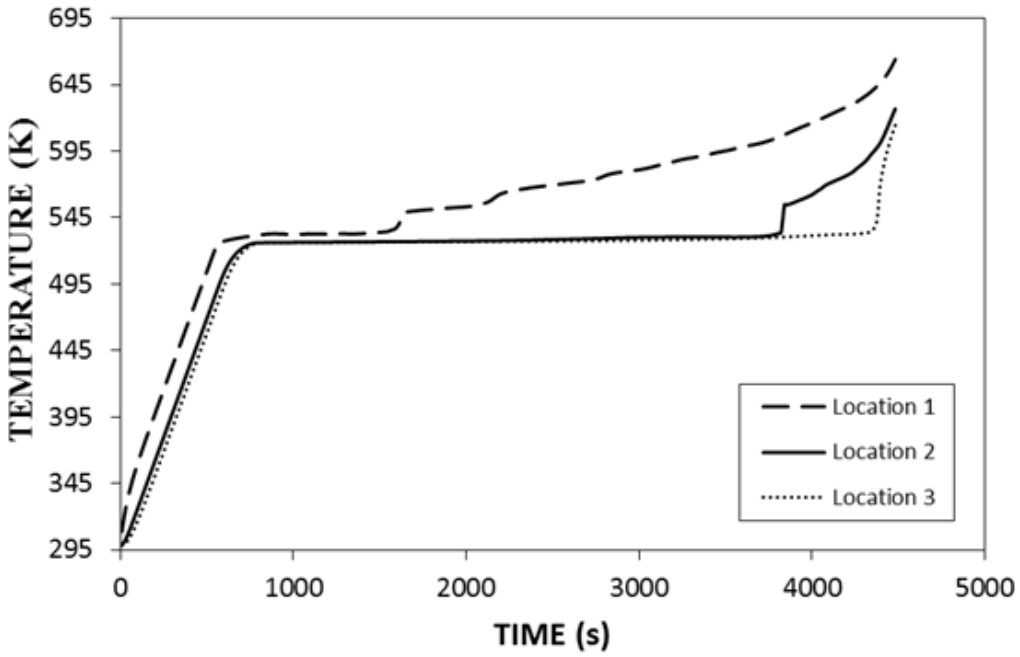

Figure 5.33 Temporal variation of temperature at three locations inside the tube.

In general, temperature rises rapidly in all the locations inside the tube during the early heating period ($t \leq 800$ s). This behavior is attributed to the solid phase heating of the phase change material inside the tube; in which case sensible heating is responsible for the rapid rise of temperature in the tube. As the time progresses, phase change takes place at solidus temperature and the time taken to reach liquidus temperature is considerably longer than that corresponding to the time taken to reach solidus temperature. This is mainly because of the energy gain of the phase change material in terms of the latent heat of melting. However, the time to complete melting is relatively shorter at location 1, and then follows locations 2 and 3. This is attributed to the temperature gradient at these locations. It should

be noted that increasing local temperature gradient results in enhanced heat conduction locally. Therefore, high rise of temperature in the solid phase is attributed to the presence of high temperature gradients between the metallic mesh and the phase change material. The early completion of the phase change at location 1 is also attributed to the rate of heat conduction due to the high temperature gradient in this region. Once the phase change occurs in this region, temperature increase in the liquid phase takes place at a lower rate than that of the solid phase of the phase change material in this region. This is associated with the thermal conductivity of the phase change material in the liquid phase, which is considerably smaller than that of the solid phase. However, as the time progresses further ($t \geq 4000$ s), temperature difference at each location becomes small. This indicates that almost uniform temperature is achieved in the tube via using the meshes. Consequently, thermal energy can be stored in a mobile thermal battery in terms of a latent heat and sensible energy storage uniformly through using metallic meshes under the arrangement of the concentrated solar heating.

5.4 Thermal Analysis with PCM ($LiNO_3$) and With Rotation of Thermal Battery

In this case, the thermal battery is rotated at different speeds and temperature and flow fields are predicted inside receiver to assess the uniform heating of the battery via solar trough.

Figures (5.34), (5.35) and (5.36) show temperature, velocity and liquid fraction contours inside the thermal battery for various rotational speeds at 2240 s of the heating duration. Temperature in the region where the focused solar radiation from the trough is located remains high in the thermal battery for all rotational speeds. The presence of the metallic

meshes improves the heat conduction in the thermal battery. This can be observed when comparing temperature rise in the metallic mesh and phase change material in the region away from the high temperature region. Due to the low thermal conductivity of phase change material ($LiNO_3$), the aluminum meshes act like a heat carriers from heated shell (tube) towards the thermal battery interior. As the rotational speed increases, high temperature region extends along the circumference of the receiver tube and receiver interior while the peak temperature remains almost same for all the cases considered. The rotation of the thermal battery provides almost uniform heating of the thermal battery interior because of reduced localized heating as observed when the battery rotation is set to zero. In the case of figure (5.35), the natural convection current generated in the liquid phase results in fluid rotation inside the cells due to solid boundaries of aluminum meshes. In addition, the rotation of the receiver tube contributes to the flow field in the cells because of the body forces generated under the gravity. In the region where the melting does not occur, due to relatively lower temperature than the liquidus temperature of the phase change material, velocity remains the rotational velocity of the receiver. In this case, the solid phase of the phase change material behaves like a solid body. This takes place in the central region of the thermal battery where temperature remains lower than the liquidus temperature of the phase material during the time period considered (t = 2240 s). This situation is also observed from the liquid fraction contours in the battery cross-section for the same heating duration (figure (5.36)). The outer cells in the solution domain are almost phase changed where the liquid fraction approaches to unity for the high rotational speed.

However, localized melting region is observed for the stationary or low rotational speeds. In this case, the heat transfer from the tube outer surface towards the phase change material inside the tube remains high in the region where the solar irradiation intensity is high. In some cells, close to the tube wall, the sensible heating takes place after the phase change

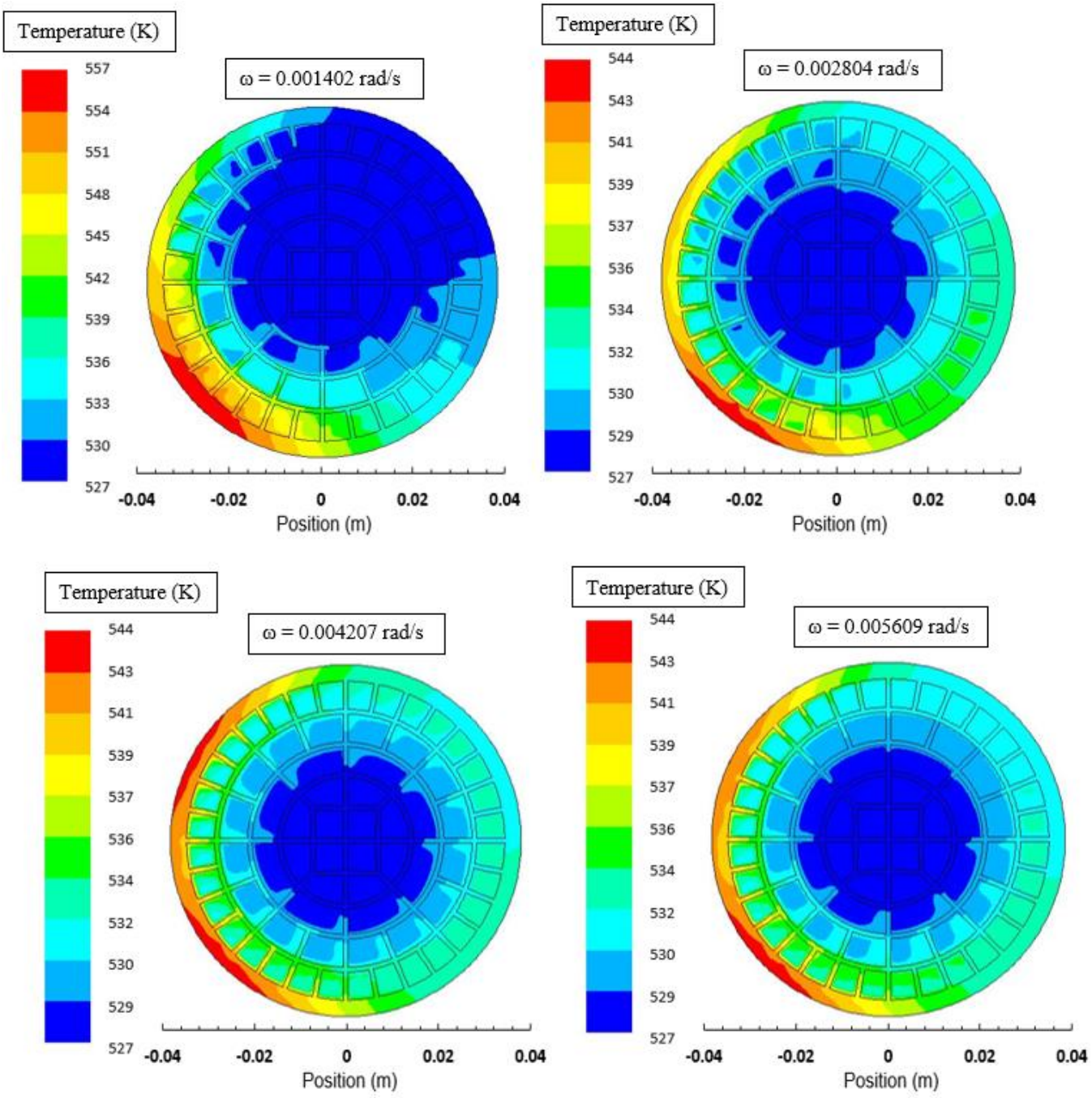

Figure 5.34 Temperature contours for different rotational speeds at t = 2240 s.

is completed. Consequently, local heating results in excessive heating of the thermal battery in some region where phase change material is in liquid form; in the other part of the battery, the phase change material remains in the solid phase.

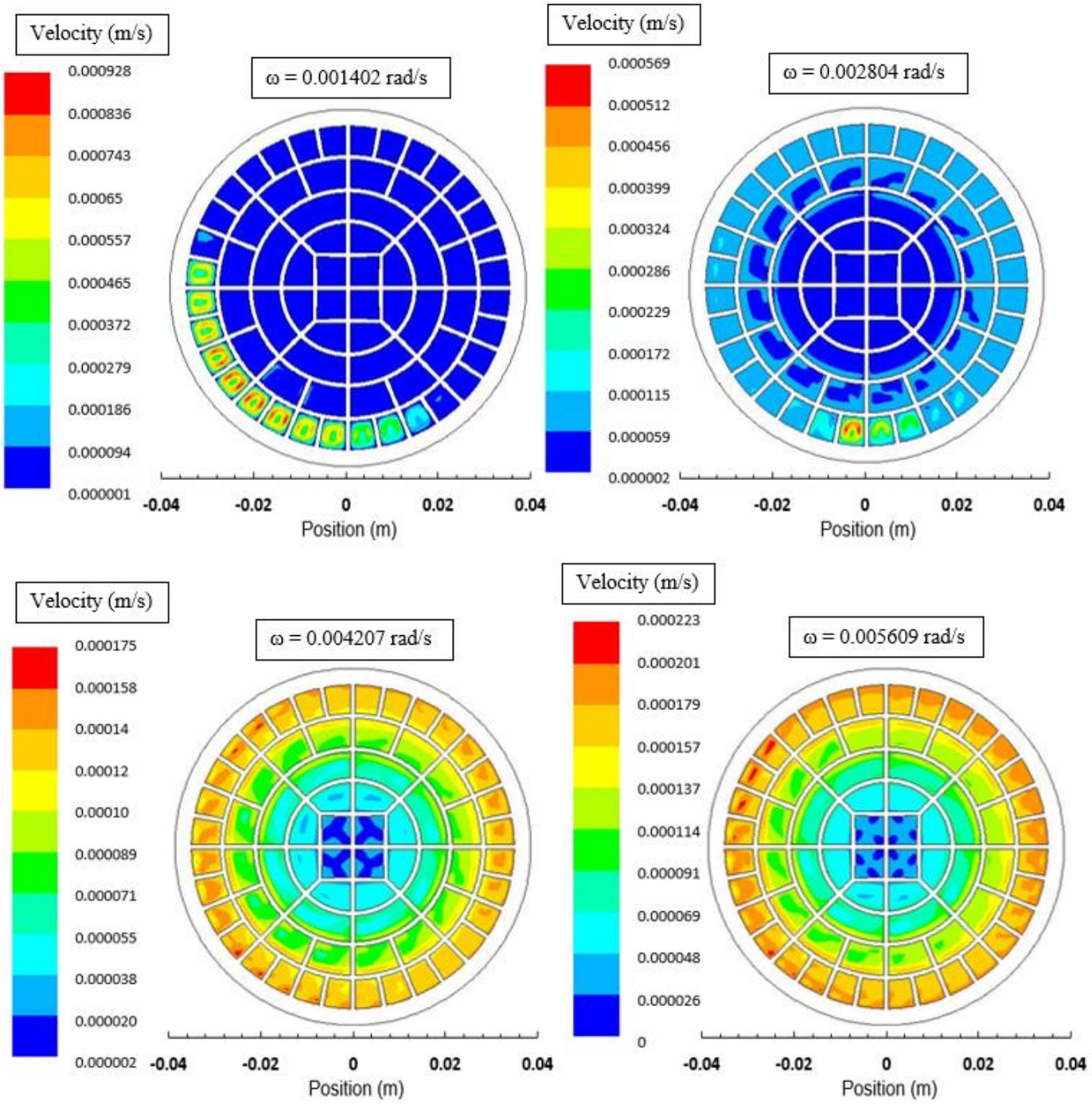

Figure 5.35 Velocity contours for different rotational speeds at t = 2240 s.

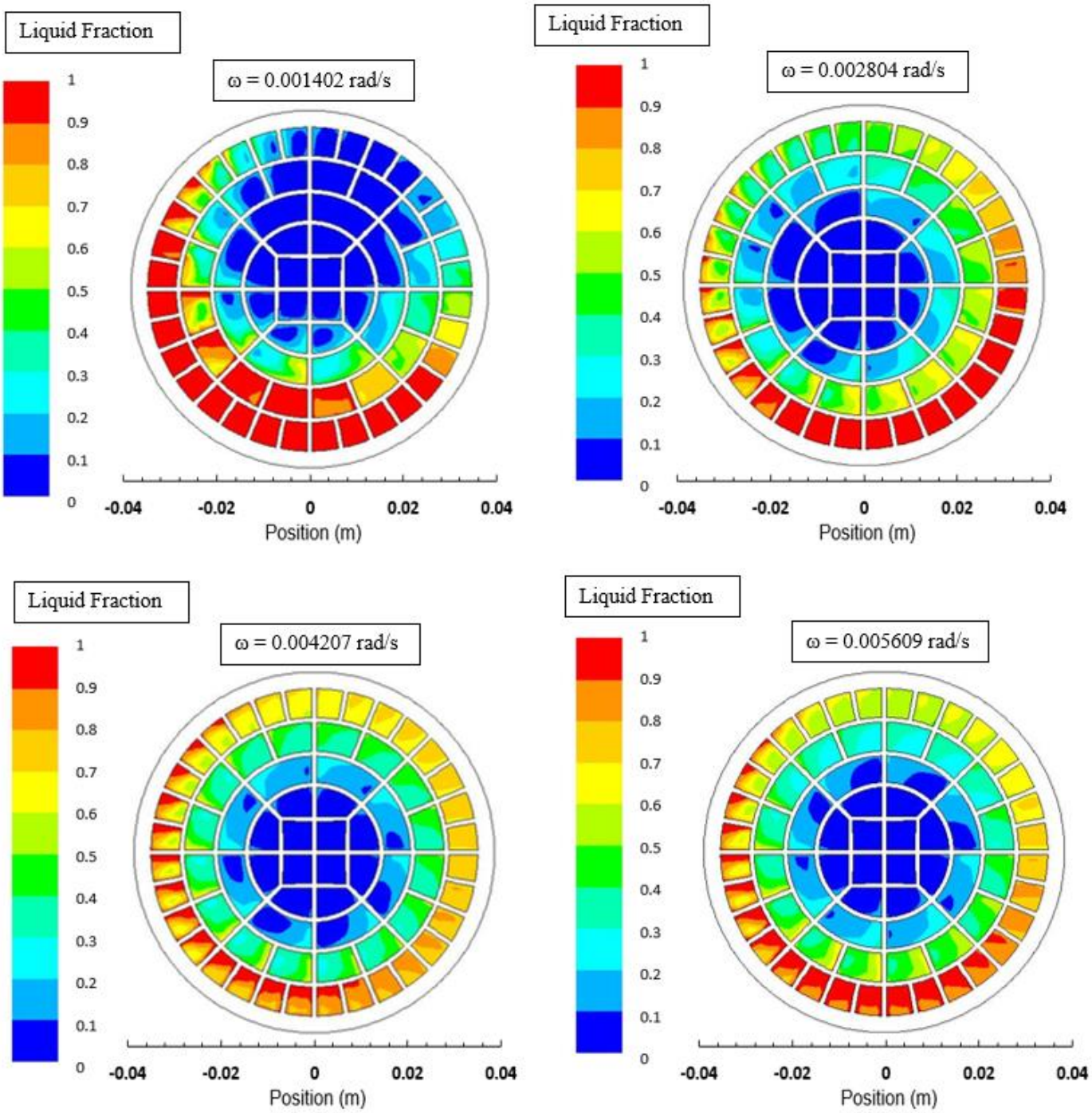

Figure 5.36 Liquid fraction contours for different rotational speeds at t = 2240 s.

Therefore, the storage of energy is localized when the thermal battery is stationary or rotating with low speeds. Moreover, at high rotational speeds, convection current generated

due to density variation in the liquid phase of the phase change material and the rotational speed influences the phase change process. In this case, in the central region of the receiver, which is slightly away from the rotational center, liquid fraction contours shows spinning like patterns. Consequently, the rotational speed of the thermal battery is responsible for this behavior. It should be noted that the melted material remains almost at liquidus temperature in this region so that the density variation in the liquid phase is small. Consequently, the contribution of the convection current to the flow filed is small.

The similar contour plots for temperature, velocity, and liquid fraction are also shown in figures (5.37). (5.38), and (5.39) for the heating time duration of t = 4480 s.

It can be observed from the liquid fraction data (figure 5.39) that the phase change material completely liquefies at this heating period. The flow field is affected by both the rotational speed and the convection current; in which case, the flow circulation is formed within each cell inside the receiver.

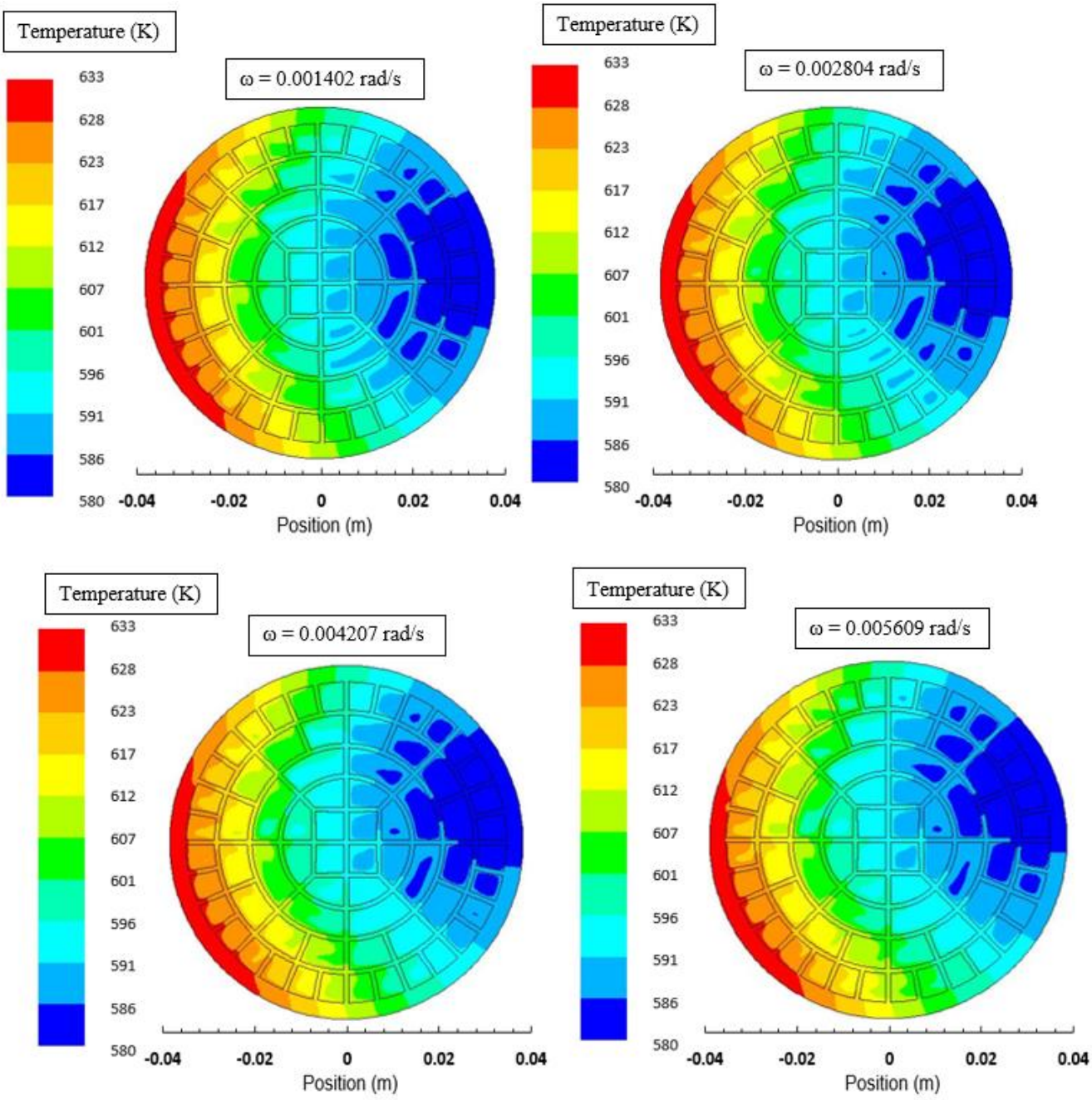

Figure 5.37 Temperature contours for different rotational speeds at t = 4480 s.

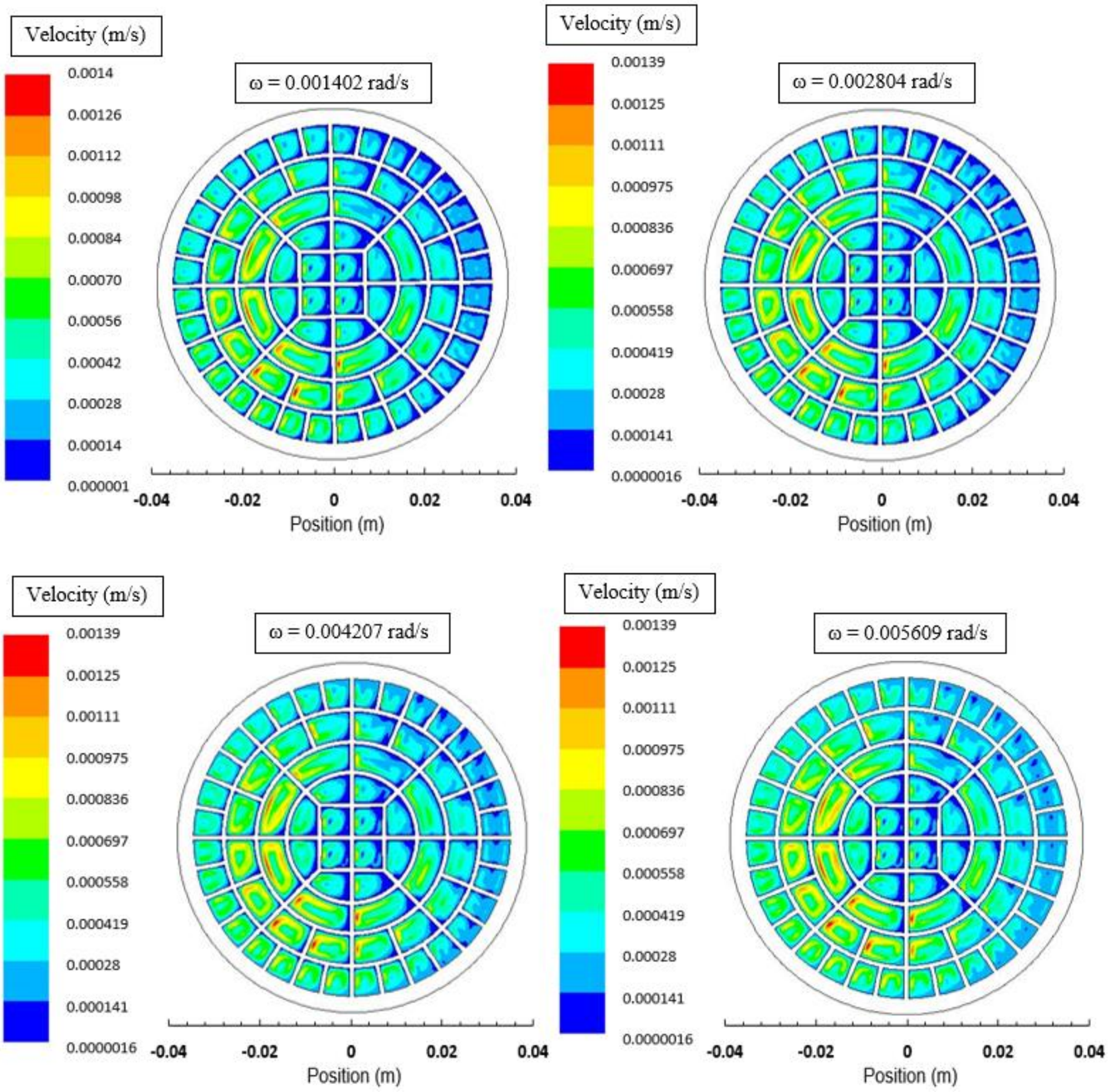

Figure 5.38 Velocity contours for different rotational speeds at t = 4480 s.

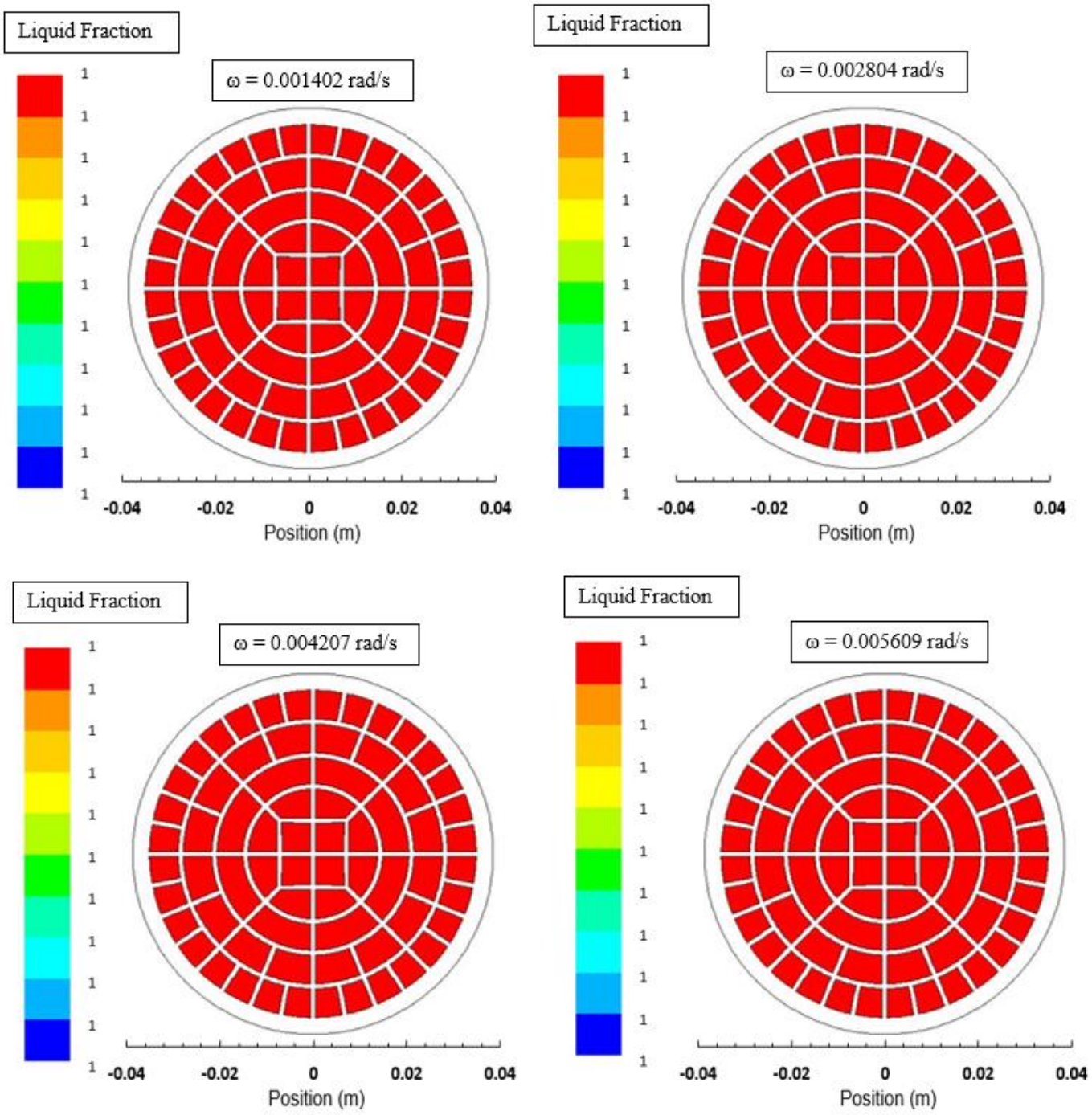

Figure 5.39 Liquid fraction contours for different rotational speeds at t = 4480 s.

Figure (5.40) shows the temperature parameter ($\varphi = \frac{T-T_{in}}{T_{max}-T_{in}}$) along the x-axis (horizontal rake, logo in figure (5.40)) for various rotational speeds of the thermal battery

and heating duration of 4480 s. The temperature parameter remains high in the region close to the thermal battery tube towards the trough site, which is associated with the attainment of high temperature difference between the current fluid temperature and initial temperature (T-T_{in}). This can be observed from figure (5.41), in which the temperature difference is shown. Temperature difference remains high for the non-rotating case because of the localized heating in the region close to the trough site. It should be noted that solar heating of the thermal battery is carried out implementing external heating source resembling the concentrated solar irradiation reflected from the trough (figure 3.8). However, rotation of the thermal battery results in low temperature difference and high temperature parameters.

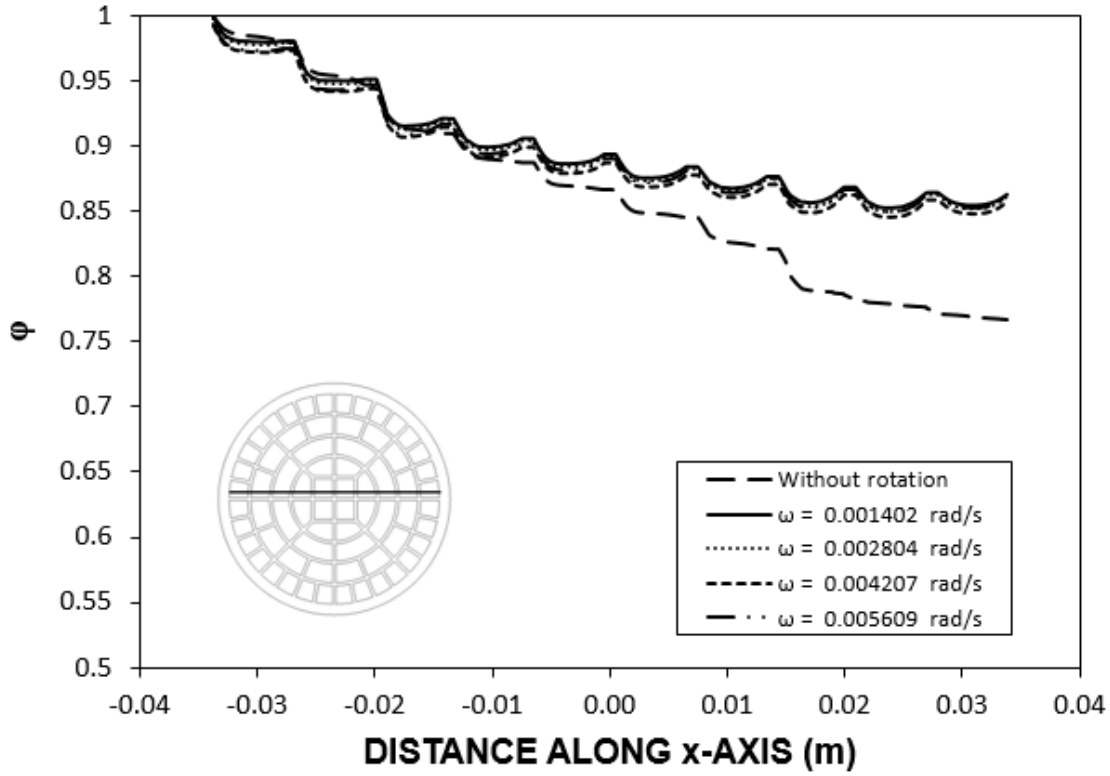

Figure 5.40 Temperature parameter (φ) along the horizontal rake located in x-axis (at t = 4480 s).

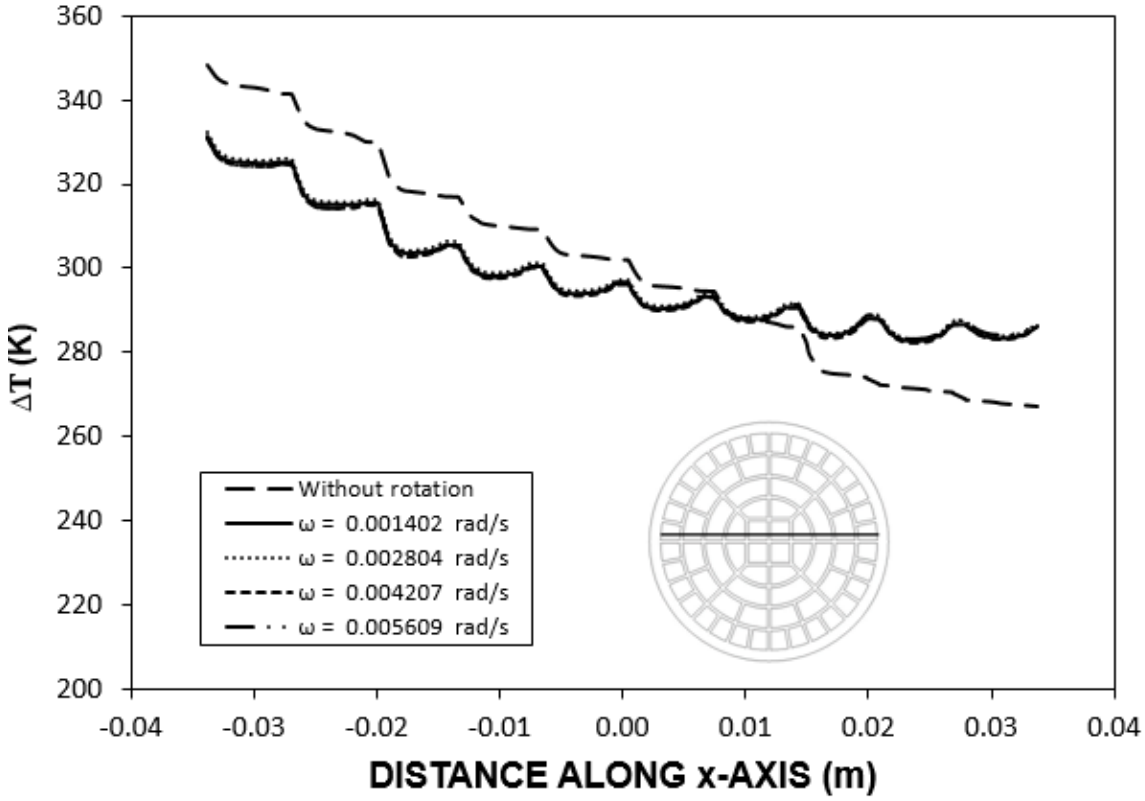

Figure 5.41 Temperature difference (ΔT) along the horizontal rake located in x-axis (at t = 4480 s).

This is attributed to the attainment of similar values of $T_{max} - T_{in}$ and $T - T_{in}$, which is more pronounced in the region close to the receiver tube wall towards the trough site. As the distance increases along the x-axis away from the trough side, the temperature parameter reduces. This is related to the heat transfer from receiver tube towards the working fluid inside the receiver. Although aluminum meshes are used to improve the heat conduction inside the receiver, temperature gradually decreases with increasing distance along the x-axis due to the low thermal conductivity of $LiNO_3$. Moreover, the wavy appearance of the temperature parameter is because of the presence of meshes inside the receiver. In this case, metallic meshes, due to high thermal conductivity, enhance conduction heat transfer and increase temperature within the metallic meshes. In addition, rise temperature of the

working fluid is suppressed by the phase change process; hence, temperature gradient is formed between the working fluid and the metallic meshes. This gives rise to a small amplitude oscillation like behavior for temperature along the x-axis. In the case of the rotation of the receiver, the influence of receiver rotation on the temperature parameter is observed to be not significant, which is particularly true in the high temperature region. This behavior is associated with the working fluid temperature (T) and the maximum temperature (T_{max}) in the working fluid. In this case, the rotation of the solar receiver reduces the maximum as well as working fluid temperature inside the receiver. This, in turn, results in almost identical temperature parameters for all rotations.

Figure (5.42) shows the temperature parameter along the y-axis (vertical rake in the figure logo) for the heating period of 4480 s. The temperature parameter behaves similar to those shown in figure (5.40), provided that the temperature parameter remains almost the same along the y-axis for all rotational speeds. However, the attainment of small decrease of the temperature parameter in the central near region of the receiver is related to the heat transfer and temperature increase in the central region, which remains relatively lower than the receiver tube vicinity due to low thermal conductivity of the phase change material (figure (5.34)). The effect of receiver rotational speed on the temperature parameter is not significant as similar to figure (5.40). However, the temperature parameter remains high in the band of 0.9 to 1 along the y-axis while it is within the band of 0.87 – 1 along the x-axis. This is attributed to the variation of temperature difference ($T - T_{in}$) along the y-axis, which remains lower than that of the case observed along the x-axis.

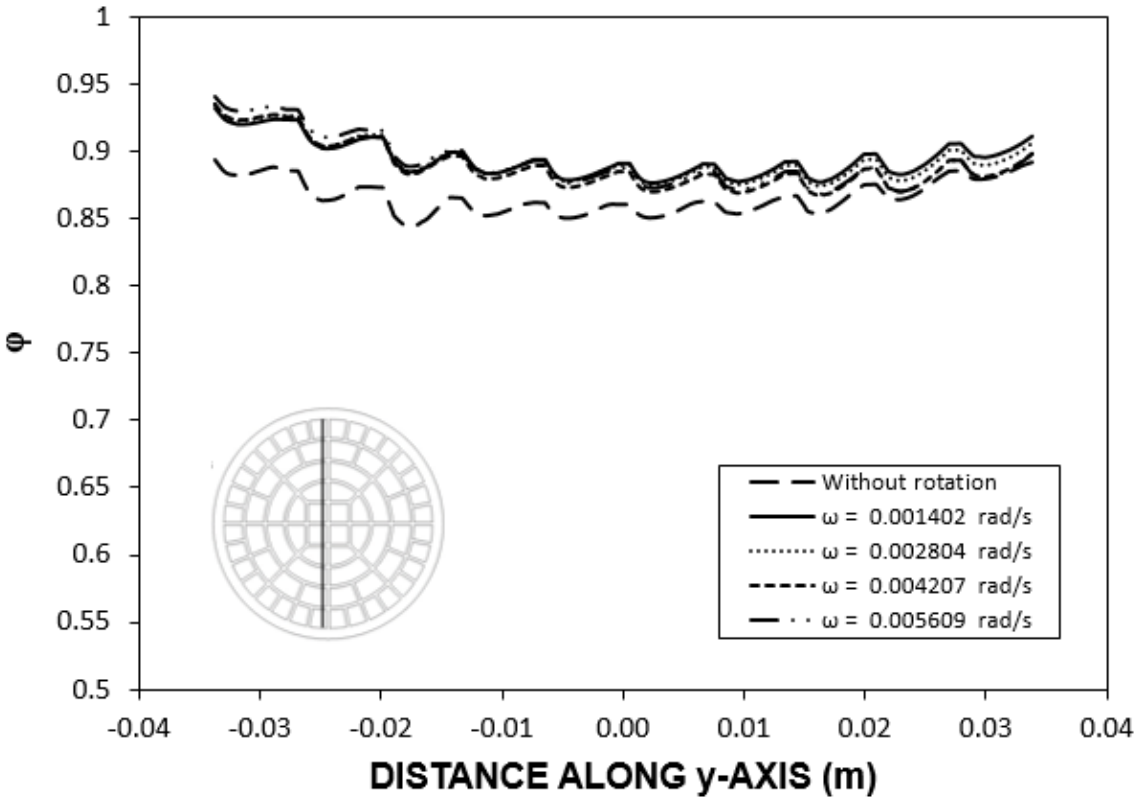

Figure 5.42 Temperature parameter (φ) along the vertical rake located in y-axis (at t = 4480 s)

This situation can also be seen from figure (5.43), in which temperature difference ($T - T_{in}$) is shown along the y-axis. This is related to the heat transfer direction, which is higher along the x-axis because of the high temperature gradients in this direction. The temperature parameter remains slightly higher for non-rotating receiver than that of rotating receiver. This is attributed to the local heating resulting in high working temperature along the y-axis as compared to that of along the x-axis (figure (5.34)). Similarly, improved heat conduction along the aluminum meshes gives rise to the attainment of higher temperature in the aluminum meshes than that corresponding to the working fluid. Consequently, temperature difference appears as temperature oscillation along the y-axis.

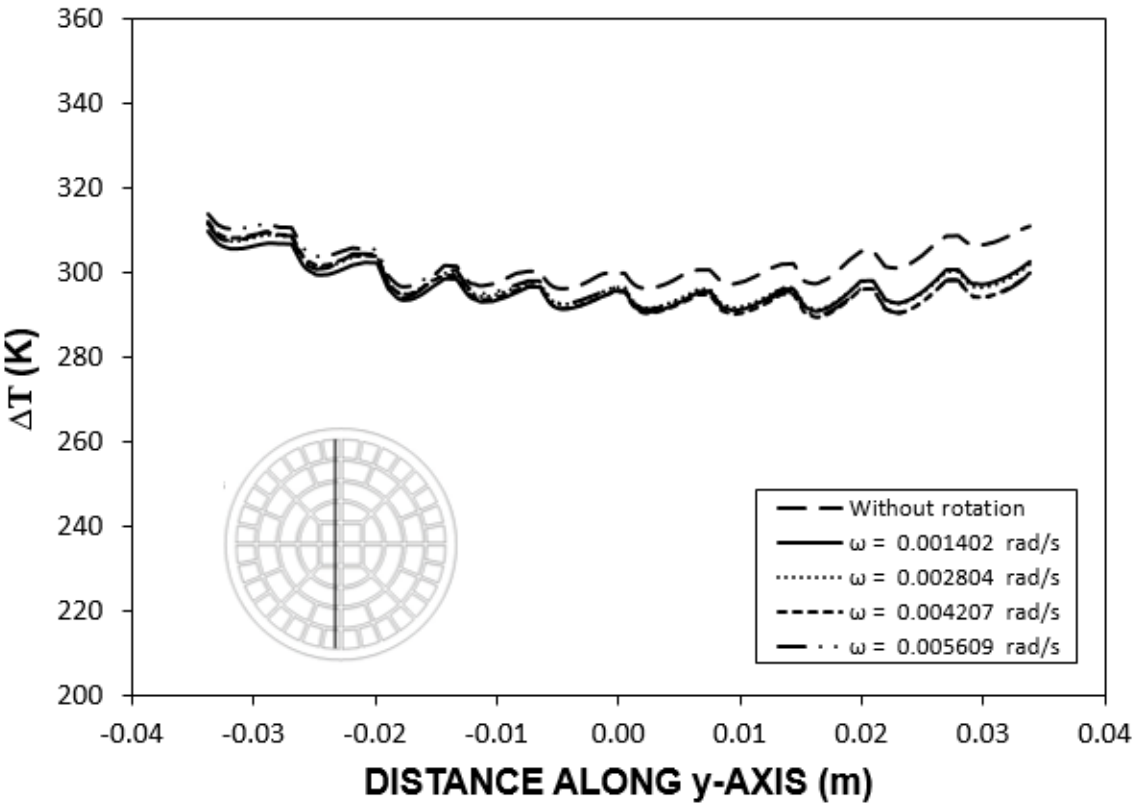

Figure 5.43 Temperature difference (ΔT) along the vertical rake located in y-axis (at t = 4480 s).

Figure (5.44) shows the temporal variation of the maximum temperature in the phase change material inside the receiver for various rotational speeds. The maximum temperature rises rapidly in the early heating period until the phase change initiates in the region close the receiver where the solar irradiation is introduced. It, then, remains same as the time progresses until the time when the heating of the phase change material starts. Although the initiation of the phase change starts almost at the same time for all the cases considered in terms of the receiver rotation, the completion of melting differs for different cases of rotation.

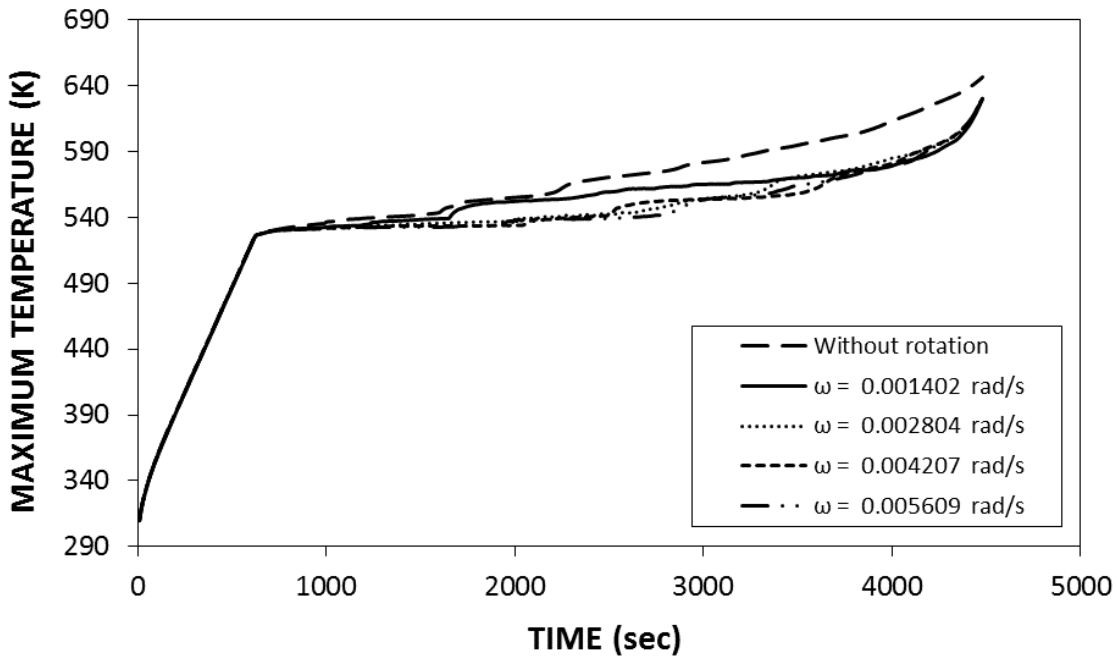

Figure 5.44 Temporal variation of the maximum temperature inside the receiver for various rotational speeds.

This is associated with the initiation of melting of the phase change material in the close region of the receiver wall for all the cases and the influence of the rotational speed on temperature distribution in the receiver. However, increasing rotational speed extends the steady duration of the maximum temperature. This indicates that phase change process continues inside the receiver with progressing time. Further increase in the maximum temperature indicates the sensible heating of the working fluid because of the localized melting and internal energy gain beyond the melting point of the working fluid. Initiation of sensible heating after the phase change process occurs first without rotational case and increasing rotational speed delays the initiation of the sensible heating in the receiver. This is because of the fact that increasing rotational speed improves the uniform heating in the receiver; consequently, localized heating and early initiation of the phase change and sensible heating is delayed. The localized heating can also be seen from figure (5.45), in

which temporal variation of temperature is shown for various rotational speeds of the receiver. The rotation of the solar volumetric receiver provides uniform heating of the working fluid while delaying the sensible heating of the phase change material due to the localized heating.

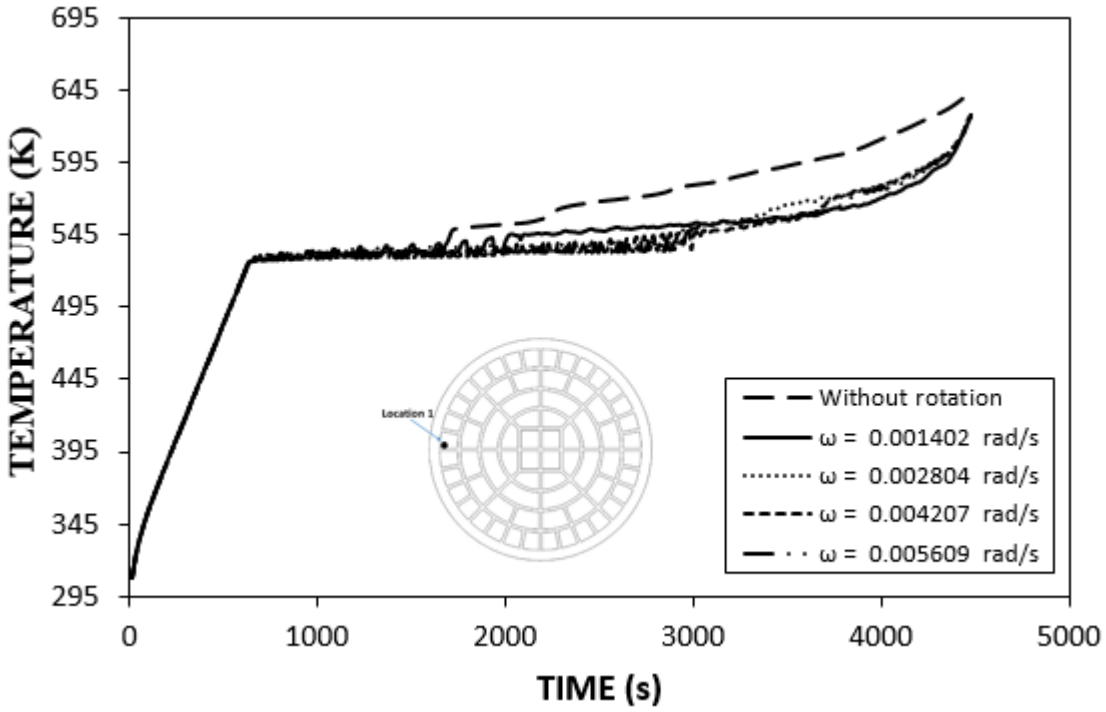

Figure 5.45 Temporal variation of temperature at location 1 where x = -0.033 m, y = 0.001 m for various rotational speeds.

Figure (5.46) shows temporal variation of the ratio of the liquid phase mass over the solid phase mass of the phase change material in the receiver for the cases with and without meshes. The ratio of liquid phase remains low with progressing time for the without mesh configuration. This indicates that heat diffusion into the receiver is suppressed by the low thermal conductivity of the phase change material. On the other hand, for the presence of meshes case, heat diffusion is enhanced because of the conduction tree generated by the metallic meshes. The difference between the temporal behaviors of liquid phase ratio

becomes significant for the later heating periods. In this case, low thermal conductivity without mesh case gives rise to localized heating in the region close to the high solar intensity around the receiver. Consequently, heat supplied by the trough is dissipated through sensible heating in the temperature range above the liquidus temperature of the phase change material in the localized region. Moreover, to assess the effect of natural convection current on the heat transfer rates in the liquid phase of the phase change material, figure (5.47) is plotted for two cases, in which the simulations are repeated incorporating the buoyancy driven flow due to density variation and non-presence of the buoyancy current.

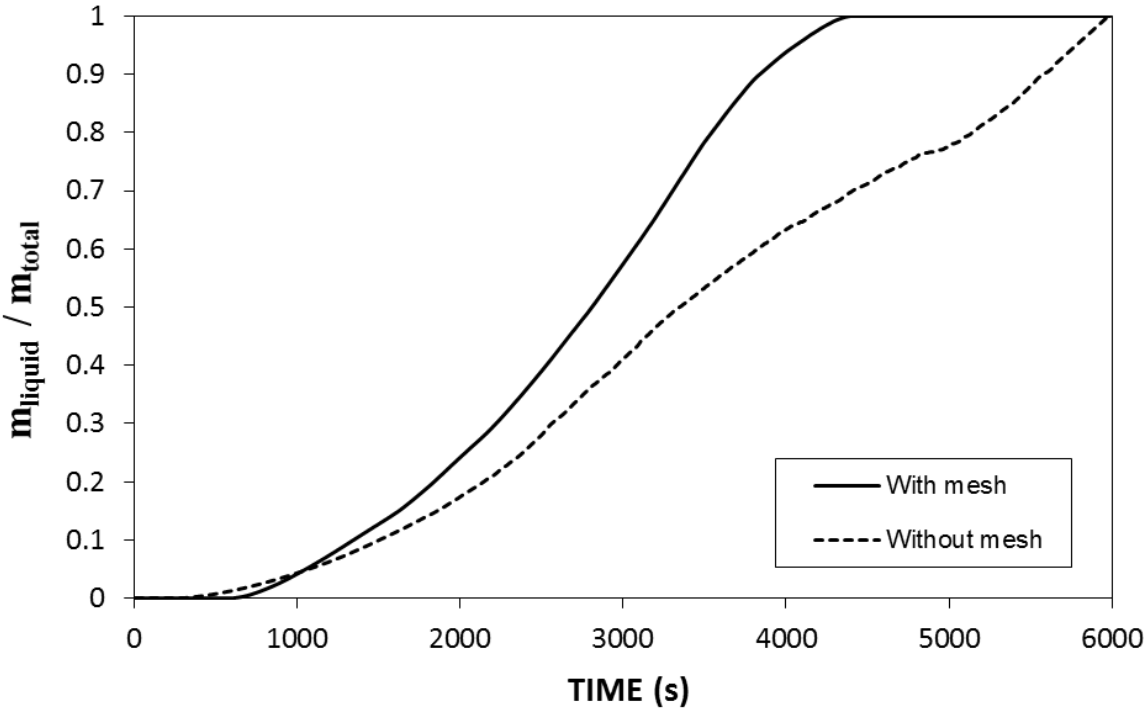

Figure 5.46 Temporal variation of ratio of liquid mass to total mass of phase change material for the cases with and without meshes.

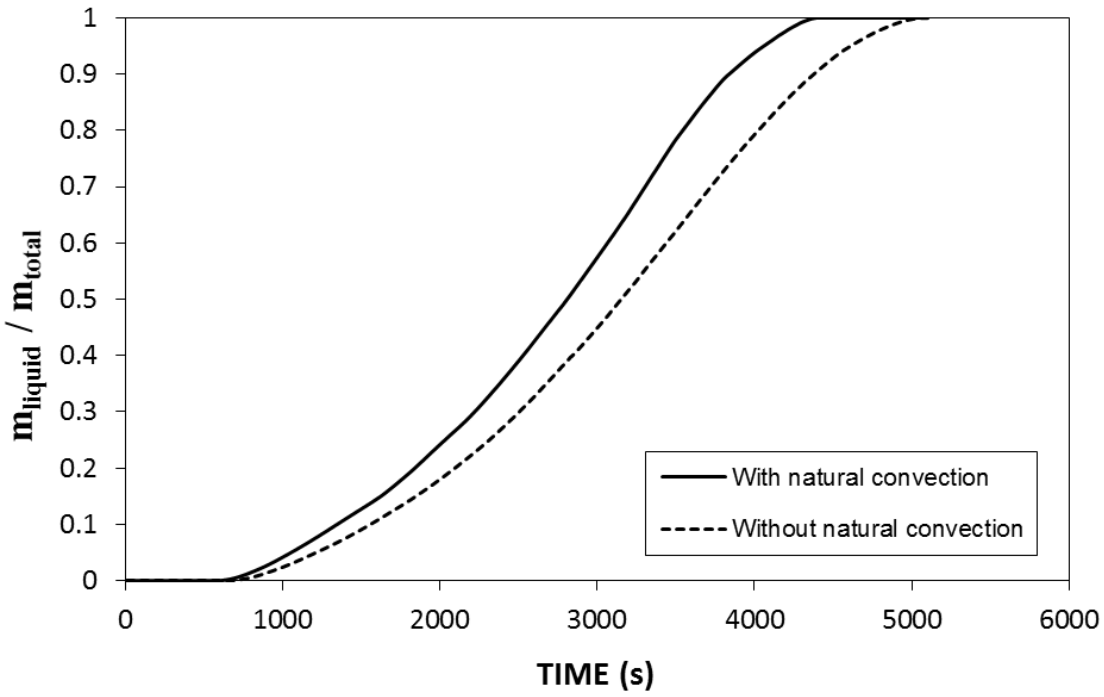

Figure 5.47 Temporal variation of ratio of liquid mass to the total mass of phase change material for the cases with and without natural convection.

It is evident that the natural convection current has significant effect on the melting rate of the phase change material. In this case, ratio of liquid phase rises faster for the case in which natural convection is incorporated as compared to that of non-natural convection case. Consequently, when modelling the phase change process, the contribution of the natural convection current on the heat transfer rates should be incorporated in the analysis. In order to examine the influence of rotation on the ratio of liquid phase in the receiver, figure (5.48) is plotted, in which temporal behavior of the ratio of mass of the liquid phase over the total mass of the phase change material in the receiver is shown for various rotational speeds.

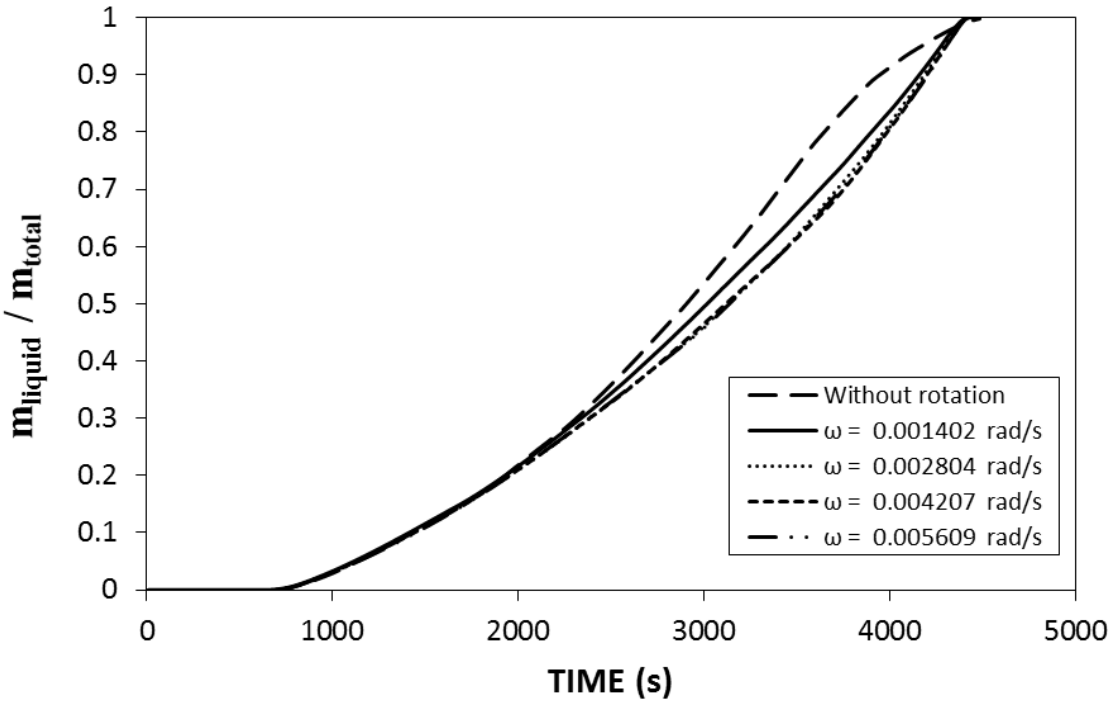

Figure 5.48 Temporal variation of ratio of liquid mass to the total mass of phase change material for various rotational speeds.

The ratio of liquid phase remains high for the case without rotation of the receiver during the early heating periods. This behavior is attributed to the localized heating and localized phase change in the receiver. However, as the heating period progresses further, the cases with rotation results in short time span for the total melting where the liquid fraction reaches unity. This is more pronounced for the high rotational speed of the receiver.

CHAPTER 6

CONCLUSIONS

6.1 Thermal Analysis with Water and Without Rotation of Thermal Battery

Thermal analysis of the solar concentrated heating of a metallic tube containing stagnant water inside is carried out. The heat transfer enhancement in water is presented introducing the metallic meshes inside the tube. In order to observe the effect of natural convection current on the temperature filed, the buoyancy-driven flow due to density variation in water is incorporated in the analysis. The side surface of the tube is considered to be exposed to a solar concentrated heating and the other side is exposed to direct solar radiation. This arrangement resembles the solar heating of the tube located at the trough locus. It is found that the local heating is resulted inside the tube in the close region of the solar concentrated irradiation for the case of without meshes inside the tube. In addition, natural convection current influences significantly temperature field in water when no mesh is used inside the tube. In the case of the presence of the meshes inside the tube, temperature increase becomes gradual during the heating period and the temperature difference between the maximum and the minimum temperature becomes small inside tube. In this case, the aluminum meshes act like a conduction tree inside the tube while enhancing heat transfer rates in water. The influence of natural convection current on the temperature field is less significant for the presence of mesh case than that corresponding to the without mesh case.

This is attributed to the small volume of water occupying the mesh cells inside the tube; in which case, temperature difference in the volume of water becomes small and the density variation remains low in the cell. The temperature coefficient variation along the x, y axes inside the tube demonstrates that local heating takes place inside the tube without mesh case. This is attributed to the attainment of the large difference between the maximum and minimum temperatures inside the tube.

6.2 Thermal Analysis with Water and With Rotation of Thermal Battery

The concept of a mobile thermal battery with rotation is introduced and thermal storage characteristics of the thermal battery are assessed. Governing equations of heat transfer and fluid flow due to fluid density variation, and Coriolis and centripetal acceleration are solved numerically and thermal performance of the storage capacity is evaluated incorporating the temperature parameter. In order to enhance the heat transfer rates in the working fluid of the thermal battery, metallic meshes are incorporated while forming a conduction tree inside the working fluid. In this case, aluminum meshes are considered for the conduction tree and water is used as the working fluid in the thermal battery system. The influence of rotational speed on the thermal storage characteristics of the thermal battery is also included in the analysis. It is found that metallic meshes improves the heat transfer rates considerably and minimizes the local heating in the working fluid due to the location of the heat source at the thermal battery outer surface. In addition, convection current and flow field developed due to the rotation of the thermal battery contributes to the heat transfer rates in the working fluid. The rotation of thermal battery along the trough centerline results in almost homogeneous distribution of the solar concentrated emitted

power at the outer surface. This shortens the duration for the fluid bulk temperature to reach the desired temperature and reduces the maximum and the minimum temperature difference in the working fluid. The temperature parameter attains almost the quasi-steady value with increasing rotational speed of the thermal battery.

6.3 Thermal Analysis with PCM ($LiNO_3$) and Without Rotation of Thermal Battery

The concentrated solar heating of a steel tube with presence of aluminum mesh inside and lithium nitrate as phase change material are considered to resemble the mobile thermal battery. The governing equations of heat transfer and flow field due to natural convection are solved numerically. Temperature difference in the phase change material remains slightly high after the completion of the melting of the phase change material; however, sensible heating in the liquid phase in the close region of the heat source resembling the concentrated heating is responsible for the local temperature rise. In general, the use of aluminum mesh inside the tube significantly enhances the heat conduction while causing almost uniform melting of the phase change material. Melting starts in the neighborhood of the aluminum mesh surfaces and the convection current developed in the liquid phase enhances the heat transfer in the mesh cell. This gives rise to increasing rate of melting inside the tube. In the case of the non-meshing configuration inside the tube, the local melting takes place while causing excessive temperature rise locally in the phase change material. The temperature parameter remains high during the phase change because of the attainment of the steady value of the maximum temperature in the tube. As the time progresses, the temperature parameter reduces because of temperature increase in the liquid phase of the phase change material while causing the rise of the increase of the maximum

temperature in the tube. The thermal energy storage through sensible heating in the phase change material results in local temperature rise inside the tube while distorting temperature uniformity. Consequently, the recyclable thermal batteries can be designed using the metallic meshes and phase change material while resulting in almost uniform temperature distribution in the battery is possible under the arrangement of concentrated solar heating.

6.4 Thermal Analysis with PCM ($LiNO_3$) and With Rotation of Thermal Battery

Solar volumetric receiver pertinent to a thermal battery, with rotation, is considered and thermal analysis related to thermal energy storage in the receiver is analyzed. In order to improve the heat diffusion in the energy storing media, which is $LiNO_3$, the aluminum meshes are incorporated in the receiver. Concentrated solar heating is introduced resembling the actual field data in the analysis. A numerical method using the finite element code is used to simulate the thermal and flow filed in the receiver. In the simulations, the natural convection current is incorporated in the liquid phase of the phase change material. To improve the uniform heating of the receiver by the concentrated solar irradiation, receiver rotation is accommodated and the effect of rotational speed on the phase change and heat transfer characteristics of the working fluid is examined. In general, the findings revealed that use of metallic meshes reduces significantly the duration of the phase change in the receiver. This behavior is associated with the enhanced heat diffusion in the receiver through the aluminum meshes. The rotation of the receiver along its symmetry axis provides almost uniform heat flux around the surface, which improves the

uniform heating in the receiver. The specific conclusions derived from the present work are listed below:

i. Temperature increase remains high in the close region where the solar irradiation is applied to the receiver. This, in turn, triggers early initiation of the phase change material inside the receiver.

ii. The maximum temperature reduces in the working fluid with increasing rotational speed of the receiver while lowering the phase change initiation in the receiver.

iii. The rotation of the receiver gives rise to the attainment of high values of the temperature parameter ($\varphi = \frac{T-T_{in}}{T_{max}-T_{in}}$) along the x-axis. This is because of attainment of low values of the maximum temperature and increased storing media temperature along this axis. Moreover, temperature parameter decreases slightly in the close region of the receiver center along the y-axis. This related to the attainment of low temperature of the phase change material in this region.

iv. Incorporating the natural convection current in the simulations improves the melting rate in the receiver despite the fact that the receiver consists of small cells bounded by the aluminum meshes.

The present study provides useful information for those designing the thermal battery utilizing the phase change material and the solar concentrated power.

References

[1] "The New Energy Outlook 2015," Bloomberg New Energy Finance report 2015.

[2] "BP Statistical Review of World Energy," The Energy Economic Report by BP 2015.

[3] H. Ye, L. Long, H. Zhang, and R. Zou, "The performance evaluation of shape-stabilized phase change materials in building applications using energy saving index," *Applied Energy,* vol. 113, pp. 1118-1126, 2014.

[4] H. E. Faith, "Technical assessment of solar thermal energy storage technologies," *Renewable Energy,* vol. 14, pp. 35-40, 1998.

[5] A. Sharma, V. V. Tyagi, C. R. Chen, and D. Buddhi, "Review on thermal energy storage with phase change materials and applications," *Renewable and Sustainable Energy Reviews,* vol. 13, pp. 318-345, 2009.

[6] Furbo, "Heat storage units using a salt hydrate as storage medium based on the extra water principle," Technical University of Denmark 116, 1982.

[7] C. S. Herrick and K. P. Zarnoch, "A rolling cylinder latent heat storage device for solar heating/cooling," *ASHRAE Transactions,* vol. 85, pp. 5-512, 1979.

[8] A. Sarı and K. Kaygusuz, "Thermal and heat transfer characteristics in a latent heat storage system using lauric acid," *Energy Conversion and Management,* vol. 43, pp. 2493-2507, 2002.

[9] E.-B. S. Mettawee and G. M. R. Assassa, "Thermal conductivity enhancement in a latent heat storage system," *Solar Energy,* vol. 81, pp. 839-845, 2007.

[10] Y. Tian and C. Y. Zhao, "A numerical investigation of heat transfer in phase change materials (PCMs) embedded in porous metals," *Energy,* vol. 36, pp. 5539-5546, 2011.

[11] C. Y. Zhao, W. Lu, and Y. Tian, "Heat transfer enhancement for thermal energy storage using metal foams embedded within phase change materials (PCMs)," *Solar Energy,* vol. 84, pp. 1402-1412, 2010.

[12] M. Gharebaghi and I. Sezai, "Enhancement of Heat Transfer in Latent Heat Storage Modules with Internal Fins," *Numerical Heat Transfer, Part A: Applications,* vol. 53, pp. 749-765, 2007/11/26 2007.

[13] A. Sarı and A. Karaipekli, "Thermal conductivity and latent heat thermal energy storage characteristics of paraffin/expanded graphite composite as phase change material," *Applied thermal engineering,* vol. 27, pp. 1271-1277, 2007.

[14] Z. Zhang and X. Fang, "Study on paraffin/expanded graphite composite phase change thermal energy storage material," *Energy Conversion and Management,* vol. 47, pp. 303-310, 2006.

[15] X. Fang, L.-W. Fan, Q. Ding, X. Wang, X.-L. Yao, J.-F. Hou, Z.-T. Yu, G.-H. Cheng, Y.-C. Hu, and K.-F. Cen, "Increased thermal conductivity of eicosane-based composite phase change materials in the presence of graphene nanoplatelets," *Energy & Fuels,* vol. 27, pp. 4041-4047, 2013.

[16] F. Agyenim, P. Eames, and M. Smyth, "Heat transfer enhancement in medium temperature thermal energy storage system using a multitube heat transfer array," *Renewable Energy,* vol. 35, pp. 198-207, 2010.

[17] U. Stritih, "Heat transfer enhancement in latent heat thermal storage system for buildings," *Energy and Buildings,* vol. 35, pp. 1097-1104, 2003.

[18] M. Xiao, B. Feng, and K. Gong, "Preparation and performance of shape stabilized phase change thermal storage materials with high thermal conductivity," *Energy Conversion and Management,* vol. 43, pp. 103-108, 2002.

[19] Y. Zhang and A. Faghri, "Heat transfer enhancement in latent heat thermal energy storage system by using the internally finned tube," *International Journal of Heat and Mass Transfer,* vol. 39, pp. 3165-3173, 1996.

[20] L. F. Cabeza, H. Mehling, S. Hiebler, and F. Ziegler, "Heat transfer enhancement in water when used as PCM in thermal energy storage," *Applied thermal engineering,* vol. 22, pp. 1141-1151, 2002.

[21] U. Stritih, "An experimental study of enhanced heat transfer in rectangular PCM thermal storage," *International Journal of Heat and Mass Transfer,* vol. 47, pp. 2841-2847, 2004.

[22] M. Costa, D. Buddhi, and A. Oliva, "Numerical simulation of a latent heat thermal energy storage system with enhanced heat conduction," *Energy Conversion and Management,* vol. 39, pp. 319-330, 1998.

[23] M. Lacroix, "Study of the heat transfer behavior of a latent heat thermal energy storage unit with a finned tube," *International Journal of Heat and Mass Transfer,* vol. 36, pp. 2083-2092, 1993.

[24] S. Z. Shuja, B. S. Yilbas, and M. M. Shaukat, "Melting enhancement of a phase change material with presence of a metallic mesh," *Applied Thermal Engineering*, vol. 79, pp. 163-173, 2015.

[25] R. Velraj, R. V. Seeniraj, B. Hafner, C. Faber, and K. Schwarzer, "HEAT TRANSFER ENHANCEMENT IN A LATENT HEAT STORAGE SYSTEM1," *Solar Energy*, vol. 65, pp. 171-180, 1999.

[26] D. K. Kim, E. E. Marotta, and L. S. Fletcher, "Thermal performance of a wire-mesh/hollow-glass-sphere composite structure," *Journal of Thermophysics and Heat transfer*, vol. 25 (2), pp. 254-261, 2011.

[27] A. Mustaffar, A. Harvey, and D. Reay, "Melting of phase change material assisted by expanded metal mesh," *Applied Thermal Engineering*.

[28] S. Z. Shuja and B. S. Yilbas, "Latent Heat Thermal Energy Storage: Effect of Metallic Mesh Size on Storage Time and Capacity," *International Journal of Thermophysics*, pp. 1-16, 2015/08/05 2015.

[29] J. M. Khodadadi and Y. Zhang, "Effects of buoyancy-driven convection on melting within spherical containers," *International Journal of Heat and Mass Transfer*, vol. 44, pp. 1605-1618, 2001.

[30] F. L. Tan, S. F. Hosseinizadeh, J. M. Khodadadi, and L. Fan, "Experimental and computational study of constrained melting of phase change materials (PCM) inside a spherical capsule," *International Journal of Heat and Mass Transfer*, vol. 52, pp. 3464-3472, 2009.

[31] A. F. Elmozughi, L. Solomon, A. Oztekin, and S. Neti, "Encapsulated phase change material for high temperature thermal energy storage – Heat transfer analysis," *International Journal of Heat and Mass Transfer*, vol. 78, pp. 1135-1144, 2014.

[32] C. Beckermann and R. Viskanta, "Natural convection solid/liquid phase change in porous media," *International Journal of Heat and Mass Transfer*, vol. 31, pp. 35-46, 1988/01/01 1988.

[33] A. R. Darzi, M. Farhadi, and K. Sedighi, "Numerical study of melting inside concentric and eccentric horizontal annulus," *Applied Mathematical Modelling*, vol. 36, pp. 4080-4086, 2012.

[34] T. Hirata, Y. Makino, and Y. Kaneko, "Analysis of natural convection melting inside isothermally heated horizontal rectangular capsule," *Wärme - und Stoffübertragung*, vol. 28, pp. 1-9, 1993/01/01 1993.

[35] S. K. Roy and S. Sengupta, "Gravity-assisted melting in a spherical enclosure: Effects of natural convection," *International Journal of Heat and Mass Transfer,* vol. 33, pp. 1135-1147, 1990.

[36] O. Bertrand, B. Binet, H. Combeau, S. Couturier, Y. Delannoy, D. Gobin, M. Lacroix, P. Le Quéré, M. Médale, J. Mencinger, H. Sadat, and G. Vieira, "Melting driven by natural convection A comparison exercise: first results," *International Journal of Thermal Sciences,* vol. 38, pp. 5-26, 1999.

[37] E. Assis, L. Katsman, G. Ziskind, and R. Letan, "Numerical and experimental study of melting in a spherical shell," *International Journal of Heat and Mass Transfer,* vol. 50, pp. 1790-1804, 2007.

[38] J. Szekely and P. S. Chhabra, "The effect of natural convection on the shape and movement of the melt-solid interface in the controlled solidification of lead," *Metallurgical and Materials Transactions,* vol. 1, pp. 1195-1203, 1970/05/01 1970.

[39] M. K. Mansour, "Effect of natural convection on conjugate heat transfer characteristics in liquid minichannel during PCM melting," *Proceedings of the Institution of Mechanical Engineers, Part C: Journal of Mechanical Engineering Science,* p. 0954406213486590, 2013.

[40] L. Tan, Y. Kwok, A. Date, and A. Akbarzadeh, "Numerical Study of Natural Convection Effects in Latent Heat Storage using Aluminum Fins and Spiral Fillers," *International Journal of Mechanical and Aerospace Engineering,* vol. 6, pp. 455-463, 2012.

[41] W. R. a. C. Martini, S. W, "Natural convection inside a horizontal cylinder," *A.I.Ch.E Journal,* vol. 6, pp. 251-257, 1960.

[42] P. Jany and A. Bejan, "Scaling theory of melting with natural convection in an enclosure," *International Journal of Heat and Mass Transfer,* vol. 31, pp. 1221-1235, 1988/06/01 1988.

[43] B. W. Webb and R. Viskanta, "Natural-convection-dominated melting heat transfer in an inclined rectangular enclosure," *International Journal of Heat and Mass Transfer,* vol. 29, pp. 183-192, 1986/02/01 1986.

[44] P. Lamberg, R. Lehtiniemi, and A.-M. Henell, "Numerical and experimental investigation of melting and freezing processes in phase change material storage," *International Journal of Thermal Sciences,* vol. 43, pp. 277-287, 2004.

[45] A. Lenert and E. N. Wang, "Optimization of nanofluid volumetric receivers for solar thermal energy conversion," *Solar Energy,* vol. 86, pp. 253-265, 2012.

[46] A. Veeraragavan, A. Lenert, B. Yilbas, S. Al-Dini, and E. N. Wang, "Analytical model for the design of volumetric solar flow receivers," *International Journal of Heat and Mass Transfer,* vol. 55, pp. 556-564, 2012.

[47] Z. Wu, C. Caliot, G. Flamant, and Z. Wang, "Coupled radiation and flow modeling in ceramic foam volumetric solar air receivers," *Solar Energy,* vol. 85, pp. 2374-2385, 2011.

[48] Z. Wu, C. Caliot, G. Flamant, and Z. Wang, "Numerical simulation of convective heat transfer between air flow and ceramic foams to optimise volumetric solar air receiver performances," *International Journal of Heat and Mass Transfer,* vol. 54, pp. 1527-1537, 2011.

[49] O. K. Siddiqui and B. S. Yilbas, "Thermal characteristics of a volumetric solar absorption system," *International Journal of Energy Research,* vol. 38, pp. 581-591, 2014.

[50] G.-G. Fabrisio, G.-A. Jose, T.-P. Sergio, O. Gabriel, and R. Manuel, "Numerical Analysis of Radiation Attenuation in Volumetric Solar Receivers Composed of a Stack of Thin Monolith Layers," *Energy Procedia,* vol. 57, pp. 457-466, 2014.

[51] W. Sun, J. Ji, and W. He, "Influence of channel depth on the performance of solar air heaters," *Energy,* vol. 35, pp. 4201-4207, 2010.

[52] H.-J. Lee, J.-K. Kim, S.-N. Lee, and Y.-H. Kang, "Numerical analysis of heat transfer in multichannel volumetric solar receivers," *Transactions of the Korean Society of Mechanical Engineers B,* 2011.

[53] N. Hasan and S. Sanghi, "The dynamics of two-dimensional buoyancy driven convection in a horizontal rotating cylinder," *Transactions of the ASME-C-Journal of Heat Transfer,* vol. 126, pp. 963-984, 2004.

[54] S. Seghir-Ouali, D. Saury, S. Harmand, O. Phillipart, and D. Laloy, "Convective heat transfer inside a rotating cylinder with an axial air flow," *International Journal of Thermal Sciences,* vol. 45, pp. 1166-1178, 2006.

[55] S. Abell and J. L. Hudson, "An experimental study of centrifugally driven free convection in a rectangular cavity," *International Journal of Heat and Mass Transfer,* vol. 18, pp. 1415-1423, 1975.

[56] F. Song, D. Ewing, and C. Y. Ching, "Experimental investigation on the heat transfer characteristics of axial rotating heat pipes," *International Journal of Heat and Mass Transfer,* vol. 47, pp. 4721-4731, 2004.

[57] G. Reich, B. Weigand, and H. Beer, "Fluide flow and heart transfer inan axially roatating pipe—II. Effect of rotation on laminar pipe flow," *International Journal of Heat and Mass Transfer,* vol. 32, pp. 563-574, 1989.

[58] F. Song, D. Ewing, and C. Y. Ching, "Fluid flow and heat transfer model for high-speed rotating heat pipes," *International Journal of Heat and Mass Transfer,* vol. 46, pp. 4393-4401, 2003.

[59] Y. J. Cheng, Y. H. Liao, and C. K. Huang, "Heat transfer on a radially rotating heated cylinder," *International Communications in Heat and Mass Transfer,* vol. 35, pp. 1355-1359, 2008.

[60] "http://www.nrel.gov/csp/troughnet/pdfs/lupfert_receiver_thermal_prop.pdf," 2015.

[61] http://www.ansys.com/Products/Simulation+Technology/Fluid+Dynamics/Fluid+Dynamics+Products/ANSYS+Fluent, 2015.

[62] Z. F. Huang, A. Nakayama, K. Yang, C. Yang, and W. Liu, "Enhancing heat transfer in the core flow by using porous medium insert in a tube," *International Journal of Heat and Mass Transfer,* vol. 53, pp. 1164-1174, 2010.

Vitae

Name	:Muhammad Khalil Anwar
Nationality	:Pakistani
Date of Birth	:1/1/1990
Email	: mkhalilanw@gmail.com
Address	House # 24, Street 5, Mohallah Qadirabad Jandiyala Road, Sheikhupura, Pakistan.
Academic Background	***M.S Mechanical Engineering***
	December, 2015
	King Fahd University, Dhahran, Saudi Arabia.
	B.Sc. Mechanical Engineering
	June, 2012
	University of Engineering and Technology, Lahore, Pakistan.

Research Contributions

1. A mobile thermal battery and thermal energy storage enhancement. (Accepted in Numerical Heat Transfer Journal, Part A; Applications, December 2015).
2. Thermal Analysis of A Mobile Thermal Battery with Presence of Aluminum Mesh and Solar Concentrated Heating (Accepted in Journal of Energy Engineering, February 2016).
3. Design of A Mobile Thermal Battery and Analysis of Thermal Characteristics (Accepted in Journal of Renewable and Sustainable Energy, February 2016).